Doctoral Dissertation

Doctoral Program in Material Science and Technology (34th cycle)

Electrospun nanofibers based sensors in the context of health monitoring

Eve Cécile J Verpoorten

* * * * * *

Supervisors

Prof. Fabrizio Pirri, supervisor

Prof. Gianluca Ciardelli, Co-Supervisor

Prof. Marzia Quaglio, Co-Supervisor

Doctoral Examination Committee:

Simone Marasso, Referee, CNR Imem Parma

Cristina Potrich, Referee, FBK – CNR Trento

Adriano Sacco, Referee, IIT

Matteo Cocuzza, Referee, Politecnico di Torino

Sergio Ferrero, Referee, Politecnico di Torino

Politecnico di Torino

October 2021

This thesis is licensed under a Creative Commons License, Attribution - Noncommercial - NoDerivative Works 4.0 International: see www.creativecommons.org. The text may be reproduced for non-commercial purposes, provided that credit is given to the original author.

I hereby declare that the contents and organization of this dissertation constitute my own original work and does not compromise in any way the rights of third parties, including those relating to the security of personal data.

Eve Verpoorten

Turin, 31 October 2021

Summary

The third goal of the Sustainable Development Goals of the United Nation is named “Good Health and well-being”. One of the strategies to reach this goal consist in the actuation of a new approach of medicine, defined as the precision medicine. The European Alliance of Personalized Medicine describe this approach as “The right prevention and treatment for the right person at the right time.” In this context, engineering has a lot to afford through the fabrication of precision devices, organ on a chip, personalized implants, cells engineering, genomics and biomaterials.

This thesis concentrates in the development of personalized devices. These devices can be divided in two categories: *i)* wearable devices, for real time information about the patient heath status; *ii)* point-of-care (POC) mostly used for diagnosis.

One important component of these devices are the sensors since they are the entry point of the information about the patient in the device. The key challenges about these sensors are their flexibility, high sensitivity, biocompatibility and easy scale up.

To rise these challenges, in my thesis, I propose nanofibers (NFs) developed as sensitive materials into sensors. Indeed, through the high surface-to-volume ratio and the nanostructuration of the NFs, the requirements of high sensitivity and flexibility can be fulfilled. Moreover, we choose electrospinning as the NFs fabrication method for the easiness of the process that led to an easy scale up and the possibility to select proper biocompatible materials.

In my thesis, I developed a multi-sensing platform based on poly(ethylene oxide)/poly(3,4-ethylenedioxythiophene):poly(styrene sulfonate) for pH and joint bending analysis for rehabilitation application as a wearable device. Moreover, I evaluated its evolution in a wire form. For what concern the development of POC for tumor biomarker, I studied the possible integration of NFs to increase the sensitivity of the devices.

Acknowledgment

I would like to acknowledge first the people that give me the opportunity to do this PhD: from my professors of the master thesis in Belgium, that gave me the will to pursue in the research field and encourage me to do it, Prof. Demoustier and Prof. Jonas; to my supervisors that effectively allowed me to work in their group: Prof. Pirri, Prof. Ciardelli and Prof. Quaglio.

In particular, I would like to thank Marzia Quaglio and Giulia Massaglia for the opportunity to work on this subject, thank you for the supervision, the support and the availability.

I would also like to thank all the people that participated in my formation: Giulia for the electrospinning, materials treatments and characterization, Adriano Sacco for the electrochemistry part, Marco Fontana for the FESEM training, Valentina Bertana for the 3D part and Alessio Testa from MicroLa for the Laser.

Thank you to all the persons with which I collaborated or that helped me characterize my materials: Adriano Sacco, Stefano Bianco, Stefano Stassi and Angelica Chiodoni. A special thanks to Gianluca Palmara, Francesca Frascella and Alessandro Chiadò. Thank you also for all the support that you gave me in these three years of work.

Thank you to Italian Institute of Technology (IIT- Center for sustainable Future Technologies CSFT@Polito) that financed my fellowship and to its whole team. Thank you to all the people of PoliTo I worked with and a particular thank you to the people of Chilab that were more than colleagues.

Thank you to all the friends from the Chilab, thank you for the support, the laughing moments and the help all along my PhD period.

Finally, thank you to my family and my friends from Belgium that were there even if there is 1000 km of distance between us.

Thank you to all my friends here in Italy for the presence and the fact that make me feel at home. Last but not least, thank you to Alberto and his family for the daily support.

Contents

Introduction 1

I.I. Research context and motivation 1

I.I.I. Personalized medicine and personalized devices 1

I.I.II. Motion State Sensors for wearable devices 4

I.I.III. Biophysical sensors for wearable devices 13

I.I.IV. Biochemical sensors for wearable devices and point of care 16

II. Aim of the proposed research 23

III. Outline of the thesis 25

Chapter 1: Electrospun nanofiber for the sensors of wearable and point of care devices: State of the Art 26

1.1. Carbon nanofibers 28

1.1.1. Carbon NFs for human motion sensors 28

1.1.2. Carbon NFs for biochemical sensors 29

1.2. Metal Oxide nanofibers 33

1.2.1. Metal Oxide NFs for biochemical sensors 33

1.3. Conductive polymer nanofibers 37

1.3.1. Conductive polymer NFs for biochemical sensors 38

1.3.2. Conductive polymer NFs for motion state sensors 38

1.4. Non-conductive polymer nanofibers 40

1.4.1. Non-conductive polymer NFs for human motion sensors 40

Chapter 2: Fabrication and measurements methods 43

2.1. Nanofibers fabrication 43

2.1.1. Electrospinning technique 43

2.1.2. Solution, parameters and post treatment 49

2.2. Characterization of the nanofibers 52

2.2.1. Morphological and Optical characterization 52

2.2.2. Chemical characterization 52

2.3. Characterization of the sensors 53
2.3.1. Electrical characterization 53
2.3.2. Electrochemical characterization 53
2.3.3. Graph plotting and Data Analysis 55
Chapter 3: Development of a wearable device sensitive to motion and pH for rehabilitation 56
3.1. Introduction 56
3.2. Optimization of thermal treatment 59
3.3. Flex sensor fabrication 67
3.4. Flex sensor characterization 68
3.5. Integration of pH sensor with Flex sensor 73
3.6. pH sensor characterization 75
3.7. Conclusion 79
3.8. Evolution of the wearable sensor in wire form 80
Chapter 4: Development of a Point-of-Care for tumor biomarker diagnosis 86
4.1. Introduction 86
4.2. Electrochemical biosensing optimization 90
4.3. Sensor fabrication 98
4.4. LIG process optimization 99
4.5. Conclusion and next steps 102
Conclusion and future perspectives 103
References 106

List of Tables

Table 1: Examples of metal nanoparticles integrated in electrospun carbon nanofibers, with their electrospinning solution. 30
Table 2: PVDF Based human motion sensors 41
Table 3: examples of composites in biochemical sensors 42
Table 4: Solution for nanofibers fabrication and proveniance of materials..... 49
Table 5: Electrospinning parameters for each solution..... 50
Table 6: Post treatments on the NFs 50
Table 7: Compression and traction maximum angles for human body joints. Reproduced with permission from [252] 70

List of Figures

Figure 1: Engineering in precision medicine. Reproduced with permission from [6] 2
Figure 2: a) Inertial Measurement Units placement example for the monitoring of human motion, b) example of an optical fiber sensor. Reproduced with permission of [22]. 5
Figure 3: Schematic illustration of electromechanical sensors: (a) capacitive, (b) piezoresistive, (c) piezoelectric 6
Figure 4: Schematic illustration of the patterned strain sensor process of fabrication. Reproduced with authorization from [50] 9
Figure 5: Structure of the piezoresistive pressure sensor and schematic diagram the drop-coating process (a) Photographs and SEM of the textile (view from top: outer layers and side: internal fibers). (b) Photograph of the sensor under stretching and bending. (c) Photographs of the textile before and after CNT/PUD coating. (d) Schematic illustration of the pressure sensor fabrication process. (e) Schematic diagram of the deformation of the sensing unit under compression and stretching. Reproduced with authorization from [64] 10
Figure 6: i) Fabrication process illustration of fish-skin-based nanogenerator. (ii) Photograph of the fish-skin-based nanogenerator showing its flexibility (scale bar ∼20 mm). Reprinted with permission from [84] Copyright 2021 American Chemical Society. 12
Figure 7: Schematic illustrations of the paired hairs geometric distortion associated to pressure, shear and torsion forces. Reproduced with permission from [86]. 13

Figure 8: Response of the sensor to the heartbeat physical force under normal (60 beats/min, +/- 100 Pa) and exercise conditions (100 beats/min, +/- 300-400 Pa). Reproduced with permission from [86]. 14
Figure 9: Smart bandage schematics (a) with and (b) without a capacitive touch panel. Photos of the smart bandage with temperature and touch sensors (c) with and (d) without a capacitive touch panel. Reprinted with permission from [91] Copyright 2021 John Wiley And Sons. 16
Figure 10: a) Scheme of the stretchable electrochemical sensor fabricated on 3D micro-patterned elastomeric substrate. b) Antibody immobilized on the WE and electrochemical response after reaction of antigens with the antibody. c) Process flow of the device fabrication. Reproduced with permission from [132]. 21
Figure 11: FESEM image of a hair and a pollen particle on a nanofiber background. [329] 26
Figure 12: TEM image of Pd/ CNFs with 1h deposition time. Deposition potential, -0.2 V. Reproduced with permission from [183]. 31
Figure 13: TEM images of IrOx nanofibers. Reprinted with permission from [198]. Copyright 2021 American Chemical Society. 35
Figure 14: Structures of typical conducting polymers for bio-sensing applications. Reprinted with permission from [206] 37
Figure 15: Schematic diagram of the set-up of electrospinning 44
Figure 16: Schematic illustration of the Taylor cone formation. Fe = electrical forces, Fs= surface tension forces 44
Figure 17: Core-Shell and Hollow NFs fabrication 46
Figure 18: Static versus dynamic collector 48
Figure 19: Example of the three-electrodes electrochemical disposition 54
Figure 20: Weight percentage evolution of PEO/PEDOT:PSS NFs along temperature increase obtained by TGA analysis. Reproduced with permission from [207]. 60

Figure 21: Rate of degradation of PEO/PEDOT:PSS NFs along temperature increase obtained by TGA analysis. Reproduced with permission from [207]. 60
Figure 22: Crosslinking reaction between PEO and PSS. Reproduced with permission from [207]. 61
Figure 23: FTIR spectrum of the reaction products along the thermal treatment: 2,5°C/min, 1h @ 70°C, 2h @ 120°C, under N2 atmosphere. Above: thermal treatment of PEO nanofibers. Below: thermal treatment of PEO/PEDOT:PSS nanofibers. Reproduced with permission from [207]. 62
Figure 24: morphology of a) PEO/PEDOT:PSS NFs mats without ThTr; b) Crosslinked NFs mats; c) Crosslinked NFs mats but without the first step at 70°C. Reproduced with permission from [207]. 63
Figure 25: Electrical conductivity variation over the duration time of the reaction of crosslinking. $\Delta S=S-S_0$, S_0 is the conductivity of the NFs non thermally treated. Reproduced with permission from [207]. 65
Figure 26: FTIR spectrum of the reaction products along the ThTr. Reproduced with permission from [207]. 65
Figure 27: Schematic illustration of the process flow of fabrication of the Crosslinked NFs Flex Sensor starting from a PDMS substrate by direct deposition of nanofiber mats by electrospinning using the PDMS substrate as the collector. Reproduced with permission from [207]. 67
Figure 28: Sensor application on the wrist. Rest, traction and compression mode illustrated. Reproduced with permission from [207]. 68
Figure 29: Resistance variation of the NFs mat under bending of the samples: a) compression mode; b) traction mode, c) model describing the determination of the traction/compression mode. Reproduced with permission from [207]. 69
Figure 30: a) PEO/PEDOT:PSS MC FESEM and b) PEO/PEDOT:PSS NFs FESEM. Reproduced with permission from [272] 70

Figure 31: Resistance variation when bending for a) the nanofibers, b) the MC. c) model describing the determination of the traction/compression mode. Reproduced with permission from [272] 71
Figure 32: FESEM image of MC material rupture when submitted to bending in traction mode. Reproduced with permission from [272]..... 72
Figure 33: Flex sensors mechanical model used to obtain the Gauge Factor, following the work of Giovanni Saggio [274]. Reproduced with permission from [207]. 72
Figure 34: Illustration of NFs pH-Flex Sensors device application. a) Description of the mechanical deformation zones. b) Description of the sensors disposition on the device. Reproduced with permission from [272]..... 73
Figure 35: NFs pH-Flex Sensor. a) Cross view, b) PEO/PEDOT:PSS Crosslinked NFs FESEM, c) top view and d) 3D view. Reproduced with permission from [272] ... 74
Figure 36: a) EIS curves of the sensor at 4 acidic pH values; b) Equivalent Circuit; electrochemical sensor variation of c) Double layer capacitance, d) Solution resistance and e) Charge transfer resistance with pH. Reproduced with permission from [272]. 76
Figure 37: Proposed model of the protons and NFs surface interactions at the material/solution interface. Reproduced with permission from [272] 77
Figure 38: FTIR analysis of the PEO/PEDOT:PSS NFs. Reproduced with permission from [272] 78
Figure 39: Electrospinning on wire..... 80
Figure 40: Percolation model illustration 81
Figure 41: Choice of material illustration for wire-shaped piezoresistive sensor. a) PEO/MWCNT and b) PAN/MWCNT composite NFs: from top to down: wire obtained after electrospinning, modality of deposition of the NFs on the wire during electrospinning, FESEM image of the morphology of the NFs; c) wire obtained after electrospinning of PEO/PEDOT:PSS blend..... 82

Figure 42: impregnated/NFs/ NFs + impregnated sensors conductivity 84
Figure 43: Piezoresistive evaluation of the wire-shaped NFs sensor. a) percolation model for PEO/MWCNT composite NFs, with emphasis on the two analyzed concentrations for the sensors; b) measurement apparatus for piezoresistive behavior characterization and model describing how this measurement was performed; c) and d) results obtained for 3.5 % wt and 5 % wt PEO/MWCNT sensors piezoresistivity characterization. 85
Figure 44: Charge-blocking effect illustration. It can be seen that more molecules immobilized on the surface, higher the Charge Transfer Resistance since the passage of the electrons from the redox couple is more difficult. 87
Figure 45: a) EIS results for 11-MUA functionalized sensors after 1 h of incubation, as example; b) Randles equivalent circuit used for the fitting of the EIS circuit; c) R_{ct} of sensor functionalized with two type of thiol derivative: 3-Mercaptopropionic acid (MPA) and 11-Mercapto-undecanoic acid (MUA) and three incubation times. 92
Figure 46: Electrochemical measurement curves at each step of the surface modification protocol: a) and d) Square-Wave-Voltammetry, LP (a)) and SP (d)); b) and e) Electrochemical Impedance Spectroscopy: Nyquist Plot, LP (d)) and SP (e)); c) and f) Scheme of the functionalization protocol, with color legend, LP (c)) and SP (f)). 93
Figure 47: Electrochemical characterization of the immunosensor: EIS and SWV for Long and Short Protocol. 95
Figure 48: ELISA results of Ang2 detection 96
Figure 49: Process flow of the fabrication of the carbon-based NFs electrodes. . 98
Figure 50: FESEM images of cellulose NFs after deacetylation treatment without washing and after LIG 100
Figure 51: Raman first analysis of cellulose NFs after LIG 101

Introduction

I.I. Research context and motivation

I.I.I. Precision medicine and precision devices

The third of the 17 Sustainable Development Goals of the United Nations is named “Good Health and Well-Being”. It aims to “Ensure healthy lives and promote well-being for all at all ages”. [1] Among the strategies studied to reach this goal, personalized (and precision) medicine stands out as a tool to improve patient care. In 2012, the European Alliance for Personalized Medicine was launched with the aim to accelerate development and diffusion of personalized medicine to offer “*The right prevention and treatment for the right patient at the right time.*” [2] The term “personalized medicine” evolved then in "precision medicine" under the approbation of the international scientific community. [3] Indeed, precision medicine aims at preventing, diagnosing, monitoring and treating diseases based on the profile of the patient. For example, thanks to this approach of the medicine, it is possible to detect the genetical predisposition of people to some diseases and therefore to act early in order to decrease the possibility or the severity of the disease. Another example is the possibility to monitor the health state of a patient that is following a cure in order to adjust this cure. A last one is to allow the patients to access their cure in autonomy and in a quicker mode. To resume, precision medicine aims at intervene on the specific individual in the right mode and at the right time, to increase the results and to decrease the frequency of unenviable events and therefore to reduce unnecessary treatments. [4]

The objective of reaching precision medicine needs to be sustained by the research in chemistry, life science, mathematics, economics and engineering fields all together to work on genome understanding and analysis, on drug development and delivery techniques, on clinical trials based on an innovative statistics and so on. [5]

Engineering has much to offer to precision medicine at least in the six following areas, as shown on Figure 1.

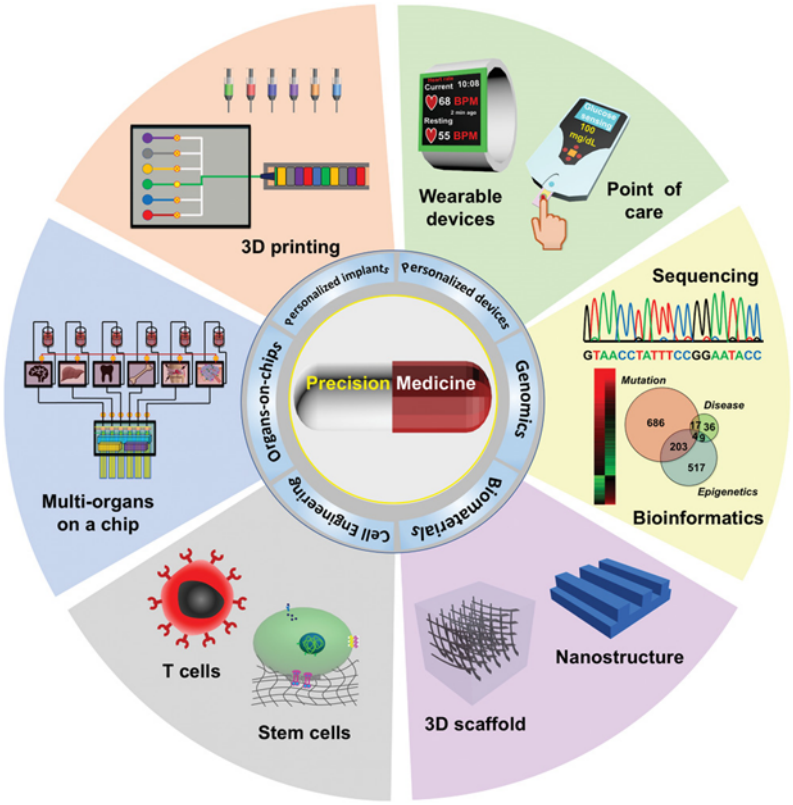


Figure 1: Engineering in precision medicine. Reproduced with permission from [6]

These six areas are:

- Organs-on-chip, that are cell cultures that using microfluidics, reproduce the way an organ or part of it work. They are useful to simulate the organ response to treatments, and the side effect of these treatments on other organs. The final goal is the fabrication of human on a chip, it will help for the testing of the cure [6,7];
- Biomaterials, that offer scaffolds for the growth of artificial tissue, tools for surgical interventions and drug delivery system for on demand release of the treatment [7–9];
- Personalized implants, that combines sensing units to detect the needs of the patient and drug delivery systems in a closed loop to respond to these needs [7];
- Personalized devices, that monitor the health status of the patient [10–12];

- Genomics that can offer accurate and prompt diagnosis, risk analysis based upon genotype and the personalized treatments capacity [5,7];
- Cell engineering that aims at harnessing the immune system of sick patients or at allowing a better organ transplant thanks to the use of patient-sourced cells [7,13].

In particular, in this work, we focused on the personalized devices, that can be divided in two categories: wearables devices and point of care devices.

A wearable device aims at giving information about the health state of the patient wearing the device. It improves the capability of precisely diagnose of a disease for the physicians and also helps the patient to be more participating in its own health monitoring. In this way, the needs of the patient can be detected in real time. The flexibility of the device, even if not necessary, is a huge advantage since it facilitates wearing in the daily life. Example of application of wearable devices are heart rate, sweat and joint bending analysis. Multisensing devices give even more precision in the health status of a patient, for example the physical activity can be monitored together with the lactose, glucose, potassium and sodium levels in sweat and temperature of the body, or also with the pH of the sweat [14]. The whole set of data informs the patient and its physician about her/his level of hydration, muscular fatigue and nutrition. It can be useful in the frame of rehabilitation. [7,15]

Point of care (POC) devices concentrate on biochemical markers rapid analysis, allowing again the monitoring of the health status of the body. In this case it will be blood, tears, saliva, urines that can be analyzed at any place and any time. Gravedance tests and fingerstick blood tests for glucose are examples of already existing POC. POC devices are useful for rapid, easy and cheap diagnosis and monitoring of heath conditions. Thanks to these devices, the treatment of some patient can be adapted based on its response to it, or diseases can be diagnosed before the apparition of some symptoms (early diagnosis of cancer for example). [7,16]

For these two categories of devices, sensors are of huge importance since they are the entry point of the information about the health of the patient.

Generally speaking a sensor is a device that is used to detect changes or events in the environment and convert the information to an electronic signal [17].

In the frame of precision medicine sensors can be divided in three large categories based on what they are sensing [15,18–21]:

- motion state sensors for the movements,
- biophysical sensors for the physiological parameters as the temperature and the heart rate,
- biochemical sensors for the analysis of chemicals in human body fluids.

I.I.II. Motion State Sensors for wearable devices

Motion state sensors mainly focus on the motion of the human being in contexts as sport, walk, sleep, rehabilitation and diseases affecting the movement (dyskinesia, tremor). The parameters measured, from dynamic physical nature, are obtained by accelerometers, goniometers, magnetometers, gyroscopes, pressure sensors and force sensors.

The key parameters to determine the performance of the sensors are:

- The sensitivity S, measured by $S = \frac{\Delta y}{\Delta x}$, with y the output signal and x the deformation imposed to the sensor.
- The Range of Detection (RoD) that is determined by the lowest and the highest value of deformation that can be distinguished

The most accurate results about motion joint monitoring can be obtained through the combination of accelerometers, magnetometers and gyroscopes. This combination gives small rigid inertial measurement units (IMU) that are usually placed above and below the joint of a person (Figure 2a)). The combination of the IMU allows calculating the angular velocity, the orientation, the 3D linear acceleration and the flexion angle of the joint with respect to the reference

coordinate system, following the second and both the inertial laws of Newton. However, the IMU suffers from drift effects and disturbance from electromagnetic noise in case of indoor measurements. Moreover, the daily life application is limited because of the rigidity of the sensors and the complicated application on the skin. [22–26]

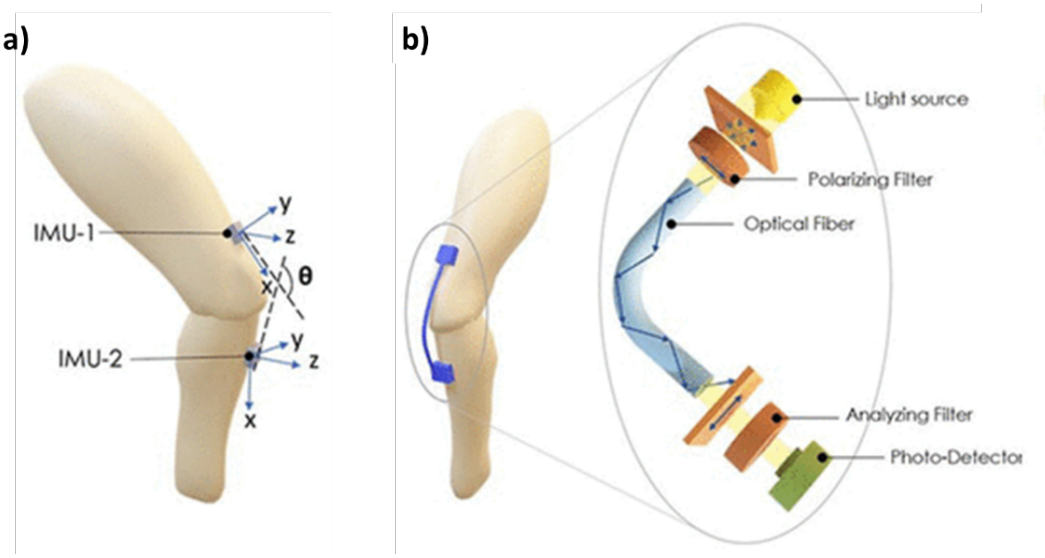


Figure 2: a) Inertial Measurement Units placement example for the monitoring of human motion, b) example of an optical fiber sensor. Reproduced with permission of [22]**.**

Another commonly used type of sensor is the optical fiber sensors (OFS) (Figure 2b)). In this case, an optical fiber, usually made of Silica or polymers, is applied on the joint, together with its light source and its photodetector. When the joint is bend, the intensity of the light that travels in the optical fiber is attenuated and the bending angle can be determined from the value of this intensity. These sensors are free of electromagnetic noise problem, but their sensitivity is low, although more and more works focused their attention on the development of several strategies employed to increase their sensitivity. [22,27–31]

Though these two categories of sensors represent the most precise, they are difficulty applicable in a life-day context, without the presence of formed personal. Moreover, their cost is a huge brake for the idea of using them in a context of health monitoring. In order to ease the use of the sensors, increase the wearing-

comfort, lower the cost and increase the range of application, flexible electromechanical sensors are more and more proposed in the literature [32]. They are sensible to pressure and tensile force and the combination of the two is enough to characterize all the mechanical stimulations that are produced by the movements of the human body. Usually, electromechanical sensors are composed of two electrodes and an active material able to respond to a mechanical stimulus assembled on a flexible biocompatible substrate that offers stability and mechanical resistance to the whole sensor. Examples of materials used for the substrate are: ecoflex, polydimethylsiloxane (PDMS), poly(ethylene terephthalate) (PET), polyimide (Kapton), poly(ethylene naphthalate) (PEN) and polyurethane (PU) [33–37]. The coupling of the active material with the substrate is of huge importance to obtain a good mechanical deformation transfer. In these sensors, the transduction of the imposed force/angle deformation to an electrical signal is mainly obtained thanks to capacitive (Figure 3a), piezoresistive (Figure 3b) and piezoelectric (Figure 3c) mechanisms. [22]

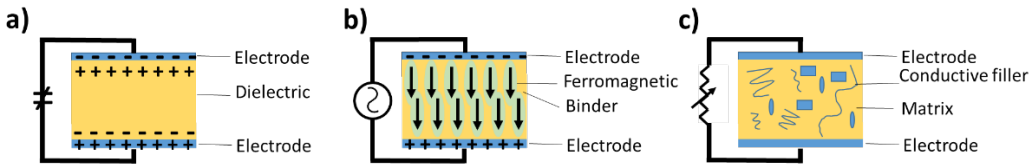


Figure 3: Schematic illustration of electromechanical sensors: (a) capacitive, (b) piezoresistive, (c) piezoelectric

Capacitive Sensors are made of two electrodes and in between a dielectric material. The capacitance (C) value, determined by $C = \frac{\varepsilon_0 \varepsilon_r A}{d}$, changes with the deformation since ε_r, the dielectric relative static permittivity, A, the area between the two electrodes and d, the thickness of the dielectric are parameters directly influenced by the applied external compression or tensile stress. ε_0 is not influenced by the stress since it is the electric constant.

Examples of dielectric presented in literature are Ecoflex [34,38], PDMS [39–41], Dragonskin [42], VHB film [43,44], Polyethylene [45] and Silicone rubber [46]. The electrodes are the fundamentals part of the capacitive sensors and therefore the choice of the material is important. Conventional materials used for capacitors

limits the range of detection because of their lack of flexibility and to deal with this problem some composites were developed: PDMS filled with AgNWs [34], PVA filled with MXenes [44], SBS filled with AgNPs [41]. Other flexible electrodes presented in literature are made of: PDMS painted with a metallic alloy [43], conductive hydrogel [45], screen-printed AgNWs [38], printed ionic conductive ink [42] and coated Au [46].

Capacitive sensors in the context of motion state sensors usually exhibits a linear response to the mechanical deformation. However, the sensitivity is often low and depends on the Young's modulus of the dielectric, and the range of detection depends on the flexibility of the electrodes.

Piezoresistive sensors are the sensors presented the most in literature in the context of motion state sensors. They can be divided in two categories: strain sensors and pressure sensors.

Piezoresistive strain sensors

The mechanical stimuli of strain sensors is transduced to an electrical resistance variation because of the change of length l and cross-sectional area A of the material. Indeed, the electrical resistance is determined by $R = \frac{\rho l}{A}$, with ρ the electrical resistivity of the material. [10,47,48] The sensitivity of the piezoresistive sensors is characterized by the Gauge Factor (GF), defined as $\Delta R/R_0\varepsilon$. ΔR corresponds to the variation of the resistance between the undeformed state (R_0) and the deformed one and ε is referred to the applied strain. Usually, the GF value ranges from 2 to 100 based on the structure and the material of the sensor.

Typical sensitive materials used for piezoresistive strain sensors are composites based on a flexible and stretchable material (PDMS [49–55], PU [56–59], ecoflex [60–62], …) as the matrix and a conductive material (CNT [49,59,63,64], graphene [65], nanowires [54,55,57,66], intrinsically conductive polymers [53,67–69]) as the filler. The employment of composite sensitive materials ensures the formation of

percolation pathway inside them. [70] According to the percolation theory, it is possible to define a correlation between final electrical conductivity of samples and the content of conductive filler. The percolation theory, indeed, defined the percolation threshold which is a certain amount of conductive filler below which the electrical conductivity is strictly correlated with the polymeric matrix and above which the electrical conductivity is due the presence of filler. In particular, above percolation threshold, electrical conductivity exponentially increases with the filler content until a certain value above which the electrical conductivity is maintained constant. [70] The deformation provokes changes in the percolative routes and therefore changes in the composite resistivity. For example, the continuity of the path created by the filler can be disrupted by the mechanical stimuli, or the filler can be disconnected from the matrix. Both cases provoke an increase of the resistance.

One common form for piezoresistive sensors is the fiber arrangement. Indeed, it enables to mount the sensor on skin, like a patch. Two techniques to develop these sensors are presented in literature: the first one consist in coating commercial fibers with conductive inks or ICPs [58,71] and the second one consist in creating directly conductive fibers through the spinning of a conductive solution [56,66,72]. Another type of piezoresistive sensor is the wire form. This form is very useful in applications in which the sensor should be sewn into the textile rather than applied as a patch on the skin. To create these sensors, usually a yarn is coated with the sensitive material. Layer-by-layer is one of the coating technique that can be used [73]. Another interesting coating that was developed is the one that allows the washing of the textile (polybutylene terephthalate [C-PBT] wire coated with first carbon and then PDMS) [51].

Finally, other forms for strain sensors were developed, as a sponge form [60,74] or a film one [50]. In the first case, a carbonized melamine sponge was infused with Ecoflex or PDMS and in the second nanoimprint lithography was used to pattern a metal/polymer composite film (Figure 4).

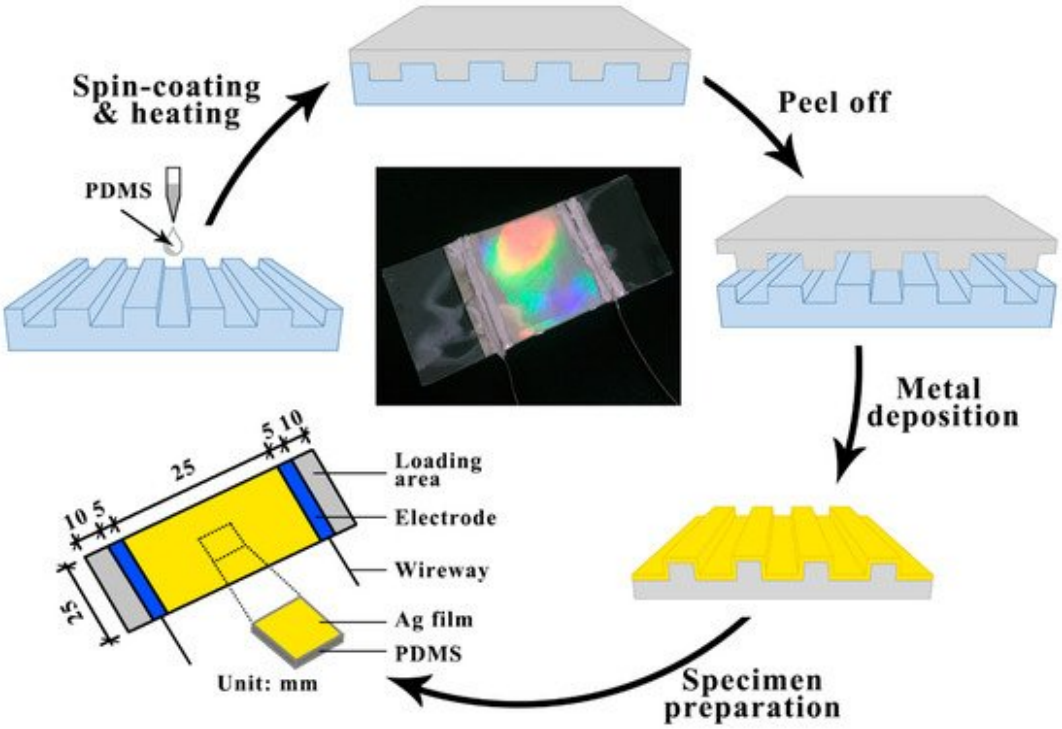


Figure 4: Schematic illustration of the patterned strain sensor process of fabrication. Reproduced with authorization from [50]

Piezoresistive pressure sensors

In the context of health-monitoring, the goal of piezoresistive pressure sensors is the detection of pulses that correspond to medium pressures (from 10 to 100 kPa) or movements/posture that are more in the range of high pressures (>100 kPa). It is therefore necessary to develop pressure sensors able to detect a wide range of pressure rather than sensors specialized in low pressure (1 Pa -10 kPa) detection. Aiming at that, sponges are again a good material form: Wu et al. [52] succeeded in sensing pressure from 91 Pa to 16.4 kPa with a strain from 0.2% to 60%, respectively with a microcrack-designed Carbon Black@PU sponges. Melanine sponges coated with PEDOT:PSS responded at compressive strain up to 80%. [69] Taking advantage of knitting technique, Kim et al. [64] invented a wide range pressure sensor (200 Pa – 50 kPa). They coated a knitted weft with CNT ink so that the fibers contact points increased under pressure leading to a decrease of the electrical resistivity (Figure 5). Another material form that allows a large pressure

range sensitivity is the structure developed by Dan et al. [55]: porous PDMS was coated with AgNW. Changing the pore size, the sensitivity can be adjusted.

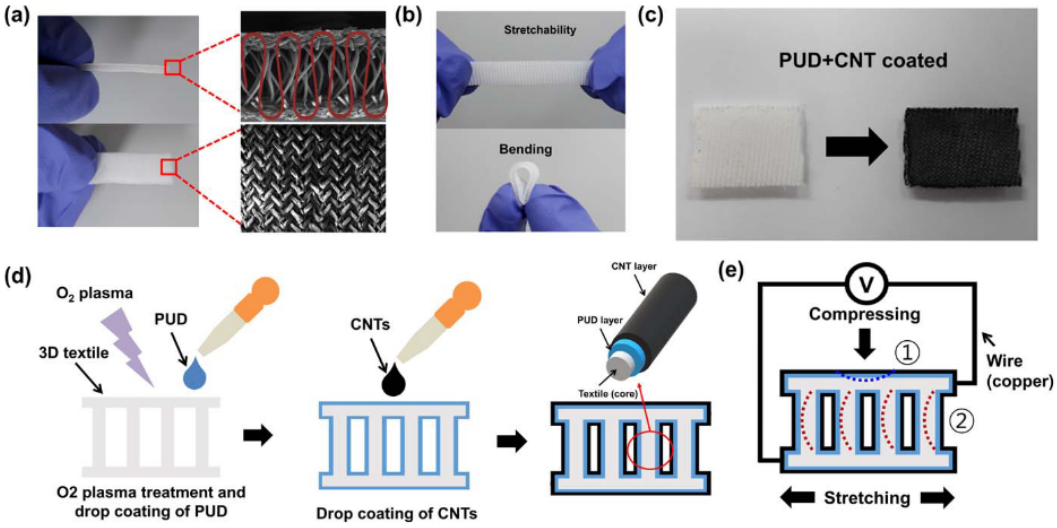


Figure 5: Structure of the piezoresistive pressure sensor and schematic diagram the drop-coating process (a) Photographs and SEM of the textile (view from top: outer layers and side: internal fibers). (b) Photograph of the sensor under stretching and bending. (c) Photographs of the textile before and after CNT/PUD coating. (d) Schematic illustration of the pressure sensor fabrication process. (e) Schematic diagram of the deformation of the sensing unit under compression and stretching. Reproduced with authorization from [64]

Piezoelectric sensors work based on another mechanism than piezoresistive sensors. In the case of piezoelectric sensors, the piezoelectricity phenomenon is exploited: when a tensile, bending or compressive force is applied, dipoles inside the material are reoriented and therefore an electrical charge, predominantly polarized normally to the sensing plane and proportional to the force applied, is generated on the crystal faces of the material. To compensate this polarization, corresponding charges are induced in the electrode faces, generating an electrical current that can be measured.

In order to deal with the need of flexibility in the context of human motion monitoring, piezoelectric polymers such as poly(L-lactic acid) (PLLA), polyvinylidene fluoride (PVDF) and poly(D-lactic acid) (PDLA) are preferred to well-known inorganic piezoelectric materials (zinc oxide (ZnO), lead zirconate titanate

(PZT), aluminum nitride (AlN), barium titanate ($BaTiO_3$), quartz and lithium niobite ($LiNbO_3$)).[8]

The most used polymer in this context is PVDF, particularly its β-phase that is the phase in which the molecular dipole moment is the largest. Liu et al. [75] electrospun nanofibers of PVDF, deposited gold films on each part of the nanofiber membrane to create the electrodes and mounted their sensitive material on a silicon substrate for mechanical stability. In this way, they proposed a piezoelectric motion state sensor able to detect respiratory signals as well as hand movements or vibrations produced by the voice of the human that wears the device. However, the β-phase of the PVDF is hard to process and therefore strategies were developed to increase the piezoelectric response of the material. [76] For example, trifluoro-ethylene (TrFE) was inserted in the chain of a new copolymer: P(VDF-TrFE) [77] and composites were done based on this copolymer and MWCNT [78] or graphene [79], each aiming at developing sensors for human motion monitoring. PVDF was also chosen as the matrix for other composites: PVDF/$BaTiO_3$ nanowire nanocomposite fibers were proposed by Guo et al. [80] and Aziz et al. [81] suggested a single-wall carbon nanotube (SWCNT)-filled PVDF/PEDOT:PSS composite blended with PDMS.

In addition to PVDF, other piezoelectric materials were used to develop motion state sensors. PLLA is another good candidate. Zhu et al. [82] took advantage of the β-crystalline form of the electrospun PLLA nanofibers to create a device able to harvest energy from the knee joint movement. Finally, two nature-inspired materials were presented in literature in the context of piezoelectric sensors for human motion monitoring: the first one is silk. Indeed, it has a natural highly oriented crystallinity that leads to a piezoelectric behavior. Lithographic or hard-mask-based techniques were used to pattern the silk. [83] The other one is fish skin, a naturally piezoelectric material thanks to its collagen nanofibrils linked by hydrogen bonds. It was used to design a pressure sensor [84].

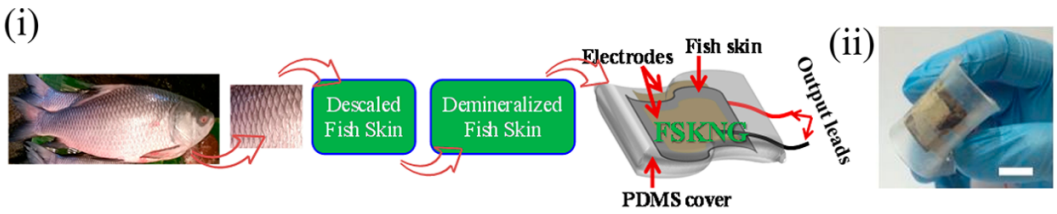


Figure 6: i) Fabrication process illustration of fish-skin-based nanogenerator. (ii) Photograph of the fish-skin-based nanogenerator showing its flexibility (scale bar ~20 mm). Reprinted with permission from [84] **Copyright 2021 American Chemical Society.**

All the sensors described above still need improvement to be part of the daily life of the humans. Indeed, their longevity is still not sufficient and therefore it is difficult to imagine continuous monitoring of the motion. Often, the response of the material is directly linked to its structure and therefore a support to mechanically protect this structure should be integrated in the sensor. The challenge here is to find the good material that can provide support without hindering the flexibility and the efficiency of the device.

Another crucial point is the repeatability of the measurements: work have to be done to find materials that offer lower hysteresis and higher linearity in the response.

In the context of health monitoring, the easiness of use and wearing of the device is also of great importance. The form of the sensors should be adapted to fit in pads or to be knitted in textile, for example.

And finally, a very great improvement is the development of multisensing units in one unique structure, still in order to ease the application of the sensors in the daily life. In this case the challenge is to be able to distinguish the different stimuli and avoid interferences in the signal.

All these challenges need to be overcome in a cheap, biocompatible and environmentally friendly way for the adoption of these sensors in our societies. [85]

I.I.III. Biophysical sensors for wearable devices

Biophysical sensors are focused of the monitoring of the heartrate and the temperature of the wearer. [18]

Heart rate sensors are of crucial importance since cardiovascular diseases are still one of the main cause of death for the human beings. Usually, the electrical activity of the heart is measured by electrocardiogram (ECG) in specialized structures. This modality, however, does not allow a *continuous monitoring* of the beats and pulses produced by the heart that can help to diagnose and cure the heart diseases before they reach an advanced status. [18] The beats and pulses can be, again, measured through pressure and strain sensors and as demonstrated before, a lot of research is done nowadays to render these sensors wearables and of easy use for health monitoring.

Pang et al. [86] developed a strain-gauge flexible and wearable sensor based on two PUA nanohair arrays supported by a PDMS layer, as shown on Figure 7. Their sensor showed a very good response to the heartbeat (Figure 8).

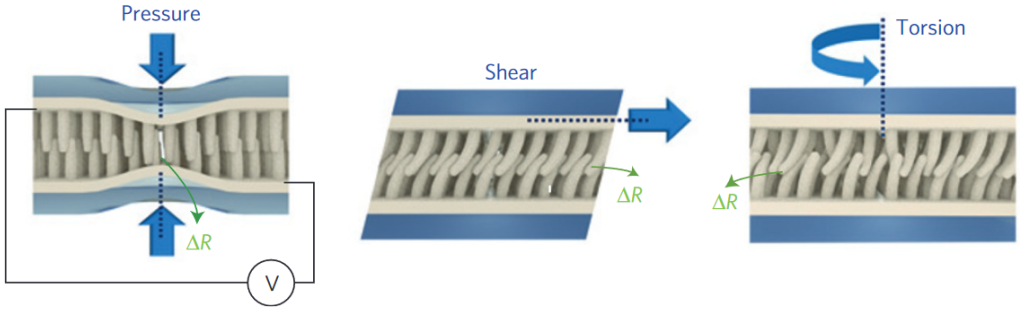


Figure 7: Schematic illustrations of the paired hairs geometric distortion associated to pressure, shear and torsion forces. Reproduced with permission from [86]**.**

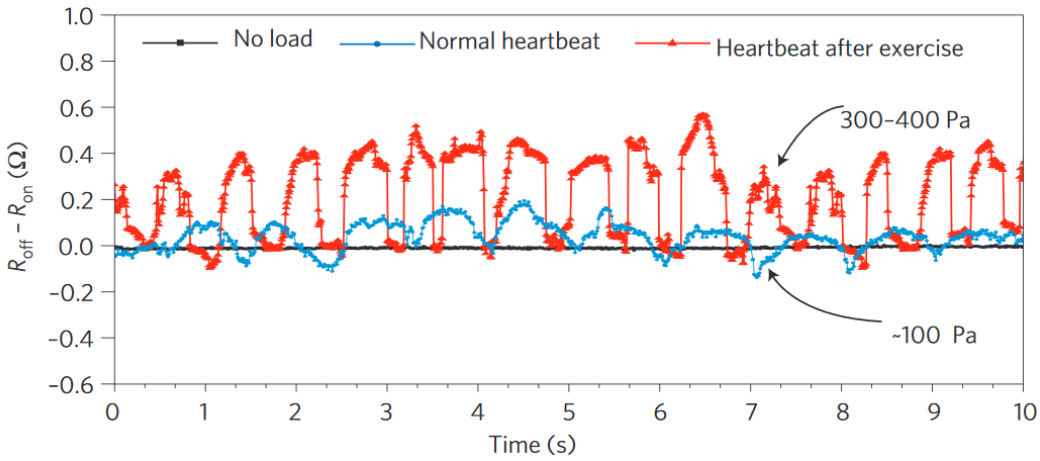


Figure 8: Response of the sensor to the heartbeat physical force under normal (60 beats/min, +/- 100 Pa) and exercise conditions (100 beats/min, +/- 300-400 Pa). Reproduced with permission from [86]**.**

Boutry et al. [87] developed a biodegradable pressure sensor array for cardiovascular monitoring. They used a microstructured (squared pyramids) array of poly(glycerol sebacate) as the sensing element and sandwiched it between two polyhydroxybutyrate/polyhydroxyvalerate films metalized with Fe-Mg. The biodegradability of the sensor was the key point to imagine that the sensor could be used in vivo. Tests were done attaching it to the femoral artery and the results of the recording of the pulse wave were promising.

In a similar way, Bae et al. [88] developed of a hierarchical structural graphene/PDMS array to make a pressure-sensitive electronic skin. Their sensor showed a high sensitivity for low pressures. The electrode material was composed of a graphene monolayer as electrode material.

Here again, the insertion in textiles to create smart clothes to facilitate the use of the heart rate sensors is largely studied and a lot of companies are already selling devices that monitor the heart rate. [89] Next steps are the integration of these sensors in multisensing platforms.

Temperature sensors are also important. Indeed, temperature is the easiest infection symptom to detect. Moreover, temperature gives information about the physical activity, the circadian cycle and the women periodic one. [18] For all these reasons, the development of wearable temperature sensors finds its place in the

context of health monitoring. Hong et al. [90] presented a temperature sensor made of stretchable polyaniline nanofibers with a thin-film of single-walled carbon nanotube as the active matrix. The nanofibers allowed a good mechanical stability, important for the good performances of a sensor that should be worn. They were able to create a sensing array in order to map the temperature of a body zone. Wu et al. [9] proposed the chemical modification of PLA to a three-arm stereocomplex PLA (tascPLA) to create a thermally stable organic transistor. The polymer also exhibited good biocompatibility and flexibility. They described their sensor as usable in post-surgery monitoring.

Multisensing devices with a temperature sensor were also studied. Honda et al. [91] integrated a temperature sensor in a “smart bandage”, i.e. fully printed wearable human-interactive device that also includes a drug-delivery system and a wireless coil for touch sensing. The whole system is flexible thanks to the polymer substrate (Figure 9).

Wang et al. [92] fabricated an E-skin sensitive to temperature and pressure. The active material was a transparent and flexible carbon fiber membrane obtained from silk nanofibers. They showed that is it possible to detect pressure and temperature at the same time because each sensor is passive to other stimuli thanks to the design they gave to their device. Moreover, its fabrication process is green and large-scalable, other advantages for health monitoring devices.

The great challenge for the biophysical sensors is their consistent contact with the human body. Indeed, the sensor should resist and be passive to the varying conditions of daily life (sweat, movements, breathing). More work should be done in that direction. [15]

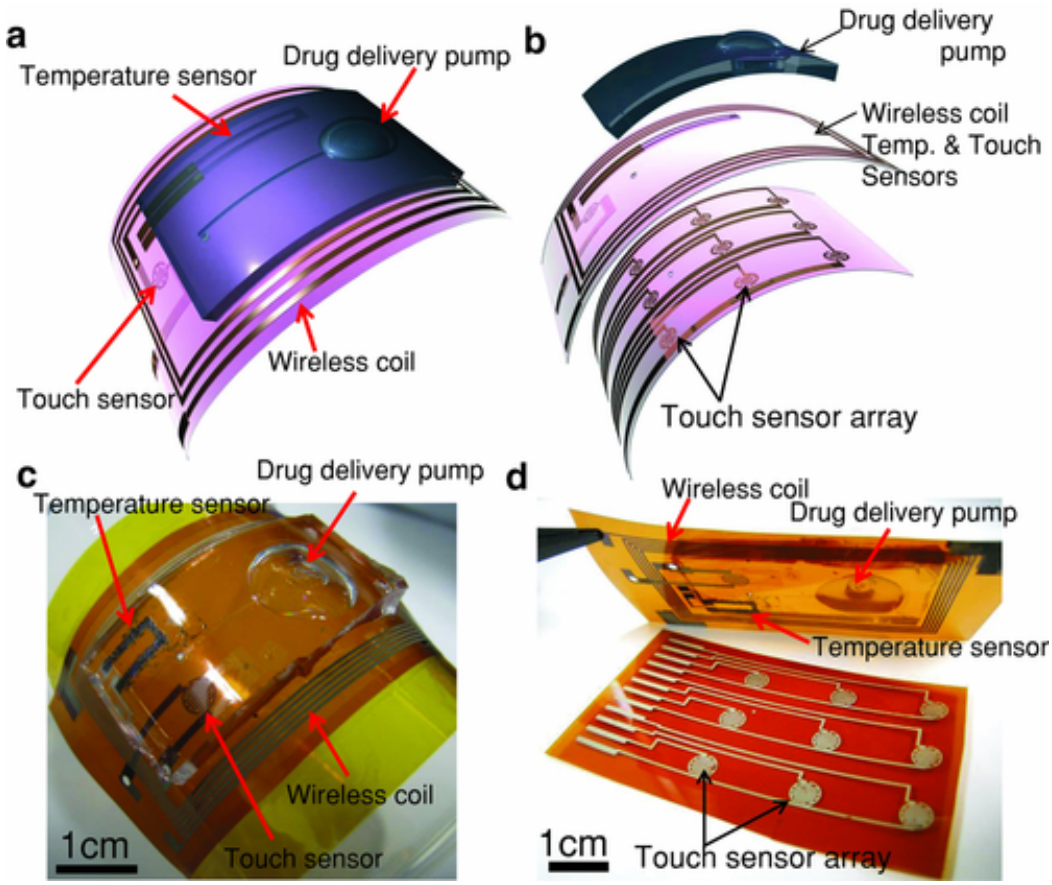


Figure 9: Smart bandage schematics (a) with and (b) without a capacitive touch panel. Photos of the smart bandage with temperature and touch sensors (c) with and (d) without a capacitive touch panel. Reprinted with permission from [91] **Copyright 2021 John Wiley And Sons.**

I.I.IV. Biochemical sensors for wearable devices and point of care

In general, biochemical sensors are devices capable to directly convert a chemical or biological species into an electrical signal. Basic components of these sensors are analyte, chemically sensitive material and transducer [93]. In the context of health monitoring, wearable biochemical sensors receive a great interest, since

their goal is the sensing of biomarkers in saliva, sweat, blood, tears, and urine. These sensors can also precisely measure respiratory gases. Indeed, they are mostly used in lab-on-a-chip technologies and therefore deal with trace samples of body fluids, which are very complex. For this reason, a lot of efforts were done in the past years. [94–97]

During last years, many works in the literature focused their attention on the development of electrochemical sensors as biochemical sensors, applied in the field of health monitoring. Indeed, electrochemistry offers a quick detection without the need of complex reading systems, an easy quantification and a high sensitivity. All these advantages can overcome the main limits offered by all other biochemical sensors employed for health monitoring applications. [20] For these reasons, in the present work, we will concentrate on electrochemical biochemical sensors.

Organic compounds sensing is useful in order to monitor the metabolism of the human body. [20] Examples of these organic compounds are glucose, dopamine (DA), ascorbic acid (AA), uric acid (UA), vitamins, lactate and alcohol. Detection and monitoring of glucose have become important since it is considered as a marker of diabetes that is one of the most widespread diseases in the world. It is also a biomarker of pancreatitis, hyperglycemia and other diseases. [89,98,99] One should be able to detect glucose in human body samples (blood), but also in the food and pharmaceutical industries. [100,101] DA, AA and UA concentration variations are related to disorders like schizophrenia, Parkinson's disease, HIV infection and addiction. [101,102] It is therefore useful to detect its concentration in human liquid samples. Because of its low concentration, dopamine is difficult to detect. Moreover, it is usually in presence of uric acid and ascorbic acid that have similar oxidation potentials, creating interferences in its detection. [101] Finally, one of the most important tissue oxygenation biomarkers is lactate. It is therefore of great importance to develop lactate wearable sensors for monitoring physical performance in sports, military or health care applications. [103]

Organic compounds sensors can be divided in two categories based on the recognition elements: enzymatic and non-enzymatic sensors.

The first ones take advantage of the enzyme high catalytic efficiency and the enzyme high specificity to produce the redox reaction when the analyte is recognized. For example, in glucose detection, glucose oxidase (GOD) is very often found in the sensors described in literature. [104–107] The current change measured comes from the oxidation of the glucose that is catalyzed by the enzyme. In 2001, Cygnus Inc. presented a watch with a glucose sensor integrated based on a Pt/C composite ink decorated with GOD. [108,109] It was the first commercial wearable glucose sensor and it opened the path to the development of health monitoring biochemical sensors. Wang et al. [110–113] used carbon graphite ink and Prussian blue together with GOD to create their glucose sensor. Carbon graphite ink, indeed, offers a good matrix for the immobilization of the enzymes thanks to its porous structure obtained after annealing. Other materials used with the same objective are: graphene [114–117], carbon nanotubes [118,119] and conductive polymers [120–123]. The detection of UA, lactate and alcohol are also often performed in an enzymatic way. [96,111,124]

However, enzymatic sensors have poor long-term stability due to the degradation of the enzymes under environmental conditions (temperature, pH, ionic strength). For this reason, non-enzymatic sensors were developed. These sensors use materials that can directly catalyze the analyte (for example glucose), as gold, palladium, platinum and metallic oxides (nickel, copper oxides), often processed in nanostructure form to increase their sensitivity. [125–128] Electrochemically active analytes, as dopamine and vitamins, are even easier to detect: carbon ink [111], CNTs [129] and conductive polymers [130] can be directly used as electrodes, offering a lower cost and a higher flexibility than metal electrode based sensors.

Ion detection is necessary to monitor human health since ions such as hydrogen ions and inorganic salts (K^+, Na^+, NH_4, Ca^{2+}, Cl^-) play a role in maintaining the pH

balance of the body and controlling water content, regulating cell membrane permeability, maintaining normal osmotic pressure, transporting elements, participating in muscle contraction and nerve activity. [131–140]

The inorganic salts ion sensors can be divided in two classes, depending on the detection mechanism. The first one is based on the combination of an ion selective and an electrode, creating an ion selective electrode (ISE). [141] ISE has a good selectivity and a short response time. The important point to select the membrane material is its interaction with the measured ions to produce electrochemical signals. To increase the sensitivity of the sensors, porous materials are usually used. For example, Roy et al. [142] developed a CNT-based wearable sensor for Na^+. They showed how the CNT increased the sensitivity of their sensor compared to Au or Pt film electrodes. Similar works were presented using conductive polymers [136], carbon ink [133] or graphene [143]. The other class of inorganic salts ion sensors is based on the flied effect transistor principle (FET). FET channels are fabricated with semiconductor materials, whose resistance changes when the ions enter in its contact. The output signal of the FET is therefore correlated to the ion concentration. [20] Examples of semiconductors used for this purpose are silicium combined with a sensible composite [143] and molybdenum disulphide (MoS_2) [143].

pH sensors are nothing else than H^+ ion sensors. The range of materials that react with H^+ is huge (metals and their oxides, carbon materials and biological enzymes) and therefore there is a lot of researches in this field. [89] Metal ink mixed with carbon one are often presented in literature [11]. It gives a good mechanical resistance and a long-term stability. Other sensors with a higher sensitivity are based on metals (silver, gold, palladium, etc.) and metals oxides (indium oxide, lead oxide, etc.). These sensors works based on a bio-FETs principle. [137,144,145] To increase furthermore the sensitivity of the sensors, nanostructures can be used. For example, Nakata et al. [138] used copper oxide nanorods, Hwang et al. [146] take advantage of a biodegradable elastomer decorated with single crystalline nanomembranes of silicon and nanoribbons and Smith et al. [147]

coated cotton yarns with different dispersions containing polystyrene sulfonate and CNT.

pH and inorganic salts detectors are yet at an advanced state of performances and easiness of wearing and use. The next step for these sensors is their integration in multisensing platforms.

Harmful agent detection sensors are more and more studied in the context of health monitoring. They are indeed the sensors that can detect biomarkers directly linked with a health issue. In the body fluid of people antigens can be found if they are injured [148,149], biomarkers of cancer if there is a growing tumor [148] and finally harmful chemicals such as toxic sulphides [150], phosphates [151–154], cocaine and nerve gas [155,156] when they were exposed in their environment.

In this case, the sensing electrodes are usually decorated with a probe (antibody, miRNA, DNA segment) able to react with the analyte. Nanostructures are often used as the support of immobilization the probe in order to increase the surface – volume ratio and therefore the sensitivity of the sensor. The strategy is similar to the one of the enzymatic sensor for organic compounds sensing. [148]

For example, Kim et al. [148] developed an electrochemical sensor for tumor necrosis factor alpha (TNF-α) (Figure 10). They decorated the WE of a 3D micro-patterned elastomeric substrate with the antibody of TNF-α. When the analyte was immobilized on the Ab, an electrochemical reaction produced electrons that could be measured. In that way, higher the analyte concentration in the solution at which the sensor is exposed, higher the current measured through Differential Pulse Voltammetry (DPV).

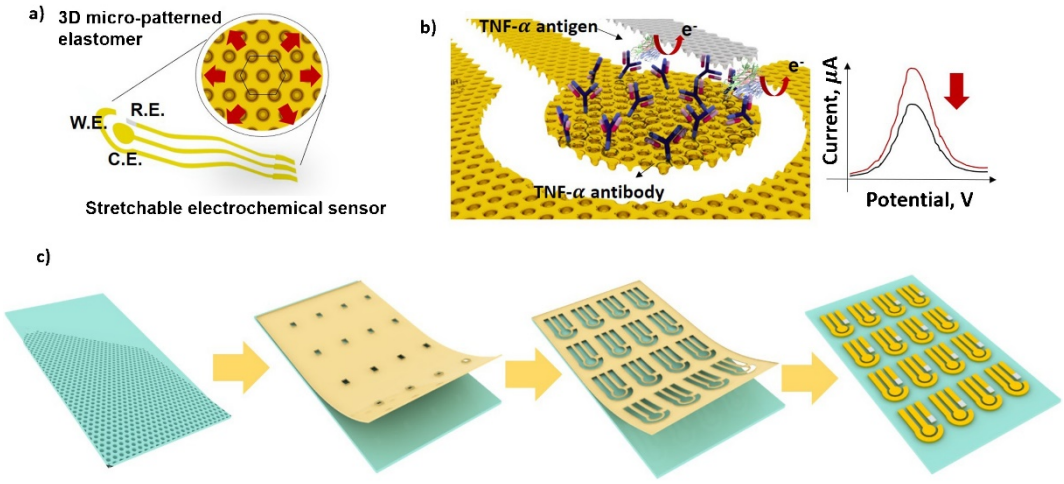


Figure 10: a) Scheme of the stretchable electrochemical sensor fabricated on 3D micro-patterned elastomeric substrate. b) Antibody immobilized on the WE and electrochemical response after reaction of antigens with the antibody. c) Process flow of the device fabrication. Reproduced with permission from [132].

For harmful agent detection sensors, the typically used materials for the fabrication of the electrodes are gold, conductive polymer and carbon materials. The choice of the material is done based on the chemical groups present on the surface to allow the immobilization of the probe.

Thanks to the development of news materials, the sensitivity, stability, and selectivity of the biochemical sensors has been hugely improved. However, numerous challenges are still to be overcome in order to truly implement them in a context of daily life health monitoring. As body fluids are rich of molecules, one of the greatest drawback of the biochemical sensors are their specificity. It is indeed difficult to avoid the electrode fouling due to the adsorption of interfering substances. In the case of ions sensors, the problem can be avoided with a Nafion membrane [110,114] or ion sensitive membranes [133,143,157], but in the case of organic compounds and harmful agent sensors, it is more difficult. Some porous materials were presented [127], but more work should be done, especially for the detection of large molecular weight molecules. Obviously, the integration of biochemical sensors in multisensing platforms is also an objective for the future

research work, as well as the pursuit of materials that confer good performances together with time-stability and flexibility. [141]

II. Aim of the proposed research

In this context and to pursue the research needed in the engineering field with the aim to respond to the objectives of the third Sustainable Goal of the United Nations, the research about the design and fabrication of a wearable multisensing device for rehabilitation and a point of care for cancer biomarker is presented.

To respond to the needs of a very high sensitivity, flexibility and biocompatibility for the sensor, electrospun nanofibers (NFs) are proposed as the sensing element of the sensors of each device. Indeed, the intrinsic properties of NFs make them the perfect candidate for such class of applications.

Nanofibers have a high surface area-to-volume ratio and a high porosity making them very attractive for sensing applications since a lot of sensing (mostly biochemical) is done through the surface.

Moreover, one of the great advantages of the electrospinning process, performed to collect final dried nanofiber mats, is represented by the possibility to obtain a wide range of materials starting from a polymeric solution. Although the greater part of the produced nanofibers are polymeric, ceramic and metal nanofibers can also be obtained through further post-treatments. A green process for the fabrication of the sensor can be ensured thanks to this huge variety of starting solutions suitable for electrospinning.

Furthermore, the nanofiber mat obtained through electrospinning can be functionalized easily by the blending of the polymeric material with a functional one prior to spinning, by the functionalization of the surface after the spinning or by the fabrication of specific nanostructures.

The electrospinning process ensures indeed to obtain a high quantity of nanostructures: classic NFs, beaded NFs, core-shell NFs, hollow NFs … The nanofibers can be deposited in a random mode, or in an ordinated one. They can be collected on a flat collector of a cylindrical one.

Finally, electrospinning is easily scaled up to an industrial fabrication process. Indeed, low cost, high quantities and green process flow are essential if we want

to imagine these devices in a daily application for a huge number of people as precision medicine aims at. [158–161]

I therefore propose in this work to take advantage of all these characteristics of the nanofibers to develop sensors for health monitoring.

III. Outline of the thesis

First, a State-of-the-Art about the electrospun nanofibers in the context of sensing for wearable devices and point of care is given to help to understand where the challenges in this context are and what is already well established and known.

A second chapter is dedicated to the materials and methods used for this work. An emphasis is given on electrospinning and electrochemistry since many time was dedicated to these two techniques in the frame of this thesis.

The third and fourth chapters concern the wearable device and the points of care studied in this work. The optimizations of the material and the detection methods are given, as well as the obtained results. Future prospective are also described in each chapter.

Chapter 1: Electrospun nanofiber for the sensors of wearable and point of care devices: State of the Art

Fibers are defined by its length that is much longer than the diameter of its cross section. Nanofibers (NFs) are characterized by a diameter smaller than 100 nanometers. On Figure 11, a FESEM image of a hair and a pollen particle on a nanofiber background is reported to give the idea of the dimension of the NFs. The nanofibers are characterized by their huge surface area-to-volume ratio, their high porosity, their flexibility and their mechanical strength. [162]

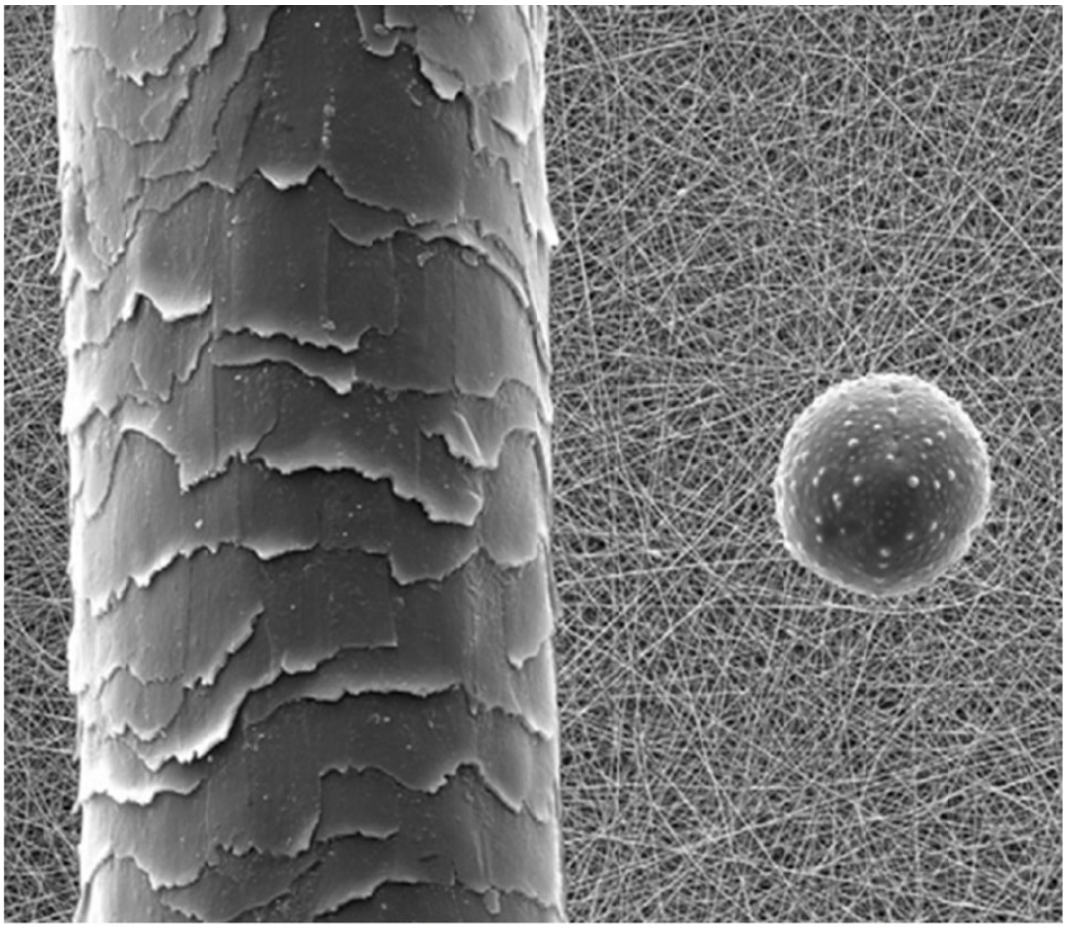


Figure 11: FESEM image of a hair and a pollen particle on a nanofiber background. [329]

Different methods are used to produce the NFs, such as drawing, self-assembly, template synthesis, electrospinning and thermal induced phase separation, but electrospinning is the most used one for its straightforwardity, its possibility to adapt it to mass production and the control of the parameters. [163]

Electrospun nanofibers can be divided in four classes of materials leading to different applications. As explained in detail in the following sections, carbon nanofibers have the advantage of simplicity and good biocompatibility. Metal-oxide nanofibers are more difficult to electrospun but have a good surface for biological receptor immobilization. Conductive polymer nanofibers are also more difficult to produce but offer a highly flexible mat, suitable for further manipulation. Finally, non- conductive polymer-based nanofibers have the same advantage of the conductive one but is also often more expensive.

1.1. Carbon nanofibers

Carbon nanofibers are interesting nanomaterials for the sensing because of their low cost, their facile electron transfer kinetics and their biocompatibility. The electrospinning solution contains polymers with high carbon yields like polyacrylonitrile (PAN), polyvinyl alcohol (PVA), polyvinylpyrrolidone (PVP), polyimide (PI), polybenzimidazole (PBI) and polyacrylic acid (PAA). [164]

Three steps are needed to form the carbon fibers: first, the polymer is electrospun. Then, the fibers are stabilized by a cross-linking step: the samples are exposed to a relatively low temperature (200 – 300°C) in an oxidative environment. The thermoplastic fibers are thus turned in condensed thermosetting fibers. Finally, the fibers are carbonized at high temperatures (800 – 1300°C) to give carbon fibers. To remove heteroatoms, the carbonization is done in an inert gas atmosphere at high temperature. [165,166]

Mao et al. [167] studied the influence of the carbonization conditions on the electrochemical properties of the carbon nanofibers. As the graphite is made of sp^2 carbon, one can estimate the graphite concentration in a material thanks to the sp^2/sp^3 ratio. The group showed that with a higher carbonization temperature induces an increasing of the sp^2/sp^3 ratio. They also showed that the graphite domains were larger. The group further studied the influence of the carbonization condition on the density of states (DOS). To estimate the DOS, they measured the conductivity of the fibers. They obtained a positive correlation between the sp^2/sp^3 ratio and the conductivity, leading to the conclusion that more graphitized are the fibers, higher the electron transfer is.

1.1.1. Carbon NFs for human motion sensors

Carbon nanofibers are difficult to use for human motion sensors even if they have a piezoresistive behavior because of their lack of flexibility due to their brittleness. [168] For that reason, only a few pressure sensors based on carbon nanofibers are

presented in the literature. Cai et al. [169] presented a highly sensitive and flexible pressure sensor based on ferrosoferric oxide (Fe_3O_4)/carbon nanofibers. The presence of Fe_3O_4 in their NFs helped to give better mechanical resistance. Their sensor worked in a wide range (0–4.9 kPa) and with a high sensitivity of 0.545 kPa^{-1}. Sengupta et al. [170] succeeded in the development of an ultralightweight and flexible strain sensor based on pyrolyzed at 950°C PAN NFs. They give mechanical stability to the NFs by embedding a bundle of them in PDMS/optically clear adhesive. The sensor was very as sensitive as able to detect wind flow velocity in the range 5–35 m/s. This sensor could be adapted to a breath sensor. Finally, Ding et al. [171] reported a highly sensitive and stretchable strain sensor based on free-standing carbon nanofibers embedded in two polyurethane (PU) elastomer substrates. The precursor of the CNFs was PAN. The sensor showed high stretchability (up to 300%), high sensitivity (GF =72) and good durability and stability under the 8000 cycles of stretch/release test. The sensor was used to monitoring the bending of the finger, wrist and elbow.

1.1.2. Carbon NFs for biochemical sensors

For the biochemical sensors, however, carbon nanofibers are very good candidates. By the doping of the fibers with heteroatoms, the electrochemical properties of carbon fiber can be modulated. For example, Liu et al. [172] integrated nitrogen atoms in the carbon nanofibers by their stabilization in a mixture of NH_3 and air at 300°C for one hour. The electron-donor ability of the carbon atoms was increased by the insertion of the nitrogen atoms, and therefore the electrocatalytic activity of the fibers toward oxygen reduction was improved. The fibers obtained were also highly flexible, which was beneficial for their further manipulation. Moreover, the electron transfer rate was higher than the one of non-doped carbon nanofibers.

In order to widen the range of analytes that can be detected by the electrochemical sensor, metal nanoparticles were incorporated in the fibers. Their role was to react with analytes that do not respond to carbon fibers. In general, metal salts were added in the polymer solution that was then electrospun. During

the thermal treatment, they were converted into metal nanoparticles. [164] Examples and their solution precursors are listed in the table 1. It can be seen from this table that the metal nanoparticles allow detecting various types of analytes. Some of these examples used enzymes immobilized on the fibers as a bioreceptor [173–175] but others detected the analyte directly thanks to the metal nanoparticles doped fibers. [176–180]

Table 1: Examples of metal nanoparticles integrated in electrospun carbon nanofibers, with their electrospinning solution.

Metal nanoparticle	**Electrospinning solution**	**Analyte**	**Ref.**
Copper	$Cu(Ac)_2 \cdot H_2O$/PAN/PVP	catechol	[174]
Carbon nanospheres	polypyrrole nanospheres/PAN	glucose	[181]
Nickel	$C_4H_6NiO_4 \cdot 4H_2O$/PAN $Ni(AC)_2/Zn(Ac)_2$/PAN	Catechol purine bases	[173] [178]
Palladium	$Pd(AC)_2$/PAN	H_2O_2 and NADH	[182]
Rhodium	$Rh_2(AcO)_4$/PAN	hydrazine	[180]
Manganese dioxide	$Mn(Acac)_2$/PAN	H_2O_2	[176]
Platinum	H_2PtCl_6/PAN	H_2O_2	[177]

Another way to allow the fibers to respond to analytes that do not react with carbon fibers, is the loading of nanostructures on their surface. These modifications occur after the steps of cross-linking and of carbonization. Wang et al. [100] modified their carbon fibers by growing Prussian blue on their surface. Prussian blue is a metal hexacyanoferrate often called “artificial peroxidase”, as it can catalyze the hydrogen peroxide at low potentials. Their sensor showed good electrochemical detection. Huang et al. [101] decorated their porous carbon nanofiber with Ag-Pt bimetallic nanoparticles. Pt shows a high catalytic activity but is expensive and has a low utilization efficiency. To counteract that, the authors proposed the use of bimetallic nanoparticles. They first immobilized Ag nanoparticles on the surface by an in-situ reduction of Ag^+ by $NaBH_4$, and finally they deposited Pt by a seed-growth reduction. Dendritic Pd structures (Figure 12)

were grown by electrodeposition on the surface of carbon nanofibers by Lin et al. [183] to increase the electrocatalytic activity reduction/oxidation of H_2O_2 and oxidation of β-NADH.

A last example is the work of Liu et al. [104]. They decorated electrospun carbon nanofibers with $NiCo_2O_4$ nanoneedles. $NiCo_2O_4$ is a good catalyzer for the glucose oxidoreduction. Nanoneedles of this compound were grown on the carbon nanofibers by a surfact-assisted hydrothermal process.

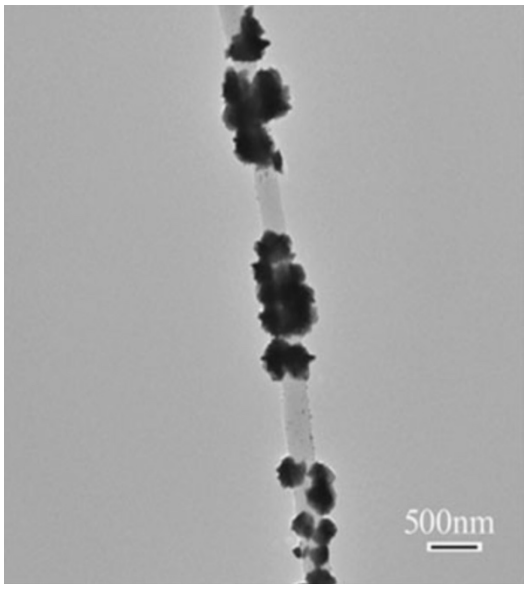


Figure 12: TEM image of Pd/ CNFs with 1h deposition time. Deposition potential, -0.2 V. Reproduced with permission from [183]**.**

The morphology of the electrospun carbon nanofibers can also be adapted. Porous fibers are interesting because the surface area is even larger. Lu et al. [178] electrospun nickel and zinc acetates with PAN. The fibers were dried at 80°C for 8h, leading to the gasification of the zinc. Therefore, nickel-loaded porous carbon nanofibers were obtained. Bae et al. [184] electrospun PAN with silica nanoparticles that they then removed thanks to hydrofluoric acid (HF) treatment. This created the pores in the carbon fibers. Finally, Huang et al. [101] obtained porous nanofibers by electrospinning a solution of PAN and PVP, followed by PVP extraction at 110°C.

The lack of flexibility is often overcome by the milling of the NFs and the fabrication of a paste by using a binder. As reported in the literature [164], polyelectrolyte binders or ionic liquid dissolved in solvent play a crucial role to consolidate the nanofiber adherence on the electrode, enhancing also the charge transfer. To ground the fibers and suspend them, violent stirring [179,184], sonication [106,107,174,176,177], boiling followed by centrifugation [100] and use of a mortar [173] were applied. The fibers were suspended in solvents alone [106,107,177,179,185], but also in more complex solutions. Nafion was generally added in the suspension as a binder, thanks to all its features, such as proton conducting, good mechanical and thermal stability and biocompatibility. [104,174,176,180] The mixture of NFs and the binder was then deposited onto the electrode surface by drop casting [101,104,187–189,106,172,173,176,177,179,184,186]. Another example of binder is represented by chitosan, which was investigated by Li et al. as a glue [190]. Electrodeposition was also used as a deposition method [178,185] as well as a post-coating of Nafion [106,191].

In conclusion, carbon nanofibers alone offer high conductivity as well as good mechanical and chemical resistance. They can be modified to improve their electrochemical properties or their sensibility to some elements by the addition of heteroatoms, nanoparticles or nanostructures, inside the fibers or on its surface. However, room for further research about carbon nanofibers for sensing is still present. Indeed, the influence of the parameters of electrospinning and thermal treatment on the electrochemical activity of the fibers is not yet well understood. Moreover, synergistic effects between carbon nanofibers and added elements were not studied enough. Knowing the existence of these effects and understand them can lead to even more efficient nanofibers structures for Health monitoring sensors. [164]

1.2. Metal Oxide nanofibers

Metal oxide nanofibers are produced by the electrospinning of a starting polymeric blend solution, obtained by dissolving a polymer, a metal oxide precursor and solvent. Basically, the polymer is used as a template to employ final nanofiber mats. Indeed, after electrospinning process, a calcination treatment is carried out to ensure the decomposition of polymer and, simultaneously, the nucleation and growth of metal oxide crystals (annealing). Polycrystalline metal-oxide nanofibers are formed. With the removing of the polymer component from the fibers, their diameter is reduced, and nanopores are created in the structure. The coexistence of these nanopores, together with the larger pores inside the nanofibers mat leads to improved mass transfer capacities as well as better electronic properties than other nanostructures of the same materials. Finally, the metal-oxide electrospun nanofibers are produced at a low cost. [165,192]

1.2.1. Metal Oxide NFs for biochemical sensors

Metal oxide NFs are mostly used for biochemical sensing. Indeed, the grafting of enzymes on the metal-oxide nanofibers is easy, and generally, the electrocatalytic activity of the enzyme is easily preserved. However, these fibers are brittle and do not have capacitive, piezoelectric of piezoresistive behavior that could be used for human motion sensors.

The most used metal-oxide for this application is the zinc oxide [102,105,185,186,193,194]. Indeed, ZnO shows a continuous electron transfer through the fiber, because of its semiconducting nature. Moreover, it is biocompatible, and the enzyme immobilization occurs through electrostatic interactions, what does not hamper the catalytic activity of the enzymes. [195] Other metal-oxides that were used as electrospun nanofibers sensor element are: Cobalt(II,III) oxide (Co_3O_4) [106], Copper(II) oxide (CuO) [105], Manganese(III) oxide (Mn_2O_3) [188], Titanium dioxide (TiO_2) [189,196], Iridium oxide (IrO_x, $0 \leq x \leq 2$) [190] and Nickel(II) oxide (NiO) [107]. The polymer more used for the template

is polyvinylpyrrolidone (PVP) [105–107,189,190,193]. Polyacrylonitrile (PAN) was also used [185,187,188,194], as well as polyvinyl alcohol (PVA) [102].

In order to better functionalize the metal oxide nanofibers, some improvements were proposed. For example, Paul et al. [186] doped their ZnO fibers to decrease their high resistivity. ZnO has a high band gap and adding Cu in the structure of the material induces an acceptor band which thus reduces this large band gap. Another result of this research is that the electric field generated at the CuO/ZnO heterojunction interface preconcentrates the target analyte onto the nanofiber surface, leading to an increased detection. Zhou et al. [105] studied electrodes modified by CuO nanofibers, ZnO nanofibers, a mixture of ZnO and CuO nanofibers and finally nanofibers obtained by the coelectrospinning of the two components. For the coelectrospinning, $Cu(Ac)_2$/PVP was the solution flowing from the inner spinneret (see 2.1.1), while $Zn(Ac)_2$/PVP was the one used for the shell of the fibers. After the annealing process, it was observed that the trunk of the nanofiber was composed of a uniform mixture of CuO and ZnO and that CuO nanoparticles were dispersed on their surface. The coelectrospun nanofibers showed better electrochemical properties than ZnO, CuO and ZnO mixed with CuO fibers. The author explained this result by the hetero-junction formation. They also determined that 20 minutes of electrospinning was the optimal time for the electrochemical detection. Multi-walled carbon nanotubes (MWCNTs) were used by Paul et al. [186] to decrease the ZnO nanofibers resistivity. MWCNTs have excellent electrical conductivity and its association with ZnO gave better results for electrochemical detection than ZnO alone. Phosphotungstic acid (PWA) was added in ZnO nanofibers by Wu et al. [102] in order to increase the catalytic properties of the fibers. Indeed, PWA belongs to the class of heteropoly acids (HPAs) that is well-known for their catalytic performance and stability. Finally, Ding et al. [107] doped their NiO fibers with Pt for the detection of the glucose. They made a comparison with NiO fibers and Pt fibers and obtained better results with the presence of nanoparticles in NiO-Pt nanofibers.

By controlling the annealing temperature, Li et al. [190] obtained IrOx wire-in-tubes, as can be seen in Figure 13. This specific morphology was obtained with a calcination temperature of 500°C. At 350°C, full fibers were obtained, at 700°C, the wire and the tube collapsed to give thinner fibers and at 900°C, the fibers were too brittle to be maintained. The authors explained the formation of the wire-in-tube by the migration of Ir ions with the solvent. When the solvent evaporated, during the electrospinning process, the ions were token with it to the surface, as they are more soluble in the solvent than the polymer. This effect was increased with the temperature, leading to a crystallization at the surface of the fiber. When all the polymer was decomposed, the small particles of the surface collapsed toward the center, while the larger remained there. The specific morphology was therefore obtained. The wire-in-tube showed improved electronic transmission rate and electrochemical signal. The sensor was also more stable.

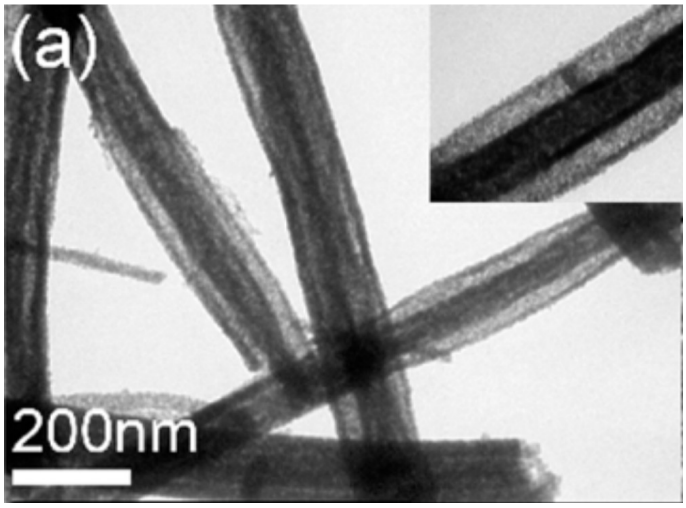


Figure 13: TEM images of IrOx nanofibers. Reprinted with permission from [198]. Copyright 2021 American Chemical Society.

Metal-oxide nanofibers show large surface to volume ratio, high electrical conductivity when doped with metallic particles [197] and easy enzyme immobilization. Non-enzymatic sensors were also developed. They were stable and did not lose their sensitivity due to protein denaturation. [198] However, the electrospinning of a mixture of polymer and metal oxide precursor is more difficult than the one of a polymer: after the ejection of the jet from the spinneret, condensation, hydrolysis and gelation of this precursor can occur. These reactions

can prevent a good electrospinning process. Therefore, the good control of all the parameters of the electrospinning is crucial. [165]

1.3. Conductive polymer nanofibers

Conductive polymer nanofibers are based on some polymers that are conductive thanks to a polymeric chain made of an alternation of single and double carbon-carbon bonds. These polymers are called intrinsically conductive polymers (ICP).

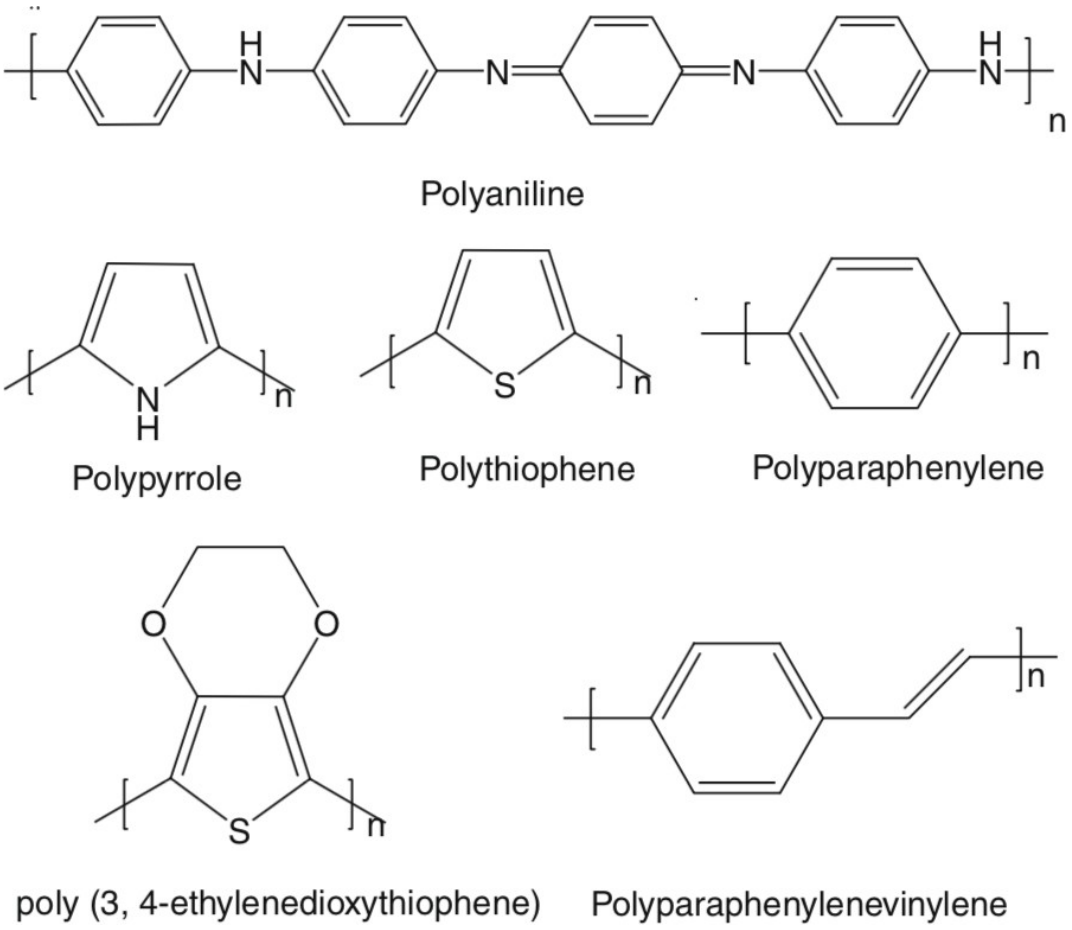


Figure 14: Structures of typical conducting polymers for bio-sensing applications. Reprinted with permission from [206]

Examples are polyacetylene, polypyrrole (PPy), polythiophene (PT), polyaniline (PANi), polyparaphenylene (PPP), poly(3, 4-ethylenedioxythiophene) (PEDOT), polyparaphenylene vinylene (PPV) and polyphenylene sulfide (PPS). The ones that are the most used for sensing application are showed in Figure 14. [199]

These polymers, through their capability of overlapping of the polymer orbitals, can con- duct the current. They can be directly electrospun and used for

electrochemical sensing without further treatment. They offer a mechanical flexibility and therefore are easily manipulated. They are also biocompatible, and the reproducibility of the polymer mat is excellent.

1.3.1. Conductive polymer NFs for biochemical sensors

However, their electrospinning is difficult because they are usually insoluble and infusible. [200] Some strategies were used to promote the electrospinnability of the ICP in the context of biochemical sensors. For example, polystyrene was added to PANi in the electrospinning solution of the nanofibers presented by Anwar et al. [201]. It also helped to immobilize the biological element for their C-reactive protein (CRP) sensor. The same strategy was used by Rodthongkum et al. [202], but they also incorporated graphene nanopowder in the electrospinning solution to increase the detection sensitivity of their electrochemical system for dopamine detection. PEDOT:PSS was used by Kumar et al. [203] and they added PVA to the electrospinning solution to facilitate the electrospinning. Their sensor aimed to the detection of cancer biomarker.

Hou et al. [204] developed a *pH sensor* based on PANi/PU core-shell nanofibers. PU served to increase the mechanical properties and the electrospinnability of PANi while PANi was the sensitive material. The sensor worked in the range of pH 2-7 with a good sensitivity. They tested the sensor on the skin and saw that the device was stable and responded to the pH changes of the sweat.

1.3.2. Conductive polymer NFs for motion state sensors

Only a few motion state sensors based on ICP are presented in literature. Liu et al. [205] electrospun PANi on an interdigitated textile electrode and wrapped the mat into a nonwoven fabric to develop a flexible, sensitive and all fabric pressure sensor. The device showed ultrahigh sensitivity of 46.48 kPa^{-1} over a wide linear range(<4.5 kPa). Nan et al. [206] created a fabric-like sensor made of GO-doped PAN NFs coated with PPy. Their sensor could detect a full range of human motion, pulse monitoring, facial expressions and human respiration. In our group, we

developed a pressure sensor based on PEO/PEDOT:PSS NFs. [207] The sensor is described in 3.3.

Even if solutions to increase the processability of electrospun conductive polymer nanofibers were proposed, this type of nanofibers remains less common than carbon or metal-oxide ones. New innovations are still needed to make use of the potential of the conductive polymers in the context of electrospun nanofibers in health monitoring.

1.4. Non-conductive polymer nanofibers

The last category of nanofibers concerns the nanofibers based on non-conductive polymer. Often, these NFs are composites of a non-conductive polymer and metallic nanoparticles or carbon nanotubes. [165] These elements are directly incorporated in the electrospinning solution, and the fibrous mat does not require other post-treatment. Moreover, the mat is more flexible than the one obtained after calcification or carbonization, what leads to an easier manipulation. However, the electrospinning has to be well controlled to avoid the aggregation of the metal nanoparticles or carbon nanotubes. Their aggregation decreases the electrochemical and catalytic activity. Besides, the conductive materials added in the electrospinning solution are expensive. [208]

1.4.1. Non-conductive polymer NFs for human motion sensors

One very common polymer used for human motion sensing is PVDF. Indeed, electrospun PVDF membranes have huge piezoelectricity. Moreover, no post treatment is required and the membranes can be integrated in piezoelectric devices directly. Table 2 summarizes the sensors that can be found in literature based on PVDF NFs. Some works used PVDF only on the electrospinning solution and reached good sensitivity. However, their sensors suffer the temperature changes. Other groups presented composites based on PVDF and fillers. The fillers can promote better performances. Finally, again to increase the performances, copolymers with PVDF were studied.

Table 2: PVDF Based human motion sensors

Composition of the NFs	Classification of the material	Type of sensing	Ref.
PVDF only	Polymer	Force sensor	[209]
		Pressure sensor	[35]
PVDF/ZnO	Composite	Pressure sensor	[210]
PVDF/MWCNT/OMMT		Force sensor	[211]
PVDF/Ag nanowire		Pressure sensor	[212]
PVDF/PPy		Pressure sensor	[213,214]
P(VDF-TrFE)	Co-polymer	Force sensor	[215]
		Pressure sensor	[216–218]
(rGO)-encapsulated P(VDF-TrFE)	Co-polymer and composite	Pressure sensor	[219]

1.4.2. Non-conductive polymer NFs for biochemical sensors

In the context of biochemical sensing, Zhu et al. [220] presented two different ways to create a nanofibrous PVA-Ag nanoparticle composite. They entrapped the nanoparticles inside the fibers, or they loaded them on the surface. For the entrapment, they made a PVA/$AgNO_3$ chelating complex solution. Then, they reduced the $AgNO_3$ with a green reductant (EGCG=epigallocatechin gallate), and they electrospun this PVA/Ag nanoparticles solution. They finally cross-linked their fibers to gain water stability with glutaraldehyde vapor. On the other hand, to load the Ag nanoparticles on the surface of the nanofibers, they first proceeded by the electrospinning of a PVA/PEI solution. They cross-linked the fibers with the same method than before and performed a thiol chemistry using mercaptopropyl-trimethoxysilane (MPTES) to provide sulfhydryl groups. Then, the functionalized nanofibers were immersed in a AgNO3 solution, and the reduction was performed. The Ag nanoparticles were anchored on the sulfhydryl groups. The second method

has the advantage of using smaller quantities of expensive Ag nanoparticles for the same results and was therefore chosen by the author as the better one. Other examples of composites are listed in Table 3.

Table 3: examples of composites in biochemical sensors

Polymer	**Nanocomponent**	**Ref.**
Nafion/Polyacrylic acid (PAA)	Au nanoparticles	[221]
Polyacrylonitrile (PAN)	Pt nanoparticles	[222]
Polyvinylidene fluoride (PVDF)	Pt nanoparticles + MWCNT	[223]
Polyamide 6 (PA6) Polymethyl methacrylate (PMMA)	MWCNT MWCNT	[224] [225]
Polyvinylpyrrolidone (PVP)/Chitosan	Reduced graphene oxide	[226]

In the context of biochemical sensing, this type of nanofibers is less used because of their higher price and the difficulty to electrospun them. Improvements were proposed, but further research still needs to be conducted.

Chapter 2: Fabrication and measurements methods

2.1. Nanofibers fabrication

2.1.1. Electrospinning technique

Electrospinning is an electrohydrodynamic process based on electrostatic fiber formation. It uses electrical forces to produce polymer fibers with a diameter ranging from 2 nm to several µm. [162,227] The base materials can be either solution of natural or synthetic polymers, or polymer melts. This technique was first described over 70 years ago [228,229], but it gained renewed attention since the beginning of the century due to the rising interest in nanoscale materials. In their review, Thenmozhi et al. [159] summarized the history of the electrospinning development in a clear table.

The basic principle is that the application of a voltage induces strong mutual electrical repulsive forces that overcome the weak surface tension of the polymer solution. There exist two different setups, either vertical or horizontal, but in both cases, the same three components are found. These are the high voltage power supply, the capillary (composed of the container and the spinneret) and a grounded metal collector (Figure 15). [230–232] It is worth to notice that the

driving force of the process is related to the applied electrical field [233] while gravity results to be neglectable.

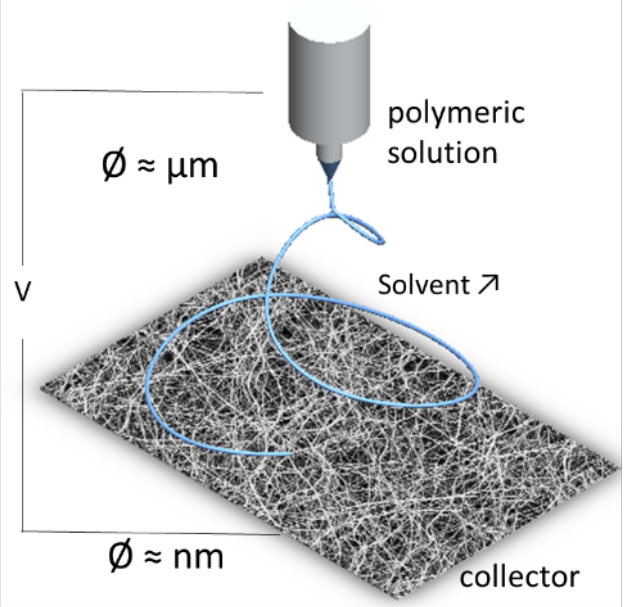


Figure 15: Schematic diagram of the set-up of electrospinning

The process of electrospinning involves three steps: the jet initiation and elongation, the further elongation and the onset of instabilities, and finally the fiber solidification (Figure 16).

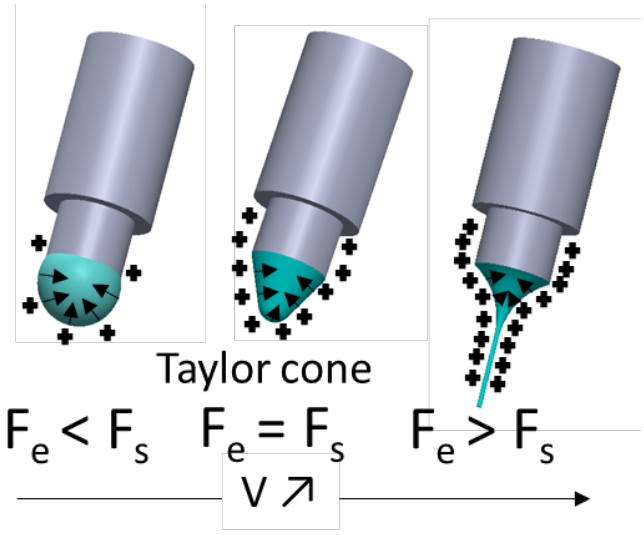


Figure 16: Schematic illustration of the Taylor cone formation. Fe = electrical forces, Fs= surface tension forces

Two kinds of forces are involved in the **jet initiation process**. The applied voltage creates electrical forces, and the solution possesses a given surface tension. The Figure 16 shows how the jet is formed: when a small voltage is applied, the droplet

at the needle tip decreases its size to maintain the equilibrium between the two forces. When the voltage is increased, the rounded droplet slightly evolves to a cone shape, called the Taylor cone. Finally, when a critical voltage is reached, electrical forces overcome the surface tension and the jet is formed from the tip of the droplet. [163,233–235]

The second step is the further **elongation of the jet and the onset of instabilities**. The diameter of the ejected jet is of the order of the micrometer, but it decreases with distance from the tip, due to the evaporation of the solvent and of the instabilities of the jet, allowing the formation of fibers in the range of the nanometer. Because of the length of the jet, charges take more time to travel, leading to local excess charges and the bending of the jet. Since several instabilities are established during the whole process, it is important to notice that the jet does not follow a straight path. [163,233–236]

Finally, a nanofiber mat is deposited on the collector and finishes **to dry**. [230,233,237]

Based on the conventional electrospinning, many variants had been made which greatly expand the applications of this technique. For example, hollow nanofibers and core-shell nanofibers have been prepared by electrospinning starting from two immiscible liquids and using coaxial, two-capillary spinneret. In the case of hollow NFs, the core are selectively removed (Figure 17). [238]

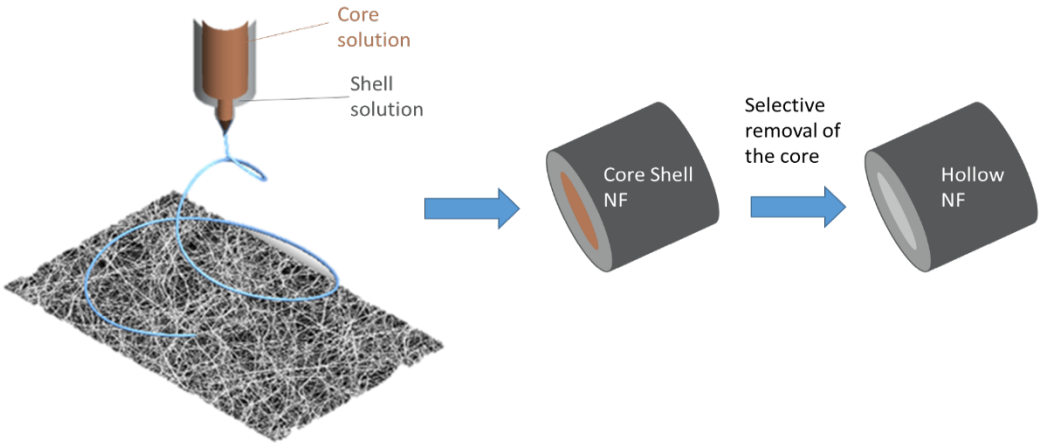


Figure 17: Core-Shell and Hollow NFs fabrication

It is also possible to fabricate multicomponent fibrous membranes by the simultaneous electrospinning of different polymers, using two parallel syringes. [239,240] Successive electrospinning of different components one of top of the other leads to multilayer mats. [241,242] Besides, traditional electrospinning can be combined with other methods, such as prototyping, polymer deposition, melt electrospinning, and so on. [243]

The morphological properties of final nanofiber mats are deeply influenced by several parameters, which can be divided in four different groups: system parameters; process parameters; type of collector; ambient conditions. As investigated in many works in the literature, indeed, these parameters directly influence the fiber diameter, formation of beads and aligned or random distribution of nanofibers. [244,245]

System parameters define the rheological properties of initial polymeric solutions. For this reason, they are directly correlated with the type of selected polymer, its concentration, its molecular weight and the solvent used. They influence mostly the diameter of the fibers and the potential formation of beads. A too low concentration in polymer on the solution leads to the formation of beads instead of fibers. Indeed, at low concentration, the viscosity of the solution is low while

the surface tension is relatively high. Therefore, the solution jet cannot maintain the proper shape at the end of the tip and a small drop is formed among the fibers. With an increasing concentration, fibers with a larger diameter are obtained. However, a too high concentration induces a very high viscosity and a continuous flow of the solution cannot be maintained. So, an optimal concentration in polymer should be found. [158] When the volatility of the solvent increases, the solidification time of the fiber decreases due to the faster evaporation, and so the fibers are kept with a larger diameter. [244] Solution conductivity has the opposite effect: when it increases, the diameter decreases. It is because the jet carries more electrical charges and thus the tensile force increases, leading to a smaller diameter. [245] Surface tension influences the stability of the jet: a too low or too high surface tension will lead to beads. In fact, surface tension determines the electrospinning window. [158,246–248]

The second important category of parameters is the **process parameters**. The effect of the voltage supply is still discussed, and researchers still do not agree on the impact it has on the fiber diameter. [158,246–248] Then, a larger volume of feed rate or a larger needle diameter leads to a larger fiber diameter. [158,246–249] Finally, the distance between the collector and the tip mostly influences the formation of beads or fibers, but also the diameter of the fibers, as it influences the time to dry before reaching the collector. [247]

The **type of collector** (static or dynamic one) influences the orientation of the fibers (Figure 18). The dynamic collector is a rotating cylinder, while the static collector is a conducting plate. With a static collector, the orientation of the fibers is random, due to the instabilities occurring during jet elongation. However, by using a suitable dynamic collector, it is possible to obtain highly orientated fibers. [163,250–252]

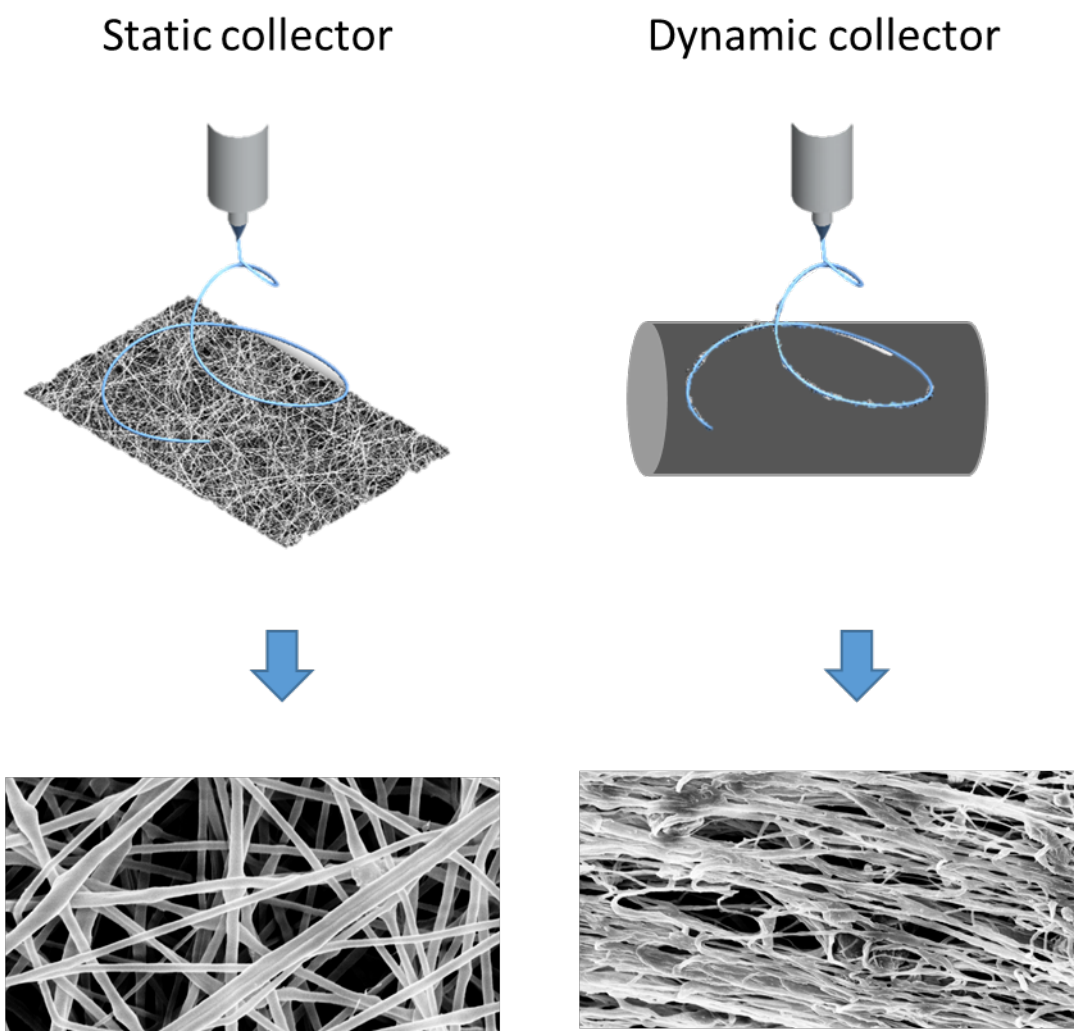


Figure 18: Static versus dynamic collector

Finally, the last category of parameters is the **ambient conditions**. The humidity, air flow and the temperature will influence the time to dry, but temperature also influences the viscosity of the solution. It is important, but difficult to take into account when processing. [247]

The electrospinning process is a trending technique because of the advantages it offers. It is a robust and simple method to produce fibers in the submicron range. The final obtained nanofiber mat offers a high surface area to volume ratio and the different parameters can be modified to tune the porosity of the produced scaffold or the composition, size and shape of the fibers. [253] Moreover, it is worth to notice how this technique leads to obtain a wide range of nanomaterials,

starting from a polymeric solution. Indeed, through several post processes, like heating treatments, it is possible to obtain carbon nanofibers, metal oxide and ceramic nanostructures. However, some elements remain challenging. For instance, the scale-up for mass production is challenging because of the limited throughput of nanofibers coming out from the spinneret. A reproducible placement of the nanofibers, as well as the control of the fiber diameter and size is hard to achieve. [158]

2.1.2. Solution, parameters and post treatment

All the nanofibers presented in this work were fabricated starting from a polymeric solution. The solution and the provenience of the material are listed in Table 4.

Table 4: Solution for nanofibers fabrication and provenience of materials

Solution	Solvent	Concentrations	Provenience	Application
PEO/PEDOT:PSS	H_2O	PEO 5 wt% PEDOT:PSS 6.66 wt%: 4 wt%	PEO: Sigma-Aldrich PEDOT:PSS: Heraeus Clevios™.	Flex and pH sensing
PEO	H_2O	PEO 5 wt%	PEO: Sigma-Aldrich	Flex and pH sensing
Cellulose Acetate	DMAc and Acetone	Cellulose Acetate 25 wt% DMAc:Acetone (1:2)	Sigma-Aldrich	Electrochemical Biosensor
PAN	DMF	PAN 8 wt%	Sigma-Aldrich	Electrochemical Biosensor
PEO/MWCNT	H_20	PEO 5 wt% MWCNT varying, see Chapter 6	PEO: Sigma-Aldrich MWCNT: Nanocyl	Pressure sensor

In particular, PEDOT:PSS solution was stirred overnight at room temperature and Cellulose Acetate and PAN ones were stirred for one hour at 60°C and then for 24h at room temperature. The solution preparation of PEO/MWCNT is more complex: first, a solution containing MWCNT (0.4 wt%) in deionized water is prepared. PSS (0.4 wt%) is added to help to suspend the nanotubes in the water-based solution, together with ultrasonic stirring. After that, the MWCNT in H_2O solution is added to a PEO solution in deionized water. Before each use of the solution, ultrasonic stirring is newly performed.

A NANON 01A apparatus from MECC Ltd was used to produce the nanofibers. A spinneret hosting a 27 Gauge x 15 mm needle was powered by a high-power supply (HVU-30P100). Connected to the spinneret, a syringe pump allowed to select a flow rate in the range of 0.1 to 99.9 mL/h.

The parameters of electrospinning for each solution are listed in Table 5.

Table 5: Electrospinning parameters for each solution

Solution	Voltage	Working distance	Flow rate
PEO/PEDOT:PSS	15 kV	15 cm	0.1 mL h^{-1}
PEO	20 kV	15 cm	0.1 mL h^{-1}
Cellulose Acetate	26 kV	15 cm	1 ml h^{-1}
PAN	30 kV	15 cm	0.1 mL h^{-1}
PEO/MWCNT	20 kV	15 cm	0.1 mL h^{-1}

Some post treatments were performed on the fibers. They are listed in Table 6.

Table 6: Post treatments on the NFs

NFs	Post-treatment
PEO/PEDOT:PSS	Thermal treatment: i) 70 °C for 1 h under nitrogen atmosphere in order to preserve the morphology of the starting nanostructures;

	ii) different temperatures and for different duration times, under nitrogen atmosphere
PEO	None
Cellulose Acetate	Deacetylation: 1 h in NaOH/Ethanol (0.05M) + optional washing (3 time 10 minutes in deionized water)
	Thermal treatment: iii) 280 °C for 2 h in air in order to stabilize the fibers; iv) 450-600-750°C for 1h under nitrogen atmosphere
	Laser treatment
PAN	Thermal treatment: i) 280 °C for 2 h in air in order to stabilize the fibers; ii) 450-600-750°C for 1h under nitrogen atmosphere
	Laser treatment
PEO/MWCNT	None

All thermal treatments were done in a Carbolite, VST furnace. The gas flow was 360 sccm (inert atmosphere obtained by N_2 or Ar flow) and the heating rate 2.5 °C min^{-1}.

More details on the sensors fabrication is given further in the dedicated chapters.

2.2. Characterization of the nanofibers

2.2.1. Morphological and Optical characterization

The morphology of the nanofibers was observed thanks to a Field Emission Scanning Electron Microscopes (FESEM, Zeiss MERLIN), that operates from 5 kV to 10 kV and that is equipped with an oxford energy dispersive X-ray detector.

Thermogravimetric analysis (TGA) was performed to analyze crosslinking reactions and thermal evolutions during the thermal treatment. The instrument used was a Perkin–Elmer Pyris 1 thermobalance. Moreover, the TGA can be coupled with a Perkin–Elmer Spectrum GX Infrared Spectrometer to analyze the gas produced by the reaction to the thermal treatment. The coupling is ensured by a Perkin–Elmer TG–IR. The condensation of the reaction product while transferring from the TGA chamber to the IR unit and inside the unit itself is avoided thanks to a gas cell heated at 220-230°C.

2.2.2. Chemical characterization

Energy dispersive X-ray spectroscopy (EDS, OXFORD X-act) were performed in order to characterize the chemistry of the samples. The samples were at 0.8 cm from the detector, the deadtime was lower than 20 %.

As well as Raman spectroscopy (Renishaw InVia Reflex micro-Raman spectrometer (Renishaw plc, Wotton-under-Edge, UK)). The laser diode source had a wavelength of 514.5 nm and the power was 5 mW.

2.3. Characterization of the sensors

2.3.1. Electrical characterization

A Keysight B2912A source measure unit was used to perform I-V measurements to characterize the electrical behavior of the nanofibers. A tension from -1 to 1V was applied at the rate of 10mV/s. The polarization of the material leaded to a current flow that was measured. The resistance of the material was then interpolated. To obtain the resistivity, the second Ohm's law was used. The thickness of nanofiber mats was evaluated by a surface profilometer (TENCOR P-10).

2.3.2. Electrochemical characterization

Diverse detection methods are used in the biochemical sensors presented in the literature, but the electrochemical methods are the most frequent since they shows great advantages such as high sensitivity, simple structure, relatively low consumption of power and fast response. [141] Electrochemical sensors detects a reduction/oxidation reaction.

Electrochemical sensors are composed of three electrodes (Figure 19):

- the *working electrode* (WE) is the electrode that transduces the signal of the electrochemical reaction. [254] It is usually in contact with the analyte. [255] Many materials can be used for the working electrode. For example, carbon-paste electrode (CPE), glassy- like carbon electrode (GCE), indium tin oxide (ITO), gold (Au), platinum (Pt) and stainless-steel electrodes were used in literature.
- the *reference electrode* (RE) serves as a reference for the measurements. Its reduction potential is known and stable. Usually, it is made of Ag/AgCl. [255]

- The *counter electrode* (CE) or auxiliary electrode let pass the charges necessary to balance the current that is observed at the working electrode. A platinum wire is often used as a counter electrode. [32]

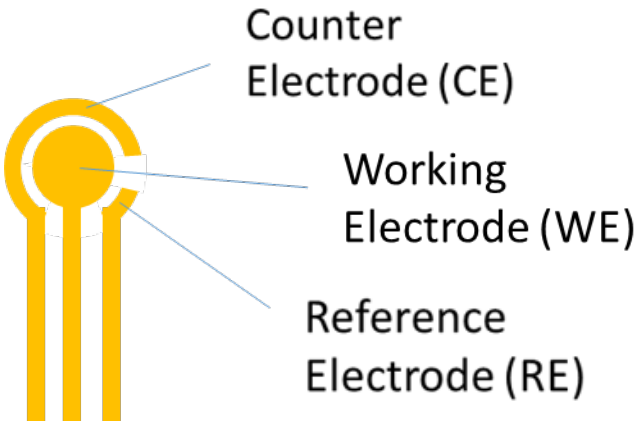


Figure 19: Example of the three-electrodes electrochemical disposition

In wearable biochemical sensors, the sensing electrodes are usually based on metal nanoparticles, polymers and carbon materials to provide better performances of the sensors, good anchoring of the analyte and flexibility. [20]

The instrument used for all the electrochemical characterization was a Palmsens potentiostat.

Electrochemical Impedance Spectroscopy (EIS) measurement were performed for the pH and for the bioelectrochemical sensor. EIS was chosen because this method analyzes the surface of the material. In the case of the wearable device, as it is explained in detail on 3.6 pH sensor characterization, it was essential to look at the surface of the NFs instead of the bulk. This strategy allowed the decoupling of the flex and the pH signal. In the case of the point of care, the surface was analyzed since the sensing was based on the Charge-Blocking effect (see 4.2 Electrochemical biosensing optimization).

The range of frequency went from 0.1 to 100 000 Hz and the perturbation amplitude amounted at 0.01 V. After collection, the EIS data was fitted into an appropriate equivalent circuit. The choice of the equivalent circuit was based on

the physical and chemical properties of the system. EIS Spectrum analyzer was the software used for the fitting.

For the pH sensor, the solution used for the measurement was water-based and of varying pH. The pH was adjusted adding HCl and NaOH to deionized water under the control of a pH meter (Hanna, HI5221).

For the biochemical sensor, a water-based solution containing $K_4[Fe(CN)_6]$ and $K_3[Fe(CN)_6]$, as the redox couple, was used.

Square Wave Voltammetry (SWV) was also performed on the biochemical sensor. The potential ranges from 0.2 to 0.6 V, the frequency was 25 Hz and the step height 50 mV.

2.3.3. Graph plotting and Data Analysis

All the graphs were plotted with Matlab or Excel. At least three measurements were done for each point of the graphs. In between the measurements, the sample went back to rest position. Error bars were calculated based on the least square method.

Chapter 3: Development of a wearable device sensitive to motion and pH for rehabilitation

3.1. Introduction

In the context of health monitoring and in particular flex sensors, composites nanomaterials, polymer-based nanofibers and nanowires showed excellent mechanical flexibility and electrical performance coupling. They have been used as the sensitive material for strain sensors. Polyvinylidene fluoride (PVDF) is the most frequently used polymer (see 1.4.1 Non-conductive polymer NFs for human motion sensors) because of its piezoelectric properties. However, doping of PVDF is usually necessary to promote the performances of the sensors. To facilitate the fabrication of the sensors, intrinsically conductive polymers (ICPs) are good candidates. [75,209,217] Indeed, they have fantastic properties such as flexibility, low cost and versatility with many applications. One of them, poly(3,4-ethylenedioxythiophene) (PEDOT), doped with poly(styrene sulfonate) (PEDOT:PSS), is often used due to its high electrical conductivity, high stability and excellent processability. Moreover, nanostructures, such as electrospinning, further improve these properties. [256]

In this work, electrospun nanofibers (NFs) based on a blend of polyethylene oxide and PEDOT:PSS (PEO/PEDOT:PSS) were optimized with the aim of developing a material sensitive to mechanical deformation and also pH. Sensors for health monitoring were then created. In this context, the good mechanical flexibility and good electrical conductivity were of huge importance for the NFs, as explained in I.I.I and I.I.II. [14,17,130]

As explained in 1.3 Conductive polymer nanofibers, PEDOT:PSS must be blended with another polymer to be able to electrospin it. Several candidates have been employed in literature, such as chitosan [257], polyvinyl alcohol (PVA) [203,258–260] and polyvinyl pyrrolidone (PVP) [261]. However, they lead to a limited electrical conductivity because of their poor electric behavior. PEO, on the contrary, is able to increase the conductivity of the nanofibers through the crosslinking under thermal treatment of its chains with PSS ones. Indeed, thanks to the crosslinking of PEO and PSS, PEDOT domains grow, improving the electron flow. [262] PEO also offers an amazing biocompatibility and Massaglia et al. [263] showed that the crosslinking also promotes a better water resistance, necessary for an application such as pH of the sweat sensing.

In this chapter, the thermal treatment (ThTr) of the NFs based on a PEO/PEDOT:PSS blend optimization is described. The crosslinking reaction, already demonstrated by Huang et al. [264] was validated by infrared spectroscopy of the ethanol released when the reaction is going and conductivity increase. The maximum applied temperature, the duration time and the heating rate were analyzed to obtain the optimized performances for the sensor.

The description of the flex sensor and the combined flex and pH sensors are also given, as well as the analysis of their performances. The piezoresistive behavior of the crosslinked NFs mat was studied inducing strain in both traction and compression mode by applying flexion. The sensor electrical resistance R has been measured and the dimensionless parameter $\Delta R/R0$ has been examined as a function of the applied deformation. A long and complicated fabrication process-flows is often required for the fabrication of a platform containing two-sensing units. If the same sensitive material is used for the two units, the whole process is hugely facilitated, and this was the reason of the development of the pH sensing based on PEO/PEDOT:PSS. However, a new challenge in terms of detection has to be took up: the mechanical stress has to not interfere with the pH analysis and the pH changes has to not interfere with the piezoresistive response of the NFs. With the aim to decouple the signals processed, we performed electrochemical

impedance spectroscopy (EIS) as the pH sensor characterization method. Indeed, EIS focuses on electrochemical interfaces rather than the bulk material, ensuring a better separation of the device response to the two kinds of stimuli.

3.2. Optimization of thermal treatment

The ThTr of the NFs has been optimized to identify the best conditions for the highly sensitive flex sensor based on PEO/PEDOT:PSS NFs. The optimization was done in order to:

- preserve the electrospun nanofibers nanostructuration, since it increases the performance of the flex sensor as showed by Amjadi et al. [10];
- promote the adhesion between the PDMS substrate and the Crosslinked NFs to obtain an optimal flex sensor;
- increase the electrical conductivity of the sensitive material by crosslinking the PEO and PSS chains. Indeed, to increase the sensor performance, the material was integrated in a nanostructured form: the electrospun nanofibers. However, to be able to electrospin PEDOT:PSS, it must be blended [257,260,261,263,265–268]. In this work, we choose PEO because, as Huang et coworkers showed [264,269], the blend electrical conductivity significally improves because of the creation of crosslinks between PSS and PEO. These links promote PEDOT domains growth.

We valuated different duration times and temperatures to obtain the best crosslinking process. The temperature at which the crosslinking happens was equal to 120°C, as demonstrated by Huang et al. [264]. Thermogravimetric analysis (TGA) was conducted on the nanofibers to verify the non-degradation of the NFs along the treatment. Weight percentage evolution with the temperature is shown in Figure 20, as well as the corresponding degradation rate in Figure 21. We can see two deflections in the weight percentage variation and therefore two peaks in the degradation rate. It corresponds to the two stages of deterioration of the material.

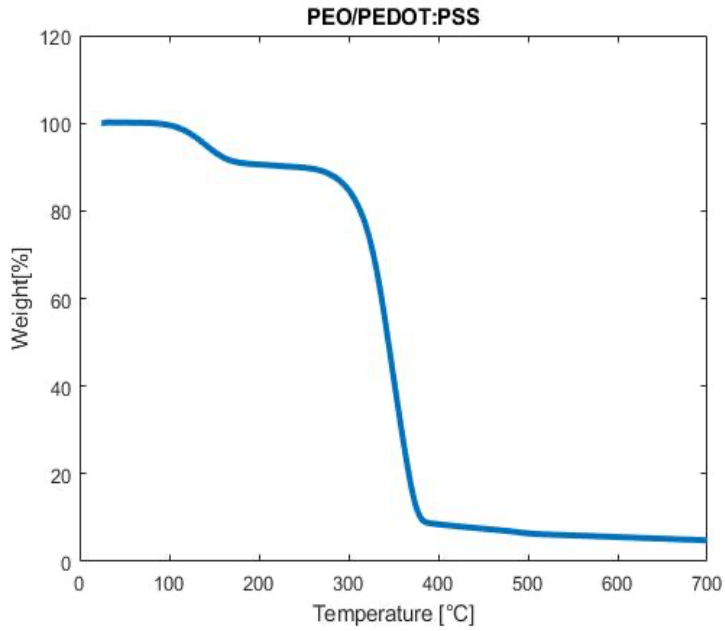


Figure 20: Weight percentage evolution of PEO/PEDOT:PSS NFs along temperature increase obtained by TGA analysis. Reproduced with permission from [207]**.**

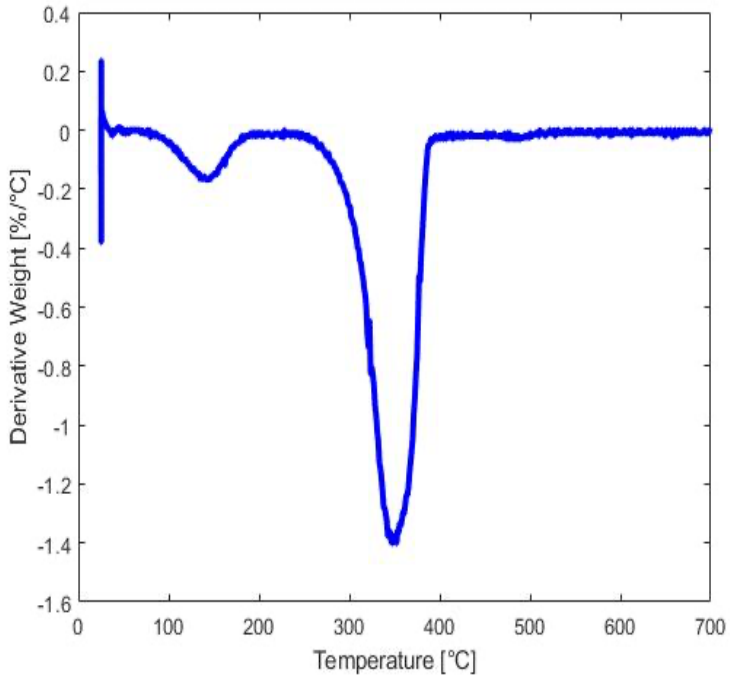


Figure 21: Rate of degradation of PEO/PEDOT:PSS NFs along temperature increase obtained by TGA analysis. Reproduced with permission from [207]**.**

We were able to attribute the first deflection peak starting at 100°C to the ethanol produced by the reaction of crosslinking (Figure 22).

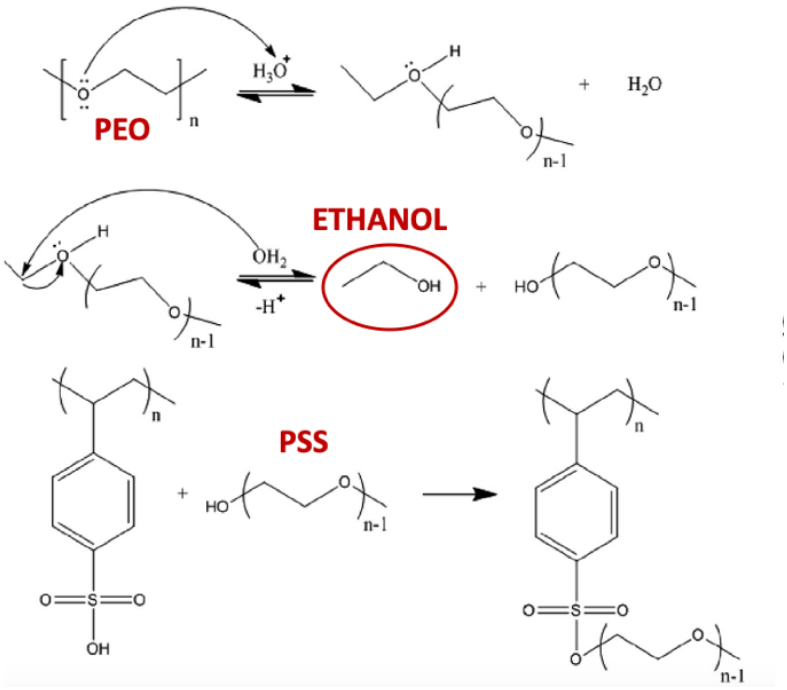


Figure 22: Crosslinking reaction between PEO and PSS. Reproduced with permission from [207]**.**

Indeed, a Fourier Transform Infrared Spectroscopy Characterization was conducted on the products of the reaction of crosslinking along the ThTr of the fibers. This analysis was performed both on PEO and PEO/PEDOT:PSS NFs to succeed in attributing the phenomenon observed at the presence of PSS on the material. The results are showed at Figure 23. The FTIR was conducted on the gas that were extruded from the chamber in which the NFs were treated. Since ambient parameters can influence the measure since PEO has a huge adsorption capacity, peaks corresponding to water and CO_2 can be observed on the results. On the spectrum of PEO/PEDOT:PSS at 120°C, CH_3, CH_2 and C-O peaks can be seen at 2870 cm^{-1} and 2960 cm^{-1}, 2850 and 2925 cm^{-1}, and at 1048-1384 cm^{-1}, respectively. These peaks are due to the production of ethanol, confirming that the crosslinking between PSS and PEO is occurring.

The O-H peak at 3610-3670 cm^{-1} is not well defined because it is covered by the H_2O production.

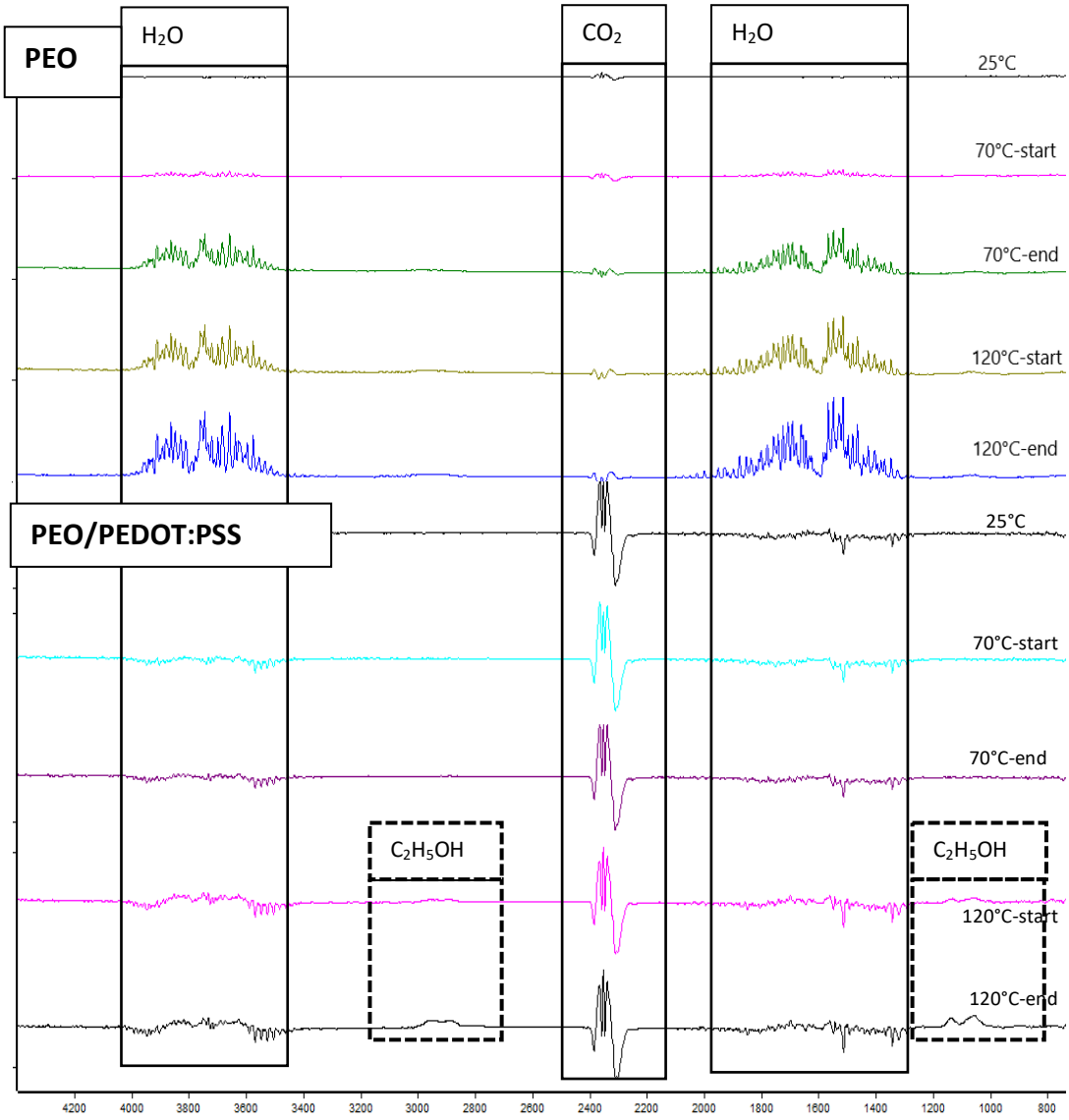


Figure 23: FTIR spectrum of the reaction products along the thermal treatment: 2,5°C/min, 1h @ 70°C, 2h @ 120°C, under N2 atmosphere. Above: thermal treatment of PEO nanofibers. Below: thermal treatment of PEO/PEDOT:PSS nanofibers. Reproduced with permission from [207].

The second deflection starting at 300°C on the TGA results (Figure 21 and Figure 20) can be attributed to the NFs components degradation. Indeed, it was already showed that PSS degrades at 320°C by rupture of the styrene sulfonate group. PEDOT degrades at higher temperatures. [270] Moreover, a TGA analysis on PEO NFs that was carried in the frame of this work showed that PEO starts to degrade at 310°C. Finally, this deflection leads to an almost complete loss of the material,

which supports the hypothesis that the degradation of all the components together appends from 300°C.

It could therefore be possible to confirm the optimal temperature (120°C) for crosslinking reaction between PEO and PSS by the combination of TGA and FTIR analysis. This result was in line with the one of Huang and coworkers [243].
A slow heating rate (2.5 °C min^{-1}) was of huge importance to preserve the nanostructuration.

Moreover, we choose to implement a first stabilization step at 70 °C for one hour. Indeed, 70 °C is slightly higher than the PEO melting temperature (67 °C), which leads to a facilitated reorganization of the polymeric chains of PEO around PSS.

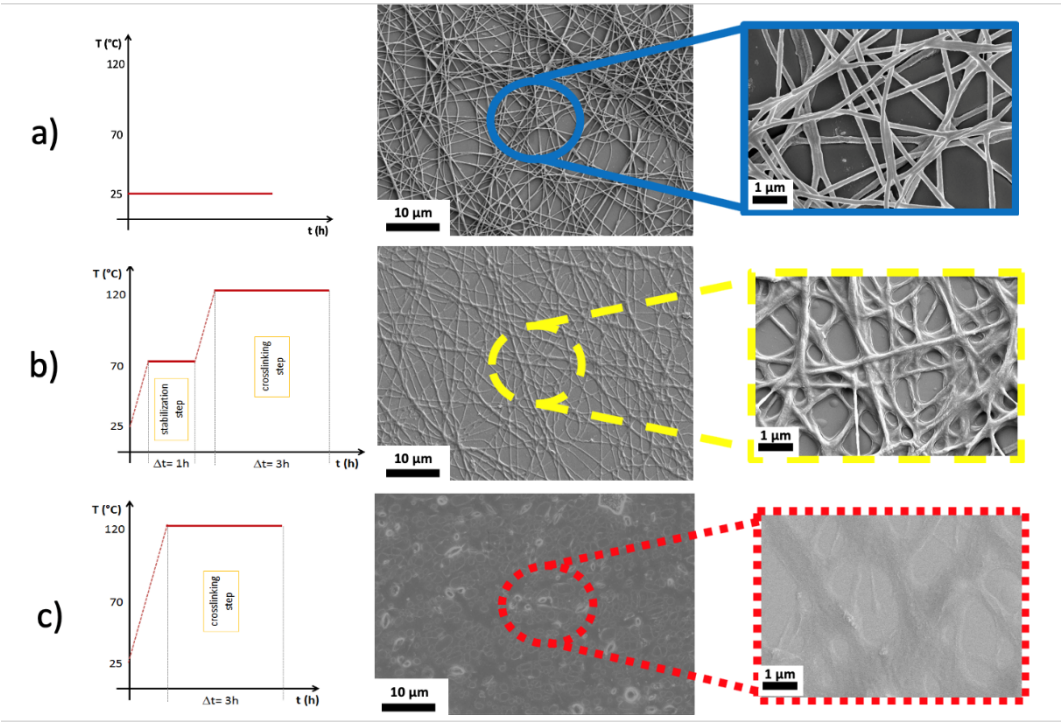


Figure 24: morphology of a) PEO/PEDOT:PSS NFs mats without ThTr; b) Crosslinked NFs mats; c) Crosslinked NFs mats but without the first step at 70°C. Reproduced with permission from [207].

FESEM images on Figure 24 a), b) and c) show the NFs without ThTr, with the full ThTr and with a ThTr but without the step at 70°C, respectively. Figure 24 b) shows the well-preserved nanostructure after ThTr confirming the integrity of NFs and

no detrimental effects on their morphology as compared to PEO/PEDOT:PSS NFs without ThTr (as shown in Figure 24 a)). Moreover, Figure 24 b) highlights the distribution of Crosslinked NFs pores, whose dimensions are in the range of some micrometers, which confirm the high surface area to volume ratio preservation after ThTr. However, Figure 24 c) clearly exposes how the destruction of the nanostructure if the step at 70 °C is not done. The diameter of the nanofiber-like structure on Figure 24 c) is definitively larger than the Crosslinked NFs one and it shows a complete NFs melting into an almost continuous film. This confirms that avoiding the stabilization step hinders the nanostructuration conservation. The one hour at 70 °C step before the one at 120 °C is therefore essential and sufficient to preserve the properties of the NFs. Moreover, the light melting of PEO [243] leads to a NFs mat perfect adhesion to the PDMS support, which insure the mechanical strain transmission from the skin to the NFs mat, i.e., the sensing element of the device.

Huang et coworkers [264] showed how the higher the PSS-PEO links, the higher the PEO/PEDOT:PSS materials electrical conductivity. We therefore correlated the variation of electrical conductivity (ΔS) with the duration time of the ThTr (up to 12h). Figure 25 shows the trend of the $\Delta S/S_0$ parameter versus the time of duration of the ThTr. ΔS corresponds to $S\text{-}S_0$, and S_0 is the conductivity of the NFs non thermally treated.

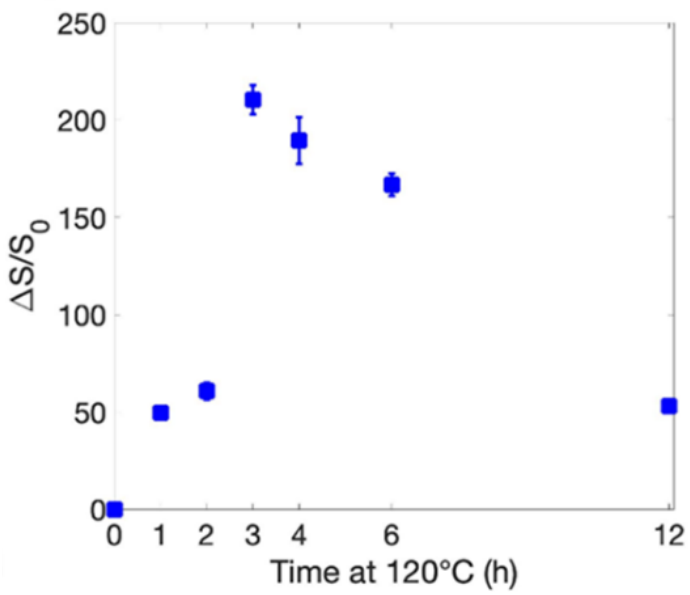


Figure 25: Electrical conductivity variation over the duration time of the reaction of crosslinking. $\Delta S=S-S_0$, S_0 is the conductivity of the NFs non thermally treated. Reproduced with permission from [207].

The electrical conductivity increases with the duration time, which confirms the correlation between the crosslinking degree between PEO and PSS and the material electrical conductivity. Within the ThTr first three hours, $\Delta S/S_0$ increases of more than two order of magnitude. However, for ThTr longer than three hours, $\Delta S/S_0$ then decreases. This decrease can be attributed to the PSS decomposition. In the FTIR spectra reported in Figure 26 the para-substituted benzene peak at

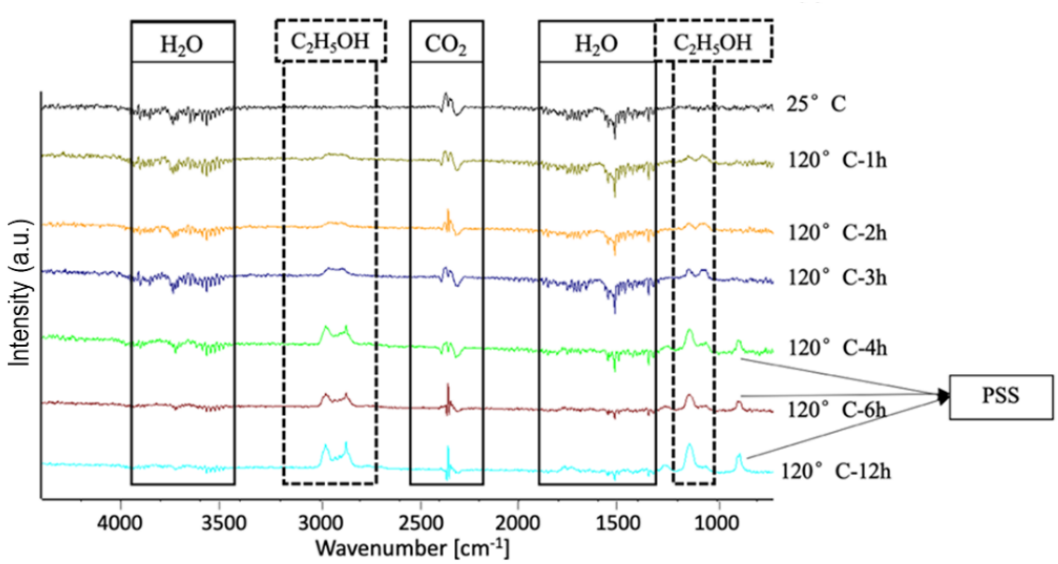


Figure 26: FTIR spectrum of the reaction products along the ThTr. Reproduced with permission from [207].

800-860 cm^{-1} observable after 3 hours of ThTr at 120°C confirmed this degradation. PSS degradation liberates PEO chains, allowing them to interfere with the electron flow.

We were therefore able to determine the optimized ThTr. It is as follow:

- One first step at 70 °C for 1 h, necessary to preserve the nanostructure
- A second step at 120°C for 3h to crosslink PEO and PSS.

Both the steps are performed with a heating rate of 2.5 °C/min under N_2 atmosphere. The ThTr promotes the adhesion between the PDMS substrate and the Crosslinked NFs, obtaining an optimal strain transfer, as well as activates the functional material electrical conductivity.

3.3. Flex sensor fabrication

The process flow of the fabrication of the sensor is sketched in Figure 27.

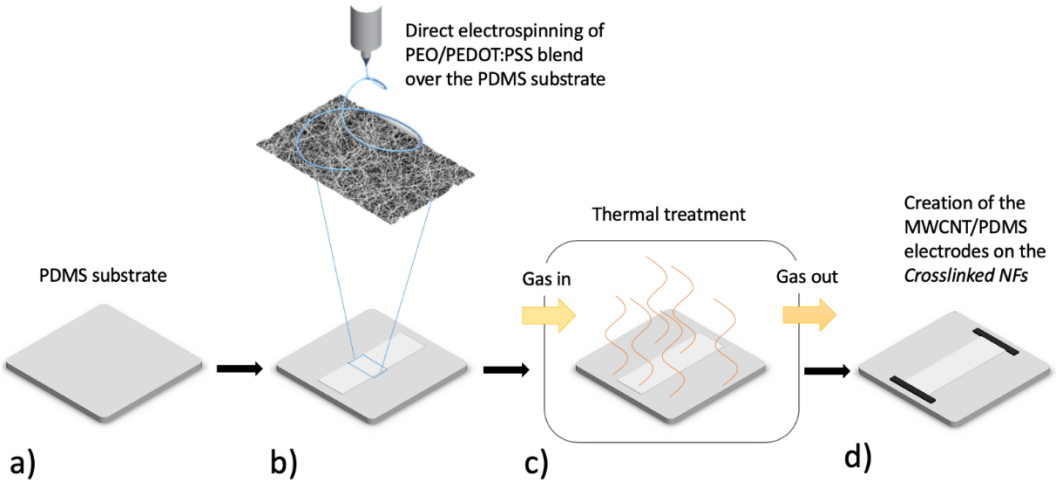


Figure 27: Schematic illustration of the process flow of fabrication of the Crosslinked NFs Flex Sensor starting from a PDMS substrate by direct deposition of nanofiber mats by electrospinning using the PDMS substrate as the collector. Reproduced with permission from [207]**.**

To provide both flexibility and stability to the sensor, a PDMS substrate (Figure 27a)) was selected. Moreover, it offers surface properties suitable for optimal mechanical coupling to the sensitive Crosslinked NFs mats. After the electrospinning (Figure 27b)), the device was thermally treated (Figure 27c)) to promote crosslinking between PEO chains and PSS into the nanofibers. Nanofiber-based sensitive piezoresistive material was freely bonded to the substrate thanks to this thermal treatment that also promote optimal adhesion between substrate and NFs. The conditions of the thermal treatment are listed in Table 6. After the treatment, the active nanostructured layer is referred to as Crosslinked NFs. Finally, as shown in (Figure 27d)), the electrodes for electrical characterizations were created thanks to a PDMS/MWCNTs paste spread at the edges of the Crosslinked NFs mat. The curing of the paste was done at ambient temperature for one night.

3.4. Flex sensor characterization

Aiming at demonstrating the great potential of the flex sensor for monitoring human body articulations, we tested it inducing strain in both traction and compression mode by applying mechanical flexion. The sensor placed in contact of the wrist showed in Figure 28 is an example of application. The sensor optimal mechanical coupling to the body is ensured thanks to the biocompatible PDMS. Indeed, PDMS has a spontaneous sticky behavior. Medical tape was also used to further improve the sensor-skin coupling and also to isolate the electrical contacts from the skin. Three main working modes were tested: rest, compression and traction. They are all illustrated on the Figure 28. It is easily seen that the sensor bending does not exceed 90° in traction mode. The sensor good coupling with the wrist, offered by the substrate of PDMS, can be appreciated in both deformation modes.

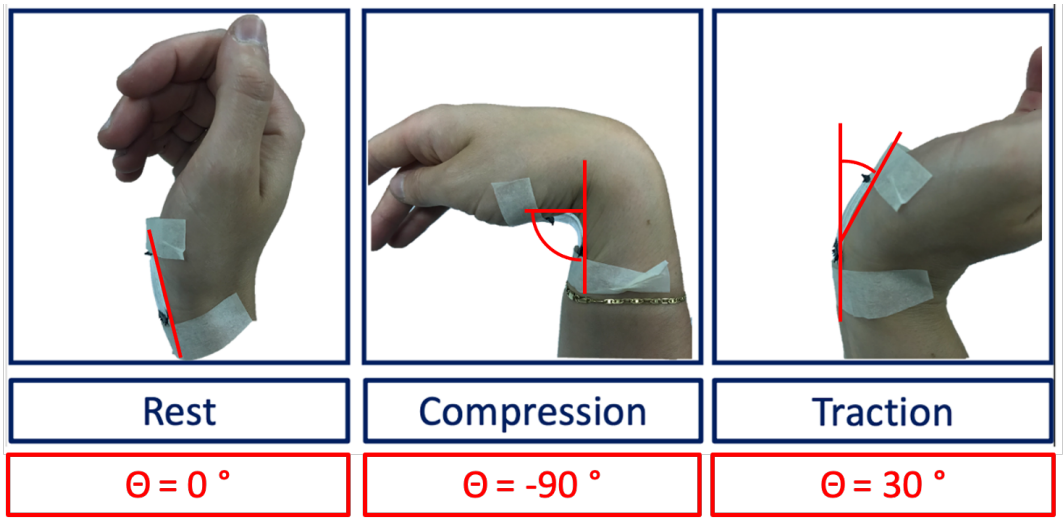


Figure 28: Sensor application on the wrist. Rest, traction and compression mode illustrated. Reproduced with permission from [207].

The correlation between the Crosslinked NFs electrical resistance variation and the applied mechanical strain was analyzed by current–voltage measurements. They were done on the samples at different angles of bending, as shown in Figure 29. $\Delta R/R_0$ is the ratio between the variation of resistance (ΔR) due to bending to the resistance R_0 of the Crosslinked NFs at rest. Figure 29 a) shows the results obtained when the sensors were compressed. A linear variation of the resistivity

is observed, showing an elastic behavior of the NFs. A huge increase of the material resistance up to 91% over a range of angular deformation of 160° was obtained. This result is much higher than the resistance changes for similar angular deformation range generally reported in literature. [10,256,271,272]

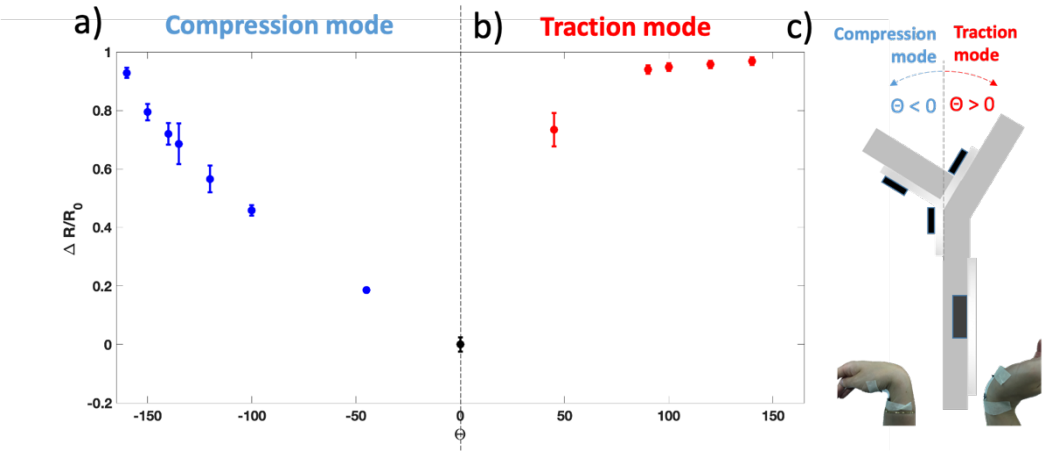


Figure 29: Resistance variation of the NFs mat under bending of the samples: a) compression mode; b) traction mode, c) model describing the determination of the traction/compression mode. Reproduced with permission from [207].

In traction mode, as shown in Figure 29 b), another huge resistance change of 90% over a range of 90° can be appreciated. However, at angular deformation over 90°, a plastic behavior of nanofibers is observed. In the context of health monitoring and rehabilitation, the plastic behavior above 90° is not considered as a problem since all the body joints bend in one unique direction (knee, elbow, fingers, hip, ankle, …) or in two directions but with one of the two directions that does not exceed 90° (see Table 7).

Table 7: Compression and traction maximum angles for human body joints. Reproduced with permission from [273]

Joint	Compression [°]	Traction [°]
Ankle	25 +/- 5	45 +/- 5
Knee	2.5 +/- 2.5	135 +/- 15
Hip	12.5 +/- 2.5	110 +/- 5
Elbow	157.5 +/- 7.5	5 +/- 25
Shoulder	40 +/- 5	85 +/- 5
Wrist	75 +/- 15	70 +/- 20
Finger	0 + 1	95 +/- 5

Aiming at demonstrating the improvement obtained by the nanostructuration, we compared two different structures: a mixed composition (MC), made of electrospun NFs immersed in a film-like arrangement (Figure 30a)) and the as-electrospun NFs (Figure 30b)). The MC structuration was obtained by increasing the working distance to 25 cm and create a floating potential using an isolating collector in the electrospinning process.

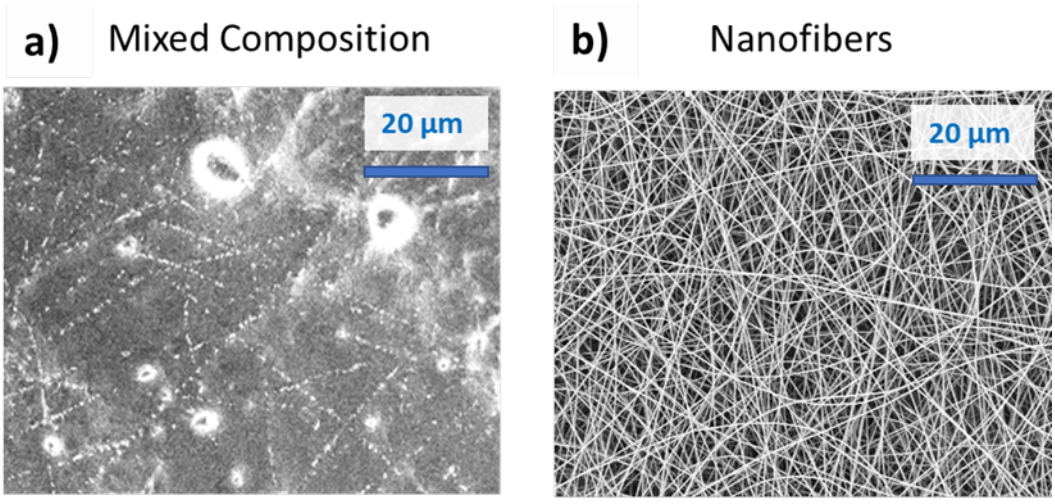


Figure 30: a) PEO/PEDOT:PSS MC FESEM and b) PEO/PEDOT:PSS NFs FESEM. Reproduced with permission from [272]

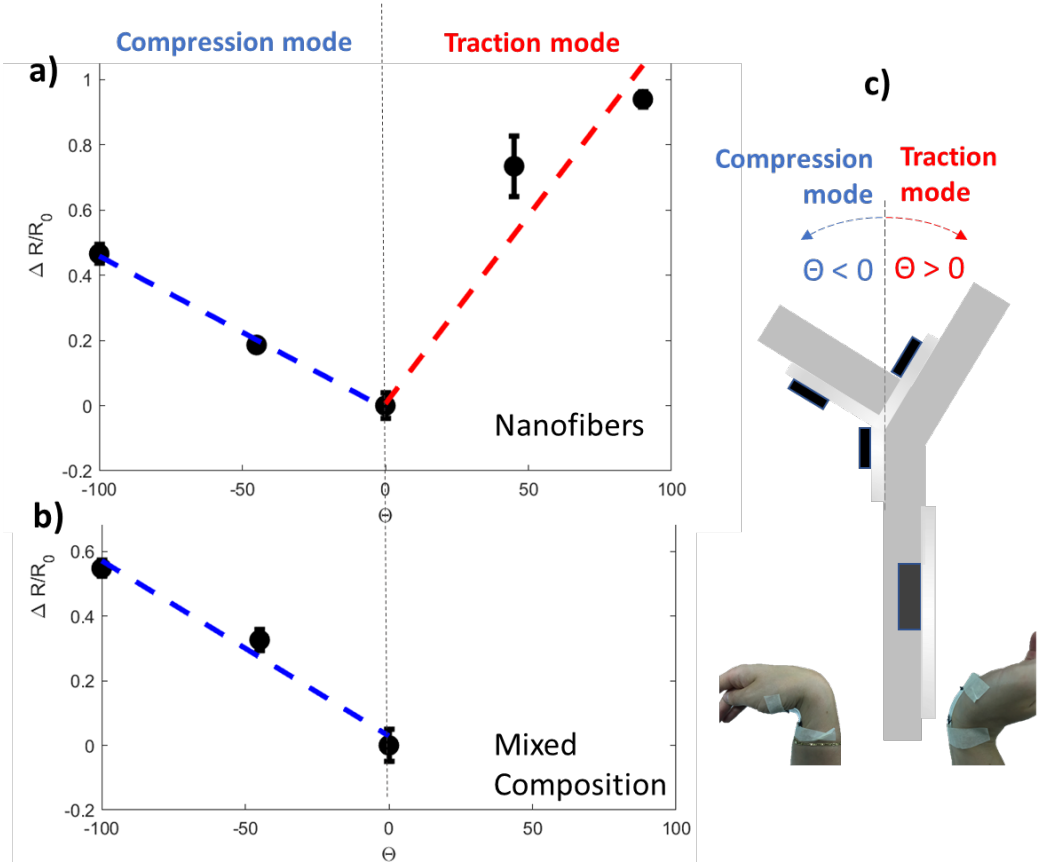


Figure 31: Resistance variation when bending for a) the nanofibers, b) the MC. c) model describing the determination of the traction/compression mode. Reproduced with permission from [272]

Figure 31 a) and b) report the resistance variation ($\Delta R/R_0$) for both of two materials with the bending angle described on Figure 31 c). R_0 corresponds to the situation of not deformed sensor.

A linear behavior was obtained for the MC in compression mode. The sensor sensitivity, i.e., the curve slope, was about -0.0052. In traction mode, a sudden rupture of the material, that inhibited the sensitive element response, was observed. A morphological analysis confirmed this observation (Figure 32). Bending severely disrupt the film-like structure of the MC, as the FESEM image shows, while the NFs are the last remaining components of this structure, competing to propagation of the fracture. According to these results and what can be found in literature [10], we deducted that film and MC are less suitable for flex sensors than nanofibers. We indeed observed a linear behavior for the NFs in traction mode as well that in compression mode. The linearity in traction mode showed how NFs are mechanically more resistant. In compression mode, the

sensitivity of the NFs was not significally different from the one of the MC (-0.0047 and -0.0052, respectively).

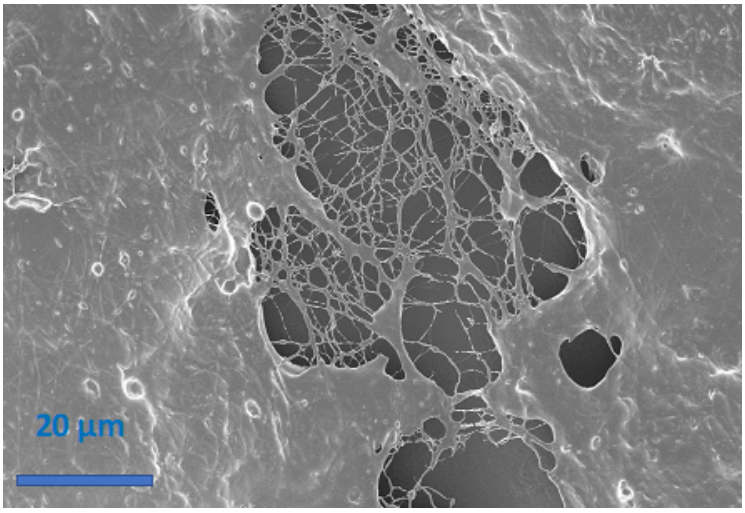


Figure 32: FESEM image of MC material rupture when submitted to bending in traction mode. Reproduced with permission from [272].

Saggio [274] showed that the Gauge Factor (GF) can be obtained by the following equation for a sensor completely adhered on the skin: $GF = \frac{\Delta R}{R_0} \cdot \frac{1}{\Delta\varphi} \cdot \frac{2l_{tot}}{h}$. $\Delta\varphi$ is the angular deformation (in rad), l_{tot} the sensible component length (the NFs length) and h the PDMS substrate thickness (Figure 33). We obtained a GF of 45.84 in traction and a GF of 208.55 in compression. The two values are very high compared with what can be found in literature [10,256,275–277] and confirm the utility of the nanostructuration and the crosslinking process to increase the material sensitivity.

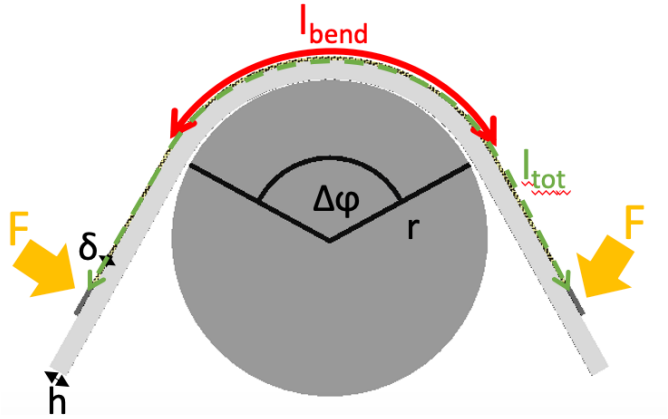


Figure 33: Flex sensors mechanical model used to obtain the Gauge Factor, following the work of Giovanni Saggio [274]. Reproduced with permission from [207].

3.5. Integration of pH sensor with Flex sensor

The first challenge for the design of the system was the identification joint zones in which place each sensing unit. Indeed, different working conditions are required for the pH sensors and the piezoresistive. The pH unit should be placed in direct contact with the skin, while the flex sensor has to be exposed to the joint deformation during flexion. Moreover, it was necessary to avoid any other perturbation and any interferences between the signals, de-coupling them.

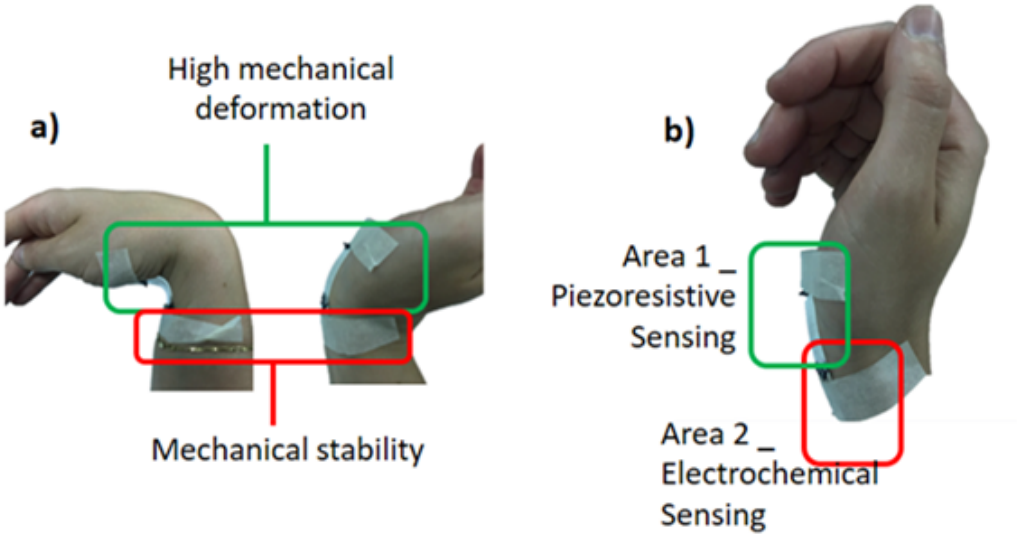


Figure 34: Illustration of NFs pH-Flex Sensors device application. a) Description of the mechanical deformation zones. b) Description of the sensors disposition on the device. Reproduced with permission from [272]

Figure 34a) describe the mechanical deformation zones when the wrist is flexed. Two main zones have been identified to satisfy the requirements described above (Figure 34b)). Area 1 offers the joint maximum deformation, while Area 2 offers a not deformed skin area. Area 1 is therefore selected for flex sensing if the nanofibers are separated from the skin to avoid the interferences from the pH changes of the sweat. Area 2 is chosen for the electrochemical sensor emplacement and the nanofibers were placed in direct contact with the skin.

In this way, and with the help of the rigid mechanical support for the pH sensor, i.e., the commercial electrode, the stimuli were separated in order to avoid any interferences.

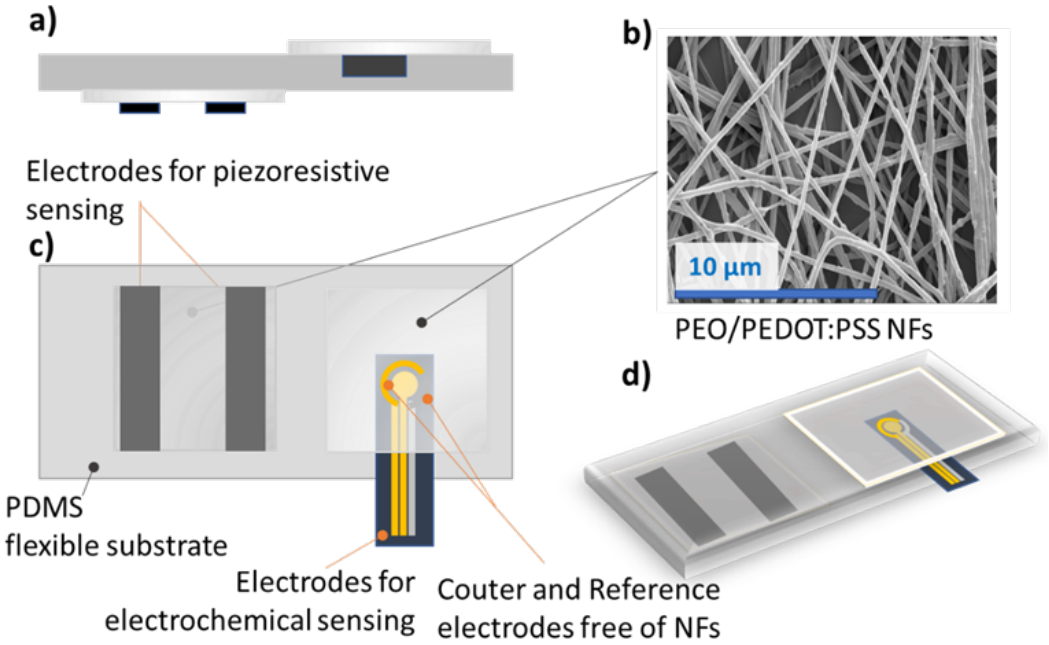


Figure 35: NFs pH-Flex Sensor. a) Cross view, b) PEO/PEDOT:PSS Crosslinked NFs FESEM, c) top view and d) 3D view. Reproduced with permission from [272]

The common sensitive element able to contemporary monitor the two signals is the great novelty of this platform. It indeed implies one single and therefore simple process flow for the whole device. On Figure 35 the design of the NFs pH-Flex Sensor is shown. Figure 35a) describes the NFs disposition to reach a skin direct contact (top) or a skin isolation (down). Thanks to the optimized ThTr leading to the crosslinking of PEO and PSS, the electrical conductivity, the mechanical coupling with PDMS substrate and the water resistance were increased.

For the measurements, the contacts were created in this way:

For the flex sensor, two conductive wires were inserted in the PDMS/MWCNT paste when it was spread to create the electrodes. For the pH sensor, we used the adaptor commercially sold with these electrodes from MetrOhm.

3.6. pH sensor characterization

The direct sensor application on the skin enabled the pH measurement that gives information about the patient health state while moving. The pH range studied was from 2 to 8.

Since the same active material was used for both sensing, it was necessary to identify the best method for pH sensing able to ensure minimal disturbance from the piezoresistive behavior of the material. We therefore choose electrochemical impedance spectroscopy (EIS). pH changes are often measured by electrochemical methods (potentiometric and amperometric), but as they analyzes the material response to the variation, we excluded them. [278] EIS study the electrochemical interfaces between the solution and the sensitive materials rather than its bulk, which enables the decoupling of the signals.

Figure 36 a) shows Bode Plots of the impedance response to acid pH. The equivalent circuit was chosen based on the sensor interface morphology and is presented in (Figure 36 b)). [279,280] This circuit was used to fit the data to obtain the following parameters:

- An ohmic resistance, R, that is the result of two in-series resistances: R_{sol} and R_{NFs}. R_{sol} is the resistance of the solution that is in direct contact with the interface of the sensor, i.e., the sweat. R_{NFs} is the resistance of the sensing material.
- A charge transfer resistance, R_{ct}, that corresponds to the resistance of the transfer of the charges from the solution is in contact with the electrode (i.e., the sweat) to the electrode. It is based on the interface nature, and therefore we expected a variation of R_{ct} with the pH.
- A double layer capacitance, C_{dl}, that is the capacitance formed at the electrode surface when the measurement is conducted. This capacitance is affected by the interface nature and therefore we also expected an evolution of C_{dl} with the pH variation.

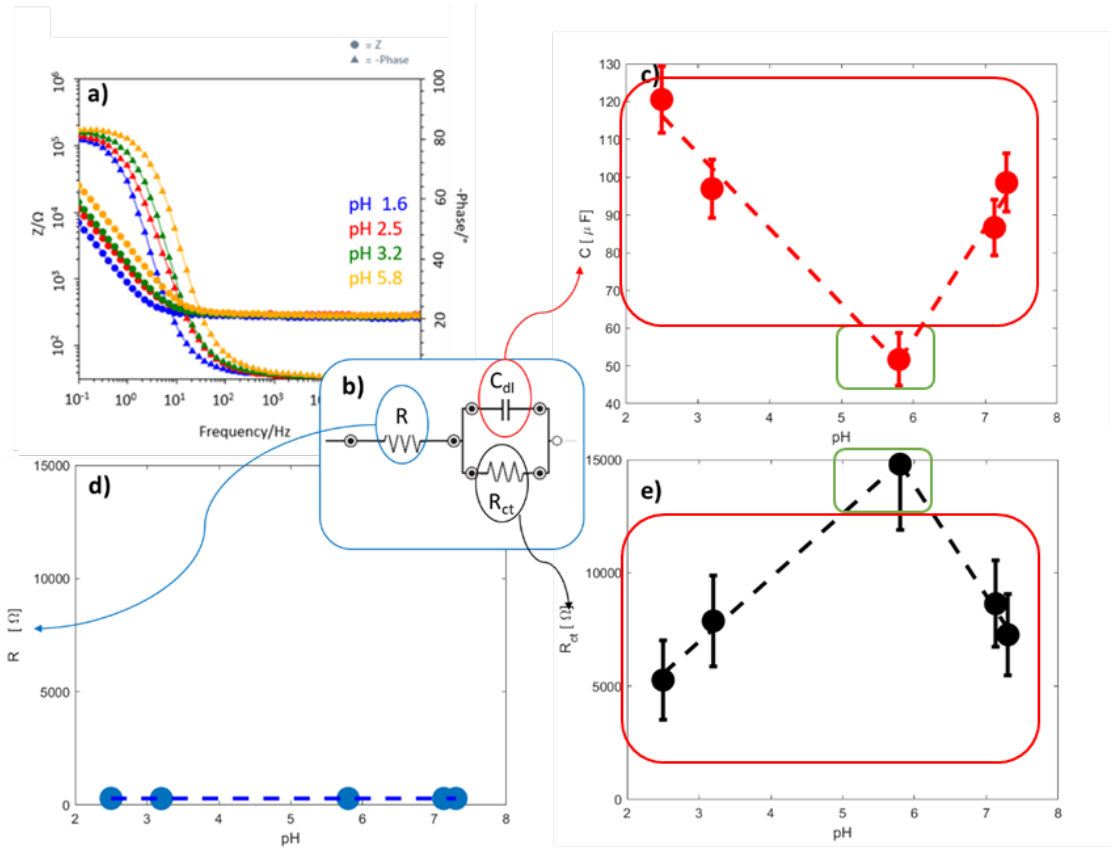


Figure 36: a) EIS curves of the sensor at 4 acidic pH values; b) Equivalent Circuit; electrochemical sensor variation of c) Double layer capacitance, d) Solution resistance and e) Charge transfer resistance with pH. Reproduced with permission from [272].

On Figure 36 c), d), and e) the three parameters variations with the pH are plotted. R did not change with pH (Figure 36 d)). R_{sol} indeed did not change since it is the same water-based solution for each pH value. The absence of variation in the global R indicates that R_{NFS} also remained constant, confirming the confinement of the pH response to the material surface and not in the bulk.

For C_{dl} as well as R_{ct} (Figure 36 c) and e)) two linear behaviors can be observed. In the range from 2 to 5.8, C_{dl} decreases and R_{ct} increases while from 5.8 to 7 it is reversed. The peak value is the same for the two parameters, which shows again that the effect is due to the response of the material to pH.

We choose to test pH in the range of 2.5-7 to be larger than the natural skin pH range (4-6) [281]. We saw that two zones can be created on the C_{dl}/R_{ct} vs pH curves: one zone in which pH value is typical of a healthy skin (green zones in

Figure 36 c) and d)), and the other zone in which the skin is too acid/alkaline (red zones) and therefore further analysis is needed.

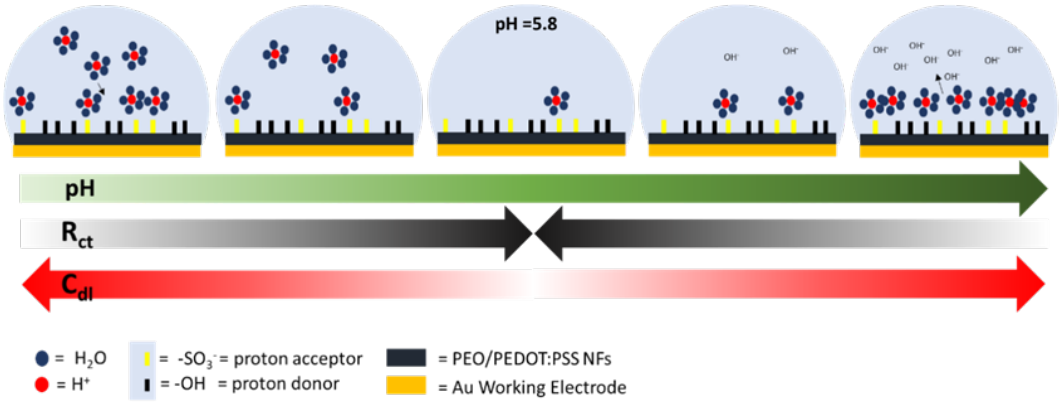


Figure 37: Proposed model of the protons and NFs surface interactions at the material/solution interface. Reproduced with permission from [272]

A hypothesis of the electrochemical mechanisms leading to the above results is given in the model described in Figure 37. The presence of $–SO^{3-}$ and –OH groups on the NFs surface is the key element and was confirmed by FTIR analysis, as shown in Figure 38. Indeed, the group $–SO^{3-}$, as a proton acceptor in acid environment, attracts the exceeding protons from the solution bulk towards the NFs, increasing the C_{dl}. With the increase of the pH, the quantity of protons available in solution decreases leading to a decrease of the C_{dl} until 5.8. At 5.8 we deducted that all the available protons are blocked on the NFs surface and the bulk of the solution is therefore neutral. Continuing to increase the pH towards basic environment, the NFs surface –OH groups start to release protons to compensate the solution charges and a capacitive layer is newly formed, growing bigger with increasing pH.

For the R_{ct}, the effect is inversed. Indeed, more charged the surface, higher the barrier for the flow of electrons from the solution bulk to the NFs and therefore higher the R_{ct}. So, when the surface groups are compensated, at low and high pH, the R_{ct} is at its lowest value.

Thanks to this analysis, we demonstrated that EIS is a good candidate for electrochemical pH sensing in wearable application, and moreover in multisensing platforms. It indeed allows to decouple the signals from the bulk of the material and its surface.

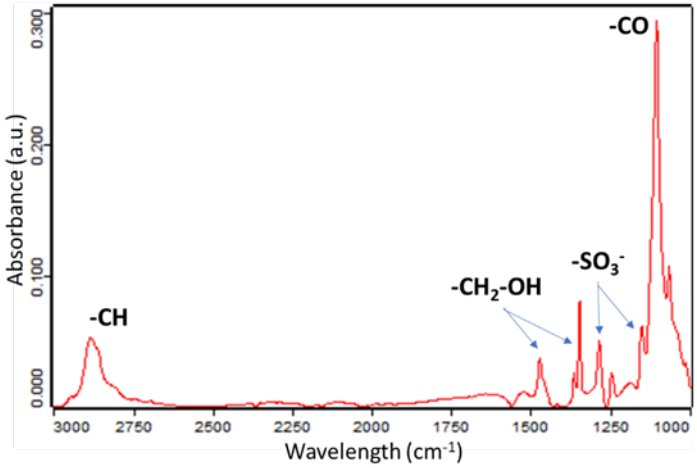


Figure 38: FTIR analysis of the PEO/PEDOT:PSS NFs. Reproduced with permission from [272]

3.7. Conclusion

In this chapter it was showed how PEO/PEDOT:PSS Crosslinked NFs are a good choice for flex and pH sensing, and moreover to combine both on a multisensing platform. The optimization of the thermal treatment gave a good electrical conductivity and an excellent adhesion of the conserved NFs to the substrate, allowing a good mechanical transfer to the flex sensor. It was optimized in terms of duration time, heating rate and maximum temperature.

The piezoresistivity of the NFs was investigated, as well as compared to the piezoresistivity of a Mixed Composition of nanofibers immersed in a film-like structure. In this way, the importance of the nanostructuration to promote the flex sensing over a larger range of deformation was demonstrated. Excellent Gauge Factors of 45.84 in traction mode and 208.55 in compression mode were obtained.

The further integration of the pH sensor with the flex sensor allowed to develop a bi-sensing platform. It was shown how the choice to perform two sensing with the same material facilitates the fabrication of the device in comparison to multisensing based on different materials. Moreover, the importance of the decoupling of the signals was demonstrated and also the modality to reach this decoupling. The placement of the sensors in the joint was of importance, but also the methods used for the analysis. It was demonstrated that EIS can provide good pH sensing results together with an analysis of the surface of the material, leaving its bulk to the flex sensing analysis.

The optimized flex-pH sensor can be useful for the monitoring of muscle fatigue during effort since skin pH is linked to the acid built-up of muscle that is doing exercise. The device can also be used for precision medicine, for example in the case of patients that needs remote assistance.

3.8. Evolution of the wearable sensor in wire form

Wire-shaped sensors are gaining of interest since their form allow the knitting of them directly in textiles such as sport tee-shirt, car seat cover and rehab induments. In this context, a wire-shaped piezoresistive sensor based on NFs electropun on wire was developed. In Figure 39, electrospinning on wire is illustrated: an isolating wire was inserted in the electrospinner and maintained by two rotating pliers. The speed of rotation can be adjusted to obtain the best distribution of NFs as possible. This procedure is similar to the electrospinning on a rotating collector as illustrated in 2.1.2. In this case, the collector is the isolating wire.

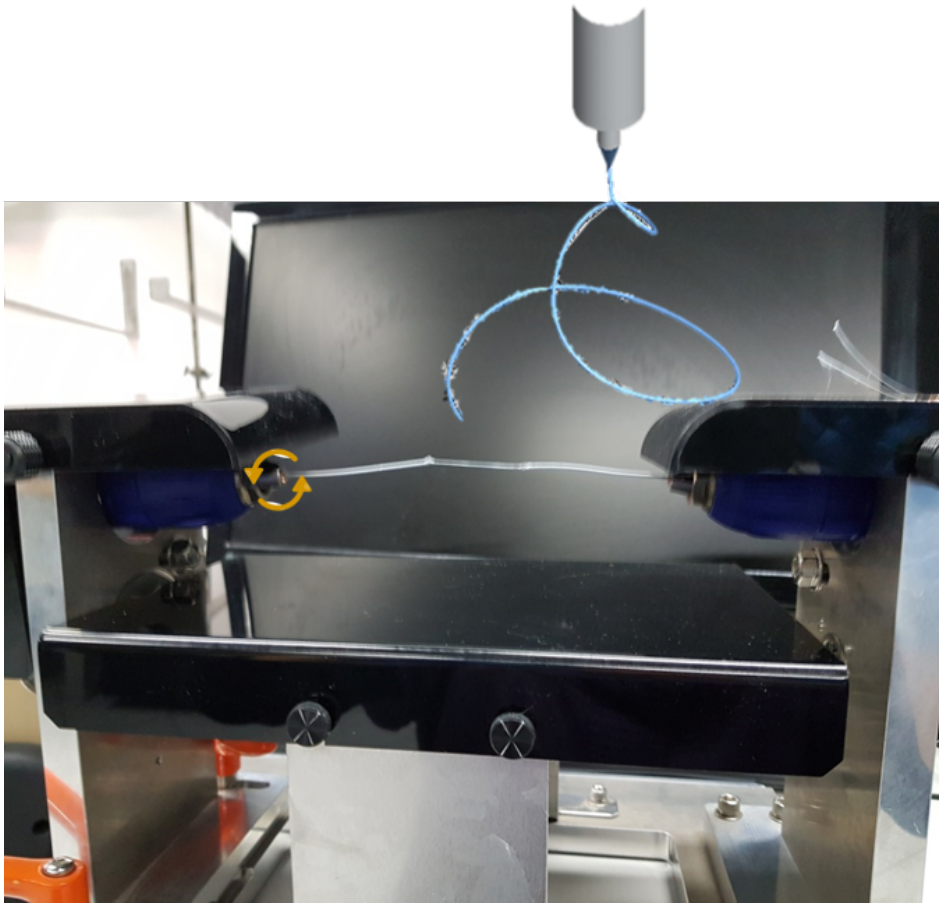


Figure 39: Electrospinning on wire

Two classes of material were evaluated for the development of the wire-shaped piezoresistive sensor: composites with PEO and PAN matrix filled with MWCNT and a blend of PEO/PEDOT:PSS. For the last one, its piezoresistive behavior was already known and studied in the previous work described in Flex sensor characterization. The piezoresistivity of the composites is based on the percolation theory. Indeed, the percolation theory (illustrated on Figure 40) defines the percolation threshold which is the concentration of conductive filler below which the electrical conductivity is strictly correlated with the polymeric matrix and above which the electrical conductivity is due to the presence of the filler. Above the percolation threshold, the electrical conductivity increases until a value above which electrical conductivity remains constant, independently from the amount of conductive filler.

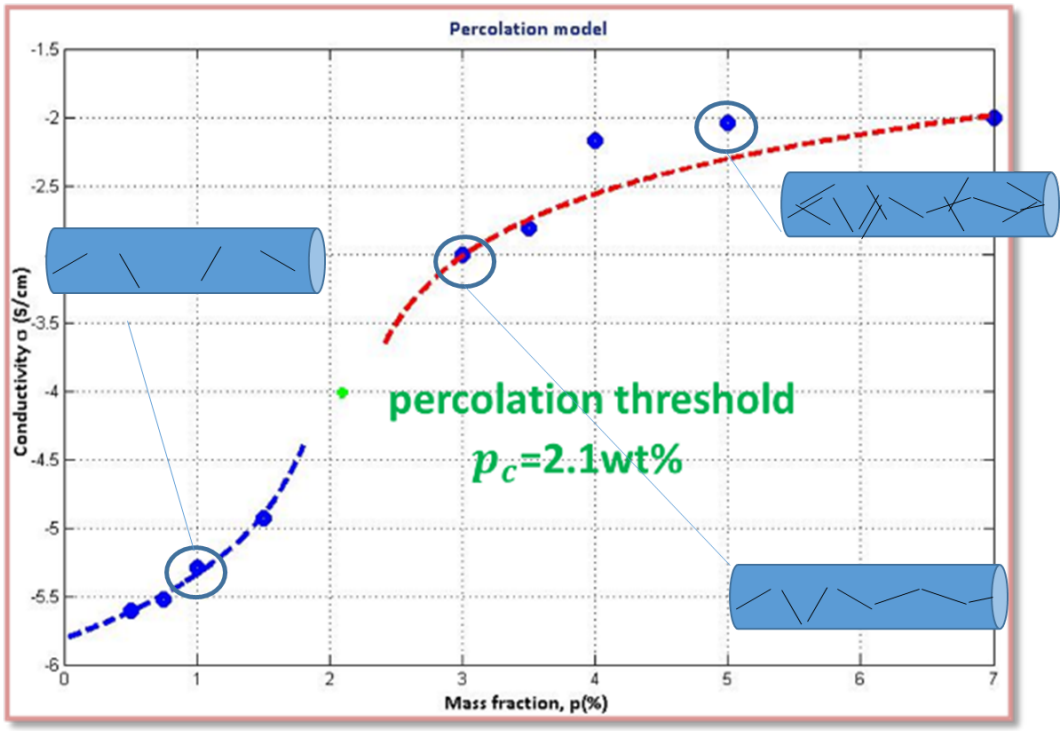


Figure 40: Percolation model illustration

The mechanical deformation induces changes in the percolative routes and therefore changes in the composite resistivity. For example, the continuity of the path created by the filler can be disrupted by the mechanical stimuli, or the filler can be disconnected from the matrix. Both cases induce an increase of the resistance.

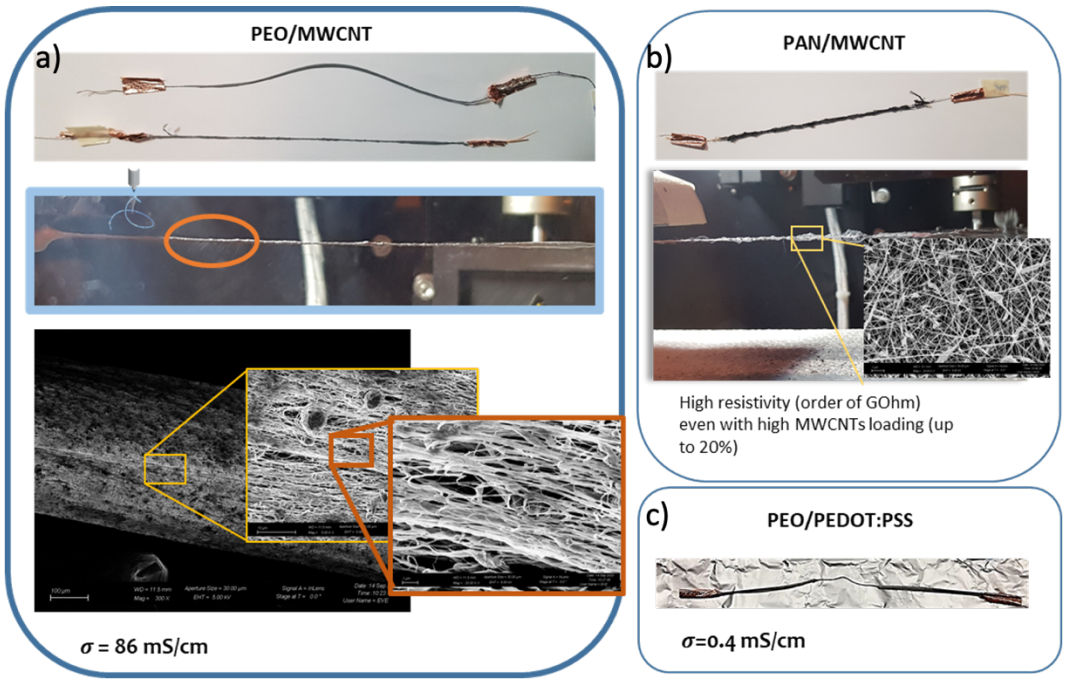


Figure 41: Choice of material illustration for wire-shaped piezoresistive sensor. a) PEO/MWCNT and b) PAN/MWCNT composite NFs: from top to down: wire obtained after electrospinning, modality of deposition of the NFs on the wire during electrospinning, FESEM image of the morphology of the NFs; c) wire obtained after electrospinning of PEO/PEDOT:PSS blend.

On Figure 41, the illustration of the electrospinning and the morphology of the sensors obtained are reported.

It can be seen how PEO/MWCNT and PAN/MWCNT deposition were different. Indeed, for PEO/MWCNT, the nanofibers reached the isolating wire and continued to fall until they were gathered thanks to the rotation of the wire. This resulted in aligned NFs as the FESEM image inset show. PAN/MWCNT composite, did not continue to fall as PEO/MWCNT did. The NFs were directly collected on the wire, leading to a random distribution and a much less regular diameter of the sensor. The blend of PEO/PEDOT:PSS had a deposition similar to PEO/MWCNT, which is also confirmed by the regular diameter of the sensor.

The electrical conductivity of the sensors was measured through IV characterization. The results are reported on Table 8. As PEO/MWCNT was the composite that gave the sensors with the higher conductivity, we choose this material as the best for these sensors.

Table 8: Wire-shaped sensor conductivity

Sensor composition	Conductivity σ [mS/cm]
PEO/MWCNT	86
PAN/MWCNT	0
PEO/PEDOT:PSS	0.4

We also evaluated two concentrations of MWCNT (3.5 and 5 wt%) and the importance of the nanostructuration. To evaluate the last condition, three types of sensors were compared:

- Sensors based on electrospun NFs on an isolating wire, named NFs
- Sensors based on an isolating wire impregnated with the composite solution, named impregnated
- Sensors based on electrospun NFs on an isolating wire followed by the impregnation with the same solution, named NFs + impregnated

The results are reported on Figure 42.

It can be seen how the nanostructuration leads to a much higher conductivity than the two other conditions. Indeed, the NFs helps the creation of the percolative way by the confinement and the organization of the filler. Moreover, it is shown how 5 wt% of MWCNT in the composite solution leads to a higher conductivity for the sensor than 3.5 wt%.

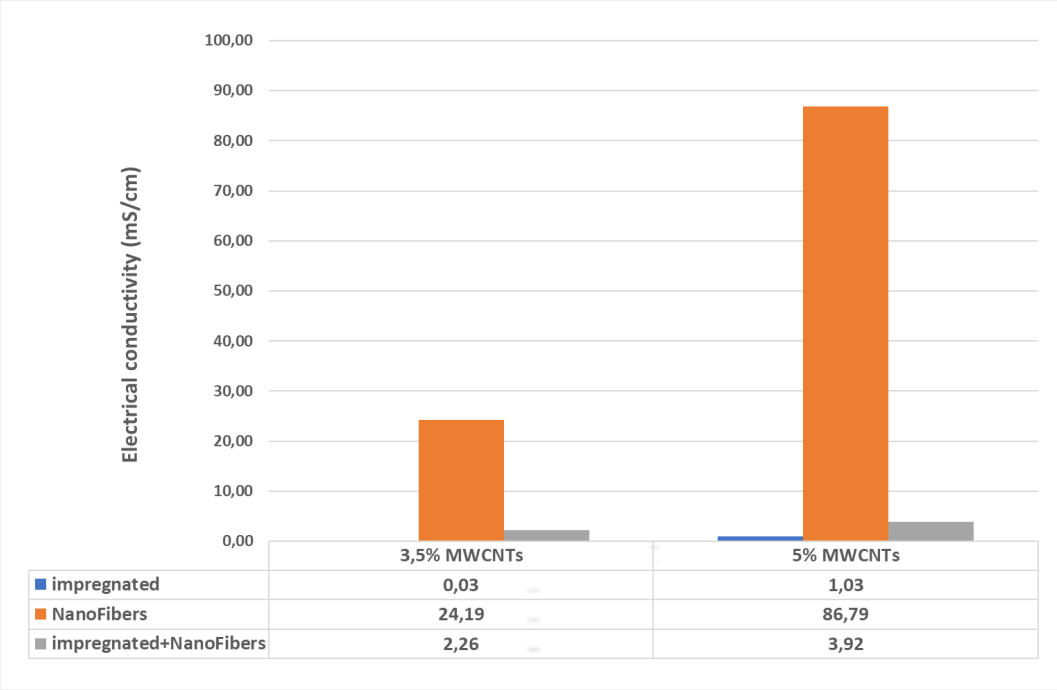


Figure 42: impregnated/NFs/ NFs + impregnated sensors conductivity

Finally, the piezoresistivity of the PEO/MWCNT (5 % wt) sensors was evaluated. Controlled bending was induced by a traction-compression machine while the resistance of the sensor was measured. $\Delta R/R_0$ versus the displacement (i.e., the amplitude of the bending) is plotted in Figure 43. It can be seen that even if the conductivity of the sensor with the higher concentration of MWCNT is higher than the one with the lower, the piezoresistive behavior is greater with 3.5 wt% MWCNT. Our hypothesis is that with less filler, the percolative path is easier to interrupt because of the reduced MWCNT concentration. This gives higher response to the same stimuli intensity.

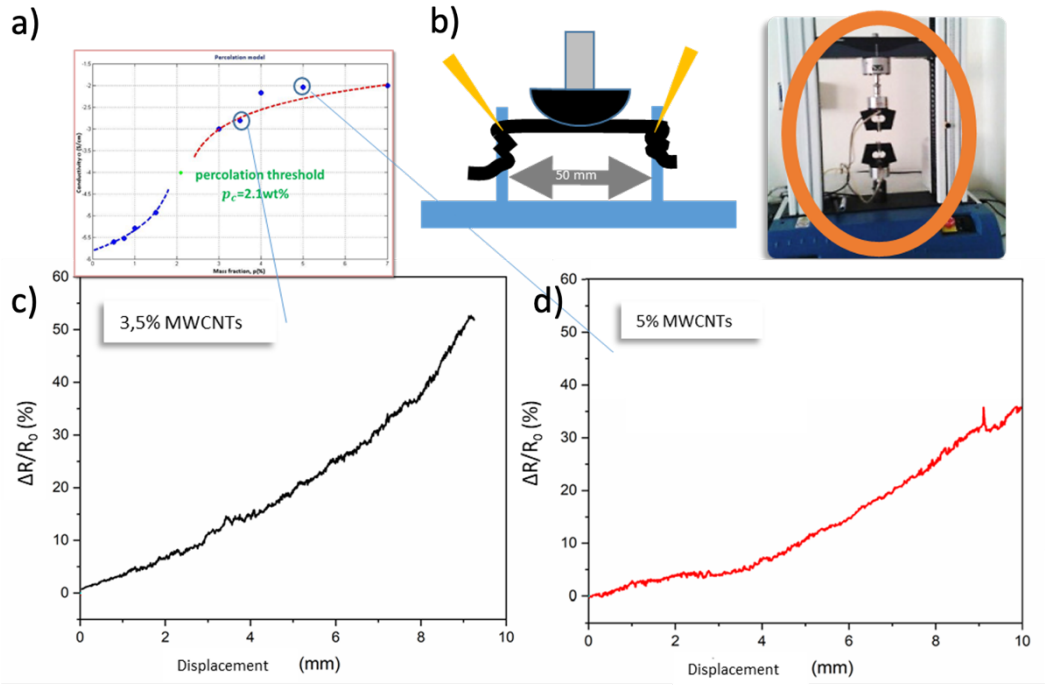


Figure 43: Piezoresistive evaluation of the wire-shaped NFs sensor. a) percolation model for PEO/MWCNT composite NFs, with emphasis on the two analyzed concentrations for the sensors; b) measurement apparatus for piezoresistive behavior characterization and model describing how this measurement was performed; c) and d) results obtained for 3.5 % wt and 5 % wt PEO/MWCNT sensors piezoresistivity characterization.

To conclude, a path for the adaptation of the wearable device to a wire form was evaluated and good results were obtained. The next step should be the electrochemical analysis of the sensor response to pH or other analytes present in sweat to develop another multisensing wearable device useful in the rehabilitation field, for example.

Chapter 4: Development of a Point-of-Care for tumor biomarker diagnosis

4.1. Introduction

The detection of biomarkers in the context of health monitoring is of huge interest since it is directly linked to the presence of some diseases. Diabetes, cancer, pancreatitis, hyperglycemia, Parkinson, HIV are examples of these diseases that can be monitored by sensing specific biomarkers. [282,283]

BioElectrochemical Detection (BED) as the methodology of detection of the biomarkers is progressively gaining attention and has increasingly been used. Recently, few works about the electrochemical detection of biomarkers were published showing the potential of the technique and highlighting its rapidness, simple instrumentation, low cost and high sensitivity [283–289].

In particular, taking advantage of the charge-blocking effect, label-free detection in BED is possible and offers great advantages. Indeed, in electrochemical detection, as in Enzyme Linked ImmunoSorbent Assay (ELISA, the usually used technique for biomarkers technique), the analyte can be linked to a label useful for the detection. In ELISA the label is responsible for a colorimetric response, in BED the label catalyzes the production of the electrons required for the detection through reduction/oxidation reactions. The most represented family of molecules in the literature as electrochemical labels are enzymes. Glucose Oxidase is often used for the development of glucose detectors [100,181,184,193,225,290,291], Horseradish Peroxidase (HRP) for various sensors among which hydrogen peroxide [221][167][292], antibiotics [293], diseases like malaria [294] and tuberculosis [295] and tumor marker sensors [296][297]. However, the labelling requires

additional manipulations and is therefore time, material and human-resource consuming. Label-free detection allows to skip steps in the process of fabrication of the sensor and in the detection itself, making faster the whole. In this case, the redox couple is inserted directly in solution and the amount of analyte immobilized on the surface of the electrode is directly correlated with the resistance of charge transfer (R_{ct}) of the electrode [289]. Figure 44 illustrates the charge blocking effect.

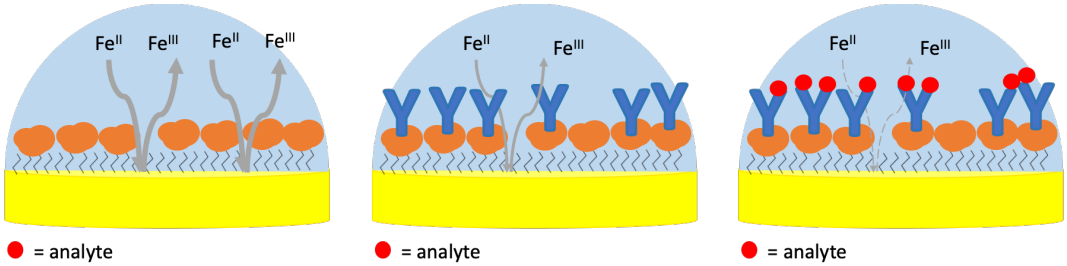


Figure 44: Charge-blocking effect illustration. It can be seen that more molecules immobilized on the surface, higher the Charge Transfer Resistance since the passage of the electrons from the redox couple is more difficult.

It is worth noting that the functionalization protocol influences in a huge way the sensibility of the sensor, since its response is directly associated to its covering. [286,298] The functionalization protocol needs therefore to be monitored to be optimized and electrochemical characterization, additionally to the detection, can perform this type of monitoring [278,282].

The bio-electrochemical sensor used to perform BED is composed of three electrodes: the working electrode (WE) in which the biomarker is immobilized and detected, the counter electrode (CE) that is usually made of the same material of the WE and that serves to close the circuit with the WE and the reference electrode (RE) that plays the role of the reference, as its name suggest. The RE is almost always composed of Ag/AgCl. The WE is fundamental for the biosensing since it is where the immobilization of the biomarker is performed. The sensitivity of the whole sensor depends therefore on the quality of the WE, which is directly correlated to its capacity to immobilize the analyte. Indeed, the WE should offer large surface area-to-volume ratio to increase the quantity of immobilized molecules, good chemistry to allow the attachment of these molecules, good

conductivity to transduce the signal from an electrochemical to an electrical one and good porosity to enable the diffusion.

In this work, electrospun carbon-based nanofibers are proposed to fulfill all these requirements. Indeed, nanofibers (NFs) are known for their huge surface area-to-volume ratio and porosity [166,299] and carbon-based ones for their excellent conductivity [165]. Through surface treatment as plasma oxygen, the surface chemistry can also be modified creating functional groups necessary for the molecules immobilization.

Usually, carbon-based NFs are obtained through in hoven carbonization under inert atmosphere of electrospun nanofibers of a polymer with a high carbon yield (PAN, PVP, PVA, PI, PBI, PAA). [165] The obtained NFs mat is brittle and therefore difficult to manipulate to integrate it in the three-electrode electrochemical system, so the NFs are milled, and a paste based on these NFs and a binder is created. This procedure, however, leads to a loss of porosity and available surface for the immobilization. Here, a new technique for the carbonization of the NFs based on the use of laser technology is presented, based on the results reported by Lee et al. [300]. This technique has the advantage of allowing the carbonization in ambient atmosphere and overall the patterning of the electrodes on the NFs mat. No milling, no paste, in this way the structure of the NFs can be exploited at its best. Moreover, Cellulose was chosen as the base polymer in order to reach green objectives to facilitate the scale-up of the sensor fabrication. After the carbonization with the laser, the NFs are treated with plasma oxygen to obtain –COOH groups on their surface to enable their biological functionalization.

In parallel, the protocol of functionalization and the detection method were studied and optimized for the detection of Angiopoietin 2 (Ang2). We started to study the electrochemical detection on gold commercial sensors to optimize the protocol and the measurement on a well-known surface before its transfer to the carbon-based NFs. Ang2 belongs to a family of growth factors that are involved in vascular development and angiogenesis [301]. The abnormal expression of this protein has been related to tumoral progression [302,303], auto-immune diseases

[304], and diverse severe illness syndromes such as sepsis, disseminated intravascular coagulation, acute respiratory distress syndrome, myocardial infarction. Acute kidney injury has been linked to its role in vascular homeostasis [305]. Several studies have identified Ang2 as a good performing biomarker from a diagnostic and prognostic perspective and as a predictor factor of patients' mortality. In particular, altered levels of Ang2 were correlated to disease outcome in patients with sepsis [306] and cardiovascular syndromes [307,308] to predict adverse pregnancy outcome [309,310], and disease severity in COVID-19 patients [311]. The detection of biomarkers, like Ang2, represents an important clinical tool to predict, diagnose and monitor the evolution of pathologies.

Label-free detection was chosen for its faster functionalization protocol. The redox couple ($K_4[Fe(CN)_6]/K_3[Fe(CN)_6]$) was inserted directly in solution and the amount of analyte immobilized on the surface of the electrode was directly correlated with the resistance of charge transfer (R_{ct}) of the electrode [282]. The functionalization protocol was monitored and optimized thanks to Electrochemical Impedance Spectroscopy (EIS) and Square Wave Voltammetry (SWV). The functionalization protocol was optimized in terms of electrode surface modification type and incubation time and in terms of length of the protocol itself. For the detection, Enzyme-Linked ImmunoSorbent Assay (ELISA) and Bio-Electrochemical Detection (BED) methods were compared. With the optimized protocol ELISA exhibited a Limit of Detection (LOD) of 1.56 ng/ml and a Limit of Quantification (LOQ) of 2.46 ng/ml. BED showed greater results, confirming the higher sensibility of the sensing technique, with a LOD of 0.3pg/ml and a LOQ of 2.1pg/ml.

4.2. Electrochemical biosensing optimization

The functionalization protocol of a biochemical sensor influences in a huge way its sensibility, since its response is directly associated to the surface covering. Indeed, the charge blocking effect is based on how the molecules immobilized on the surface hinder the passage of the charges from the bulk of the solution toward the electrode. More molecules immobilized, higher the charge transfer resistance (R_{ct}). As in this case we are interested to the sensing of Ang2, it is important to optimize the functionalization protocol to achieve its detection without saturating the surface, case in which we would not be able to do a proper detection.

To optimize the functionalization protocol and the biosensing detection methods, we choose to work with commercial electrodes (DropSens). They were supplied by Metrohm. They present a working and counter screen-printed electrode made of gold, while the reference electrode is made of Ag/AgCl.

The first step of the protocol consisted in the functionalization of the electrode, through the anchoring of thiol-based molecules -COOH terminated. These molecules were useful in order to render specific the link between the antibody and the electrode. Indeed, two strategies are possible to link the antibodies to gold surface: the physical adsorption of the antibody directly on the gold surface or the modification of this surface with reactive groups that can be covalently linked to the antibody after activation. We choose the second option since it have a better reproducibility, better control of the orientation and higher stability. [312]

Thanks to Electrochemical Impedance Spectroscopy we checked the formation of a Self-Assembled Monolayer (SAM) or a partial-SAM based on the incubation time. [313–316] After the functionalization of the electrode surface, the following step consisted in the activation of the terminal carboxyl groups by means of EDC/sulfo-NHS bio-conjugation [317–319]. Then, two strategies were compared:

Long Protocol (LP) consisted in the introduction of the control of the orientation of the antibody by means of protein G (PtG) incubation, at the beginning of the procedure [320]. This protein could then interact with the a-Ang2 antibody through its constant region and exposing the two variable regions for the recognition of the analyte. Thus, this antibody orienting protein immobilization step was followed by the incubation with the a-Ang2 antibody. Finally, Ang2 was incubated, and the detection of the analyte was afterwards performed.

Short Protocol (SP) consisted in the tethering of the a-Ang2 antibody through the incubation of a PBS solution containing 5 μg/mL of the protein on the working electrode. After washing three times in PBS supplemented with 0.05% Tween-20 (PBS-t) for 5 minutes, Ang2 was incubated at different concentrations to establish the interaction with the antibody. After the washing steps were performed as described before, the detection of the analyte was investigated by electrochemical measurements.

The protocol optimization was done in term of the electrode surface modification type and quality and length of the protocol itself:

- Electrode surface modification type was analyzed based on the choice of thiol-based molecules -COOH terminated: the Au surface of the electrodes was modified by grafting one between 3-Mercaptopropionic acid (3-MPA) and 11-Mercaptoundecanoic acid (11-MUA));
- The quality of the electrode functionalization was analyzed through EIS and the best time was selected from this analysis;
- The length of the protocol (SP o LP) determined the quality of the sensing and therefore only one was selected.

SWV and EIS characterizations were performed on the sensor at each step of the functionalization protocol and the charge transfer resistance was extrapolated from EIS through fitting of the Randles (Figure 45b)) equivalent circuit.

The results obtained about the surface electrode functionalization are shown in Figure 45. Two different molecules (3-MPA and 11-MUA) were immobilized on the surface of the sensor and three incubation times (0.5 h, 1 h and 17 h (i.e., overnight)) were compared. The Au surface of the WE was modified by grafting 3-MPA or 11-MUA, in order to choose the best candidate for further grafting exploiting -COOH groups. The electrodes surface was then washed twice in fresh ethanol and once in deionized water.

Since 3-MPA is composed of a chain of only 3 carbons, it probably gives a thinner coating to the sensor leading to an R_{ct} smaller than the one of 11-MUA functionalized sensors that has an 11-carbons long chain. [321,322] Moreover, for the two types of thiols, an increase of R_{ct} is observed from 0.5 h to 1 h of incubation, while no increase is observed from 1 h to 17 h. This indicates a better organization of the molecules, and eventually the formation of the Self-Assembled Monolayer (SAM) after 1 h of incubation [313,314,316,323]. To avoid an electrochemical saturation of the signal due to a too big coating of the sensor, 3-MPA was retained as the thiol derivative useful for the present work and 1h of incubation was applied for this step of the protocol.

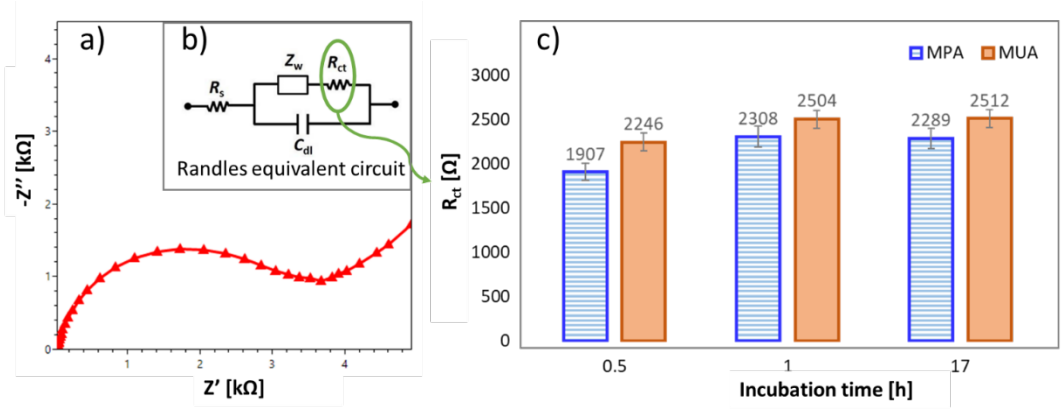


Figure 45: a) EIS results for 11-MUA functionalized sensors after 1 h of incubation, as example; b) Randles equivalent circuit used for the fitting of the EIS circuit; c) R_{ct} of sensor functionalized with two type of thiol derivative: 3-Mercaptopropionic acid (MPA) and 11-Mercapto-undecanoic acid (MUA) and three incubation times.

The results about the monitoring of each step of the protocol done thanks to SWV and EIS characterization are plotted in Figure 46, as well as the ideal scheme of the

protocols. The difference between the LP and the SP consisted in the introduction of the control of the orientation of the antibody by means of a protein (G protein (PtG)) incubation, at the beginning of the procedure. In this way, it is possible to control the orientation of the biorecognition elements and minimize the potential effects of steric hindrance. Beside this advantage, the introduction of another protein lengthens the overall time required to prepare the devices before the electrochemical measurements and increase the quantity of molecules immobilized on the surface, risking its electrochemical saturation or a weaker sensibility of the sensor.

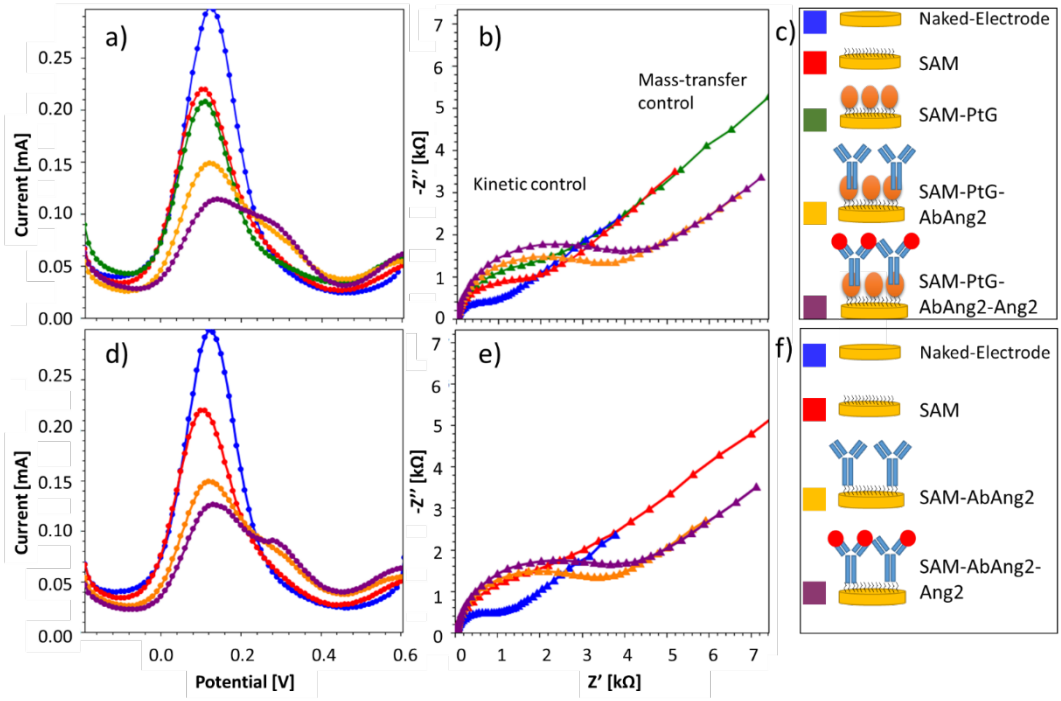


Figure 46: Electrochemical measurement curves at each step of the surface modification protocol: a) and d) Square-Wave-Voltammetry, LP (a)) and SP (d)); b) and e) Electrochemical Impedance Spectroscopy: Nyquist Plot, LP (d)) and SP (e)); c) and f) Scheme of the functionalization protocol, with color legend, LP (c)) and SP (f)).

As reported in Figure 46, when more molecules were immobilized on the electrode surface, the resistance of the interface was higher (so the current was lower) due to the charge transfer blocking. A huge difference was observed in terms of resistance between the naked electrode (blue line) and the electrode functionalized with the SAM (red line), probably due to the density of the monolayer. Another great variation in the curves can be appreciated when the a-

Ang2 antibody is added to the previous layer of immobilized molecules (yellow line). This increase in the R_{ct} is probably due to the larger size of the antibody, compared to the size of the thiol-based molecules or the one of the PtG. Finally, a secondary redox peak at 0.28 V appears in the SWV curves from the a-Ang2 antibody immobilization step, showing an electrochemical behavior of the antibody. This behavior can also be observed on the Nyquist Plot (Figure 46b) and e)) through the translation of the straight-line in the mass-transfer control region. However, since the concentration of the antibody immobilized on the surface of the electrode is fixed for all kind of experiments, this electrochemical behavior does not interfere in the performance of the sensor.

Thanks to the electrochemical measurements and the good agreement between the results obtained by the two methods (SWV and EIS), the optimization of the fabrication of the immunosensors could be performed. The good accomplishment of this fabrication could also be demonstrated for the two immunosensors (LP and SP) and therefore they could be characterized for the detection of Ang2 in term of sensitivity, Limit-of-Detection (LOD) and Limit-of-Quantification (LOQ). Moreover, the performances of the immunosensors could be compared to the performances of the ELISA.

The Ang2 bio-electrochemical detection is shown in Figure 47. To be able to compare the two electrochemical methods, the data is presented in the $\Delta x/x_0 = (x - x_0)/x_0$ form. SP and LP gave very different results. In the case of SP, a trend can be observed and an interpolation with a straight line is possible for the two methods while in the case of LP no trend appears and therefore no fitting occurs. Moreover, for LP, the variability of the results is high (the error bars are huge), especially for EIS. These results lead to the conclusion that, even if the functionalization is well accomplished, as the monitoring of all the steps already proved (Figure 46), LP is not suitable for this kind of characterization. SP, however, is suitable and it is therefore possible to hypothesize that electrochemical saturation of the surface is achieved with LP. This saturation induces no differences in the signal when varying the concentration of Ang2, confirming the

importance of the functionalization protocol choice for the construction of the immunosensor in case of BED.

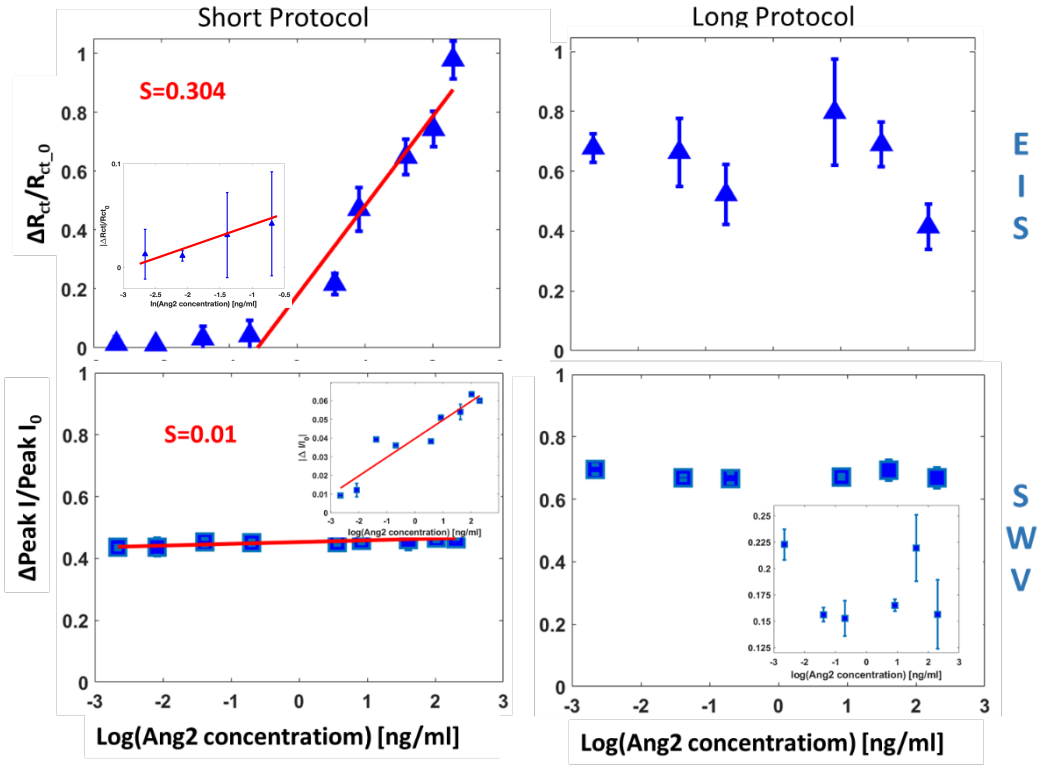


Figure 47: Electrochemical characterization of the immunosensor: EIS and SWV for Long and Short Protocol.

For the short protocol, two linear fits can be obtained and from the slope of these fit the sensitivity of the method can be deduced. EIS offers a better sensitivity than SWV since the slope of the straight line is about 0.3 compared to 0.01 for SWV. However, the LOD and the LOQ of SWV are lower than the ones of EIS, as shown in Table 9. The two types of characterization are therefore useful in a combined modality: one give information with a good sensitivity and the other one detects very low amounts of Ang2 in the sample.

Table 9: Limit Of Detection (LOD) and Limit Of Quantification (LOQ) for the three types of measurement

	LOD [ng/ml]	**LOQ [ng/ml]**
SWV	0.3×10^{-3}	2.1×10^{-3}
EIS	0.68	1.17
ELISA	1.56	2.46

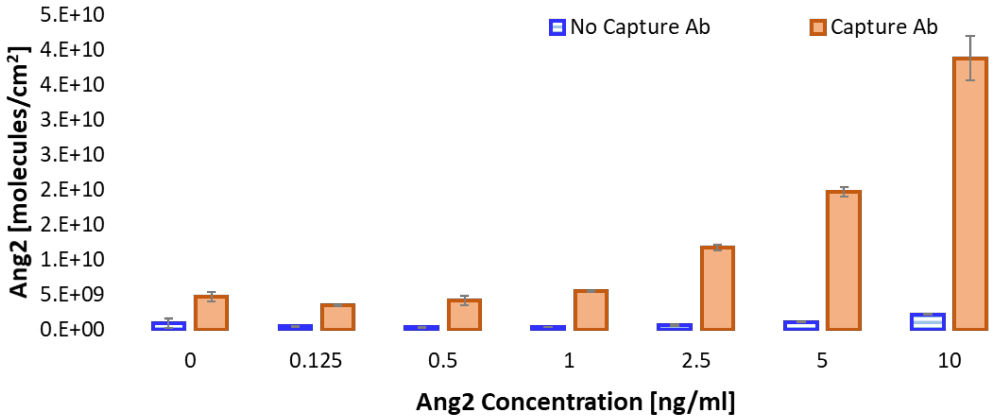


Figure 48: ELISA results of Ang2 detection

Finally, the BED-based sensor was compared to a sandwich ELISA based detection (Figure 48). The sandwich ELISA analysis was performed using a 96-well plate and each experimental condition was tested in triplicate. First, 5 µg/mL of capture antibody in PBS were incubated overnight (O/N) at 4 °C, followed by three washings in PBS-tween 0.05% for 5 minutes on an orbital shaker. Bovine Serum Albumin (BSA) 1% in PBS was incubated for 1 hour at room temperature (RT) to avoid non-specific interactions. A solution of Ang2 in PBS + BSA 0.1% was incubated at different concentrations for 1 hour at RT. After the washing steps were performed as before, 0.5 µg/mL of biotinylated detection antibody in PBS + BSA 0.1% were incubated for 1 hour at RT. The excess was then washed away as previously described and 0.5 µg/mL of HorseRadish Peroxidase (HRP) conjugated Streptavidin in PBS + BSA 0.1% were incubated for 1 hour at RT. Finally, the last washing procedure was performed and (3,3', 5,5'-tetramethylbenzidine) (TMB) chromogen solution was employed for the development of the colorimetric assay. A solution of sulfuric acid (H_2SO_4) 0.5 M was added in equal volume to the TMB solution and the optical density (OD) of the resulting solution was measured using a Thermo Fischer Varioskan™ Microplate Reader. On Figure 47, a linear range is also observed with ELISA, but the LOD and LOQ is higher than the one of the two other types of characterization, as reported in Table 9.

In this work, we showed how BED methods can be useful as a tool to monitor the immunosensor construction. Moreover, we showed how EIS and SWV are valid detection methods for label-free sensing of Ang2, offering the advantages of rapidity, low cost, simplicity and higher sensitivity than ELISA.

4.3. Sensor fabrication

The process flow of the fabrication of the carbon-based NFs electrodes is shown in Figure 49. First, the NFs are obtained through electrospinning of Cellulose Acetate solutions (see Nanofibers fabrication for the composition). Before the laser-induced-graphitization (LIG) process, i.e., the process used for the carbonization, the as-spun NFs mat have to be pretreated in order to guarantying the NFs structuration preservation and the graphitization instead of the burning of the materials under ambient atmosphere. The pre-treatments are discussed below. After the LIG, oxygen plasma treatment should be performed before the biological functionalization process. Plasma treatment, indeed, increases the carbonyl, hydroxyl and carboxyl groups on the surface of the material. The carboxyl group is necessary to anchor the molecules that will further capture Ang2.

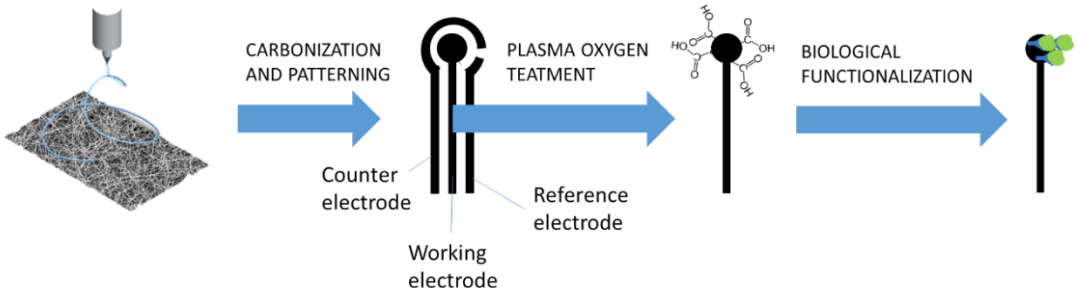


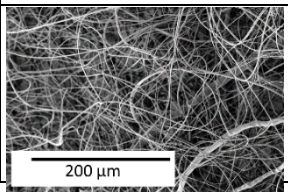
Figure 49: Process flow of the fabrication of the carbon-based NFs electrodes.

4.4. LIG process optimization

Aiming at performing the LIG step under ambient atmosphere in order to easier the fabrication process to be able to scale it up, the big challenge was to reach the conditions of a graphitization without burning of the material. Indeed, for the carbonization to occur, high temperatures have to be reached, temperatures at which these polymers burn in the presence of O_2. We therefore needed to find the pre-treatment of the NFs mat that allowed a carbonization of the material without burning.

In Table 10, the pre-treatments analyzed for cellulose acetate NFs are described.

Table 10: Pre-treatments needed for the graphitization of the cellulose NFs mats under LIG

	Pre-treatment	**Result after LIG**
Cellulose Acetate	1. NaOH 0.05 M in ethanol, 1 h 2. Washing	Burned
	1. NaOH 0.05M in ethanol, 1 h	

For the Cellulose Acetate NFs, a deacetylation step is needed to obtain cellulose NFs. This step is performed through an immersion in a NaOH 0.05 M in ethanol for one hour. We observed that if we do not wash the sample before LIG, the carbonization occurs. However, washing the samples leads to burning of the sample when the LIG is performed. We deduced that the salt present in the deacetylation solution was the key. Indeed, as shown in Figure 50, the NaOH observable in the FESEM before the LIG disappear in the sample carbonized.

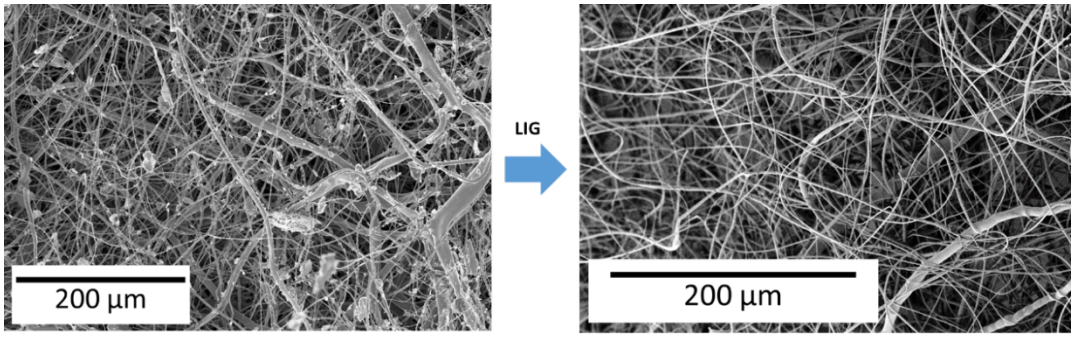


Figure 50: FESEM images of cellulose NFs after deacetylation treatment without washing and after LIG

A hypothesis is that NaOH sublimes under the laser beam, creating an atmosphere free of O_2 that allows the carbonization without burning of the material. Knowing that NaOH boiling temperature is 1388°C [324] and knowing the laser parameters for which we obtained a carbonization of the material, we could verify that the laser temperature reached at least 1388°C with the following equation:

$$T_{exp} = \frac{E}{m} \cdot \frac{1}{C_p} = \frac{P \cdot t}{m} \cdot \frac{1}{C_p} = \frac{P \cdot d/v}{m} \cdot \frac{1}{C_p}$$

Where T_{exp} is the temperature during the laser treatment, m the mass of the sample, C_p the specific heat capacity (for cellulose ≈ 1.4 J/g C° [325]), P the power that reached the sample (that we measured with a powermeter and obtained 0.24W), t the exposition time of the sample, d the distance of the sample analyzed and v the velocity of the laser beam (in this case 500 mm/s).

Considering a length of sample of 1 mm, the condition to reach 1388°C in the material was that the mass of the sample weighted less than 0.25 µg:

$$\begin{cases} T_{crit} = 1388 \\ T_{exp} = \dfrac{P \cdot 1/v}{m} \cdot \dfrac{1}{C_p} \end{cases}$$
$$\Longrightarrow T_{exp} \geq T_{crit}$$

$$\frac{P \cdot 1/v}{m} \cdot \frac{1}{C_p} \geq T_{crit}$$

$$\frac{P \cdot \frac{1}{v}}{T_{crit}} \cdot \frac{1}{C_p} \geq m$$

$$0.25\ 10^{-6} \geq m$$

It can also be noticed in Figure 50 how the nanostructuration is perfectly maintained.

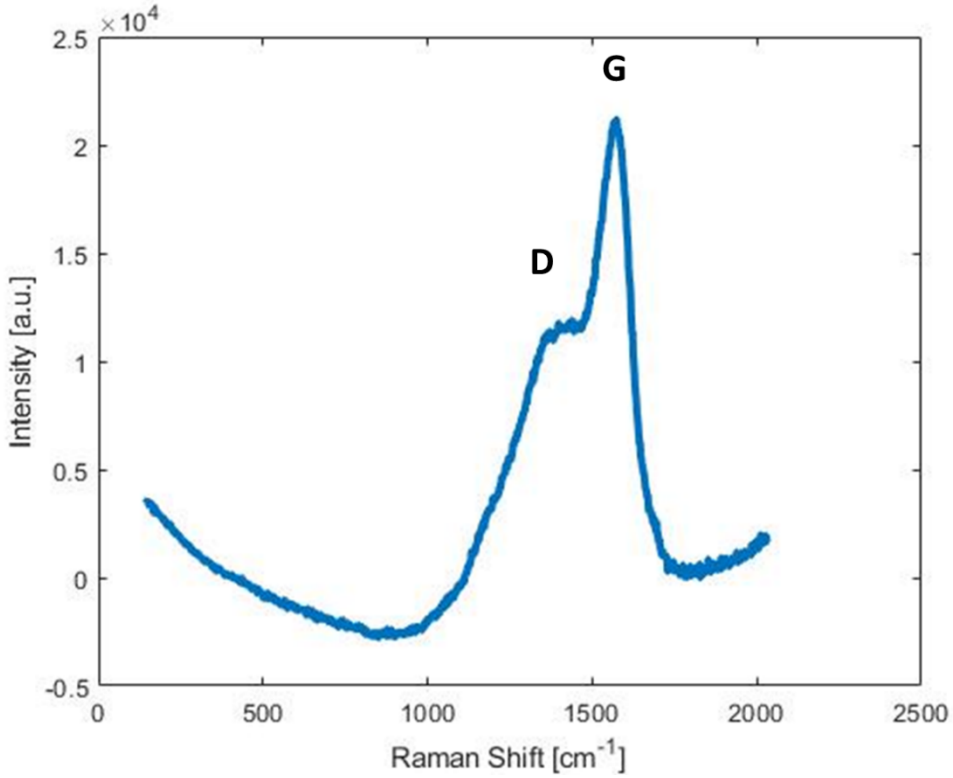


Figure 51: Raman first analysis of cellulose NFs after LIG

A first Raman analysis was conducted on a sample of cellulose after LIG. Figure 51 displays the results. The G band, characteristic of graphite, can be observed and confirms the graphitization of the material.

Further analysis about the conductivity of the NFs should be done to continue the analysis of the material.

4.5. Conclusion and next steps

In this chapter, a promising new technique for the fabrication of carbon based bioelectrochemical sensor was demonstrated, as well as the biosensing optimization.

It was showed how Cellulose NFs can be a suitable material to create electrodes for biosensing with an easy and green scale up. Indeed, through LIG, cellulose NFs mat can be carbonized, perfectly maintaining the nanostructure that offers huge surface area-to-volume ratio and porosity. The great novelty of this carbonization technique consist in the possibility to perform the LIG in air in comparison with the usual carbonization techniques that are performed under inert atmosphere [326–328]. Moreover, LIG allow to pattern the NFs mat, which answer to the big problem of having to mill the carbon NFs and create a paste to form the sensor. With the patterning, indeed, the electrode design is directly applied on the mat.
Further, the biosensing functionalization protocol and detection methods were studied and optimized on commercial gold electrodes. It was shown how, based on charge blocking effect, a shorter protocol gives better sensitivity and how EIS and SWV are complementary methods for the bioelectrochemical sensing. The comparison with ELISA led us to the conclusion that, even on gold, the electrochemical methods give lower LOD and LOQ than classic ELISA, showing again the potentiality of electrochemistry in the context of health monitoring.

To conclude the fabrication and development of this sensor, more analysis should be done on the carbon-based NFs about their conductivity. Plasma treatment should be performed and optimized in order to create the carboxyl groups that can host the molecules necessary for the anchoring of the analyte. The specificity of the sensing should also be checked. And finally, proper biochemical detection should be performed and characterized.

Conclusion and future perspectives

In the frame of my PhD thesis and to respond to the need of a Precision Medicine, I worked on multi-sensing platform for pH and joint bending analysis for rehabilitation application as a wearable device and a Point Of Care (POC) for tumor biomarker and viral detection. In the two devices, electrospun nanofibers are the sensitive element that offer a huge sensitivity, flexibility and ease of fabrication.
For what concerns the wearable device, the first challenge was about the nanofibers fabrication optimization in terms of thermal treatment optimization to obtain highly conductive, mechanical and water-resistant NFs. It was showed how PEO/PEDOT:PSS crosslinked NFs are a good choice for flex and pH sensing, since the same NFs can be employed to develop a multisensing platform. One of the great advantage of these nanomaterials is represented by PEDOT:PSS that is an intrinsically conductive polymer. Furthermore, the optimization of thermal treatment gave a good electrical conductivity and an excellent adhesion of the conserved NFs to the substrate, allowing a good mechanical transfer to the flex sensor. It was optimized in terms of duration time, heating rate and maximum temperature.

The piezoresistivity of the NFs was investigated, as well as compared to the piezoresistivity of a Mixed Composition of nanofibers immersed in a film-like structure. In this way, the importance of the nanostructuration to promote the flex sensing over a larger range of deformation was demonstrated. Excellent Gauge Factors of 45.84 in traction mode and 208.55 in compression mode were obtained.

Another challenge was the decoupling of the signals from the flex and the pH sensors that were integrated on the same platform. It was shown how the choice to perform two sensing with the same material facilitates the fabrication of the device in comparison to multisensing based on different materials. Moreover, the importance of the decoupling of the signals was demonstrated and also the modality to reach this decoupling. The placement of the sensors in the joint was

of importance, but also the methods used for the analysis. It was demonstrated that EIS can provide good pH sensing results together with an analysis of the surface of the material, leaving its bulk to the flex sensing analysis.

The optimized flex-pH sensor can be useful for the monitoring of muscle fatigue during effort since skin pH is linked to the acid built-up of muscle that is doing exercise. The device can also be used for precision medicine, for example in the case of patients that needs remote assistance.

The future perspectives for this work are the adaptation of the platform to a wire form in order to be able to integrate the wire in textiles for even easier daily use.
In the case of the POC for tumor biomarker analysis, the first challenge was the optimization of the functionalization protocol in order to do the best electrochemical detection possible in terms of sensitivity, range of detection and limit-of-detection and –quantification. The second challenge was the fabrication of the electrode based on highly conductive carbon-based NFs. Indeed, these NFs are brittle and hardly shaped into an electrode form.

A promising new technique for the fabrication of carbon-based bio-electrochemical sensor was demonstrated, as well as the biosensing optimization.

It was showed how Cellulose NFs can be a suitable material to create electrodes for biosensing with an easy and green scale up. Indeed, through LIG, cellulose NFs mat can be carbonized, perfectly maintaining the nanostructure that offers huge surface area-to-volume ratio and porosity. LIG played a crucial role to induce the carbonization of nanofibers in air, differently from the most common heating treatments, which ensured the carbonization under inert atmosphere. Moreover, LIG allow patterning the NFs mat, which answer to the big problem of having to mill the carbon NFs and create a paste to form the sensor. With the patterning, indeed, the electrode design is directly applied on the mat.

Further, the biosensing functionalization protocol and detection methods were studied and optimized on commercial gold electrodes. It was shown how, based on charge blocking effect, a shorter protocol gives better sensitivity and how EIS and SWV are complementary methods for the bioelectrochemical sensing. The comparison with ELISA led us to the conclusion that, even on gold, the electrochemical methods give lower LOD and LOQ than classic ELISA, showing again the potentiality of electrochemistry in the context of health monitoring.

The carbon-based electrode still needs to be functionalized and tested for the detection. These steps represent the future perspective of the work about the POC for tumoral biomarker detection.

References

1. UN DESA THE 17 GOALS | Sustainable Development Available online: https://sdgs.un.org/goals (accessed on Oct 12, 2021).
2. European Alliance for Personalised Medicine European Alliance for Personalised Medicine - Who we are Available online: https://www.euapm.eu/who-we-are.html (accessed on Oct 13, 2021).
3. Juengst, E.; McGowan, M.L.; Fishman, J.R.; Settersten, R.A. From "Personalized" to "Precision" Medicine: The Ethical and Social Implications of Rhetorical Reform in Genomic Medicine. *Hastings Cent. Rep.* **2016**, *46*, 21–33, doi:10.1002/hast.614.
4. Medicina personalizzata | CCM - Network Available online: https://www.ccm-network.it/pagina.jsp?id=node/1750 (accessed on Oct 12, 2021).
5. Lee, V.H.L. Personalized medicine: Transforming drug development and healthcare. *Ther. Deliv.* 2010, *1*, 615–619.
6. Wang, Z.; Samanipour, R.; Koo, K.I.; Kim, K. Organ-on-a-chip platforms for drug delivery and cell characterization: A review. *Sensors Mater.* **2015**, *27*, 487–506, doi:10.18494/SAM.2015.1086.
7. Sun, W.; Lee, J.; Zhang, S.; Benyshek, C.; Dokmeci, M.R.; Khademhosseini, A. Engineering Precision Medicine. *Adv. Sci.* 2019, *6*, 1801039.
8. Chorsi, M.T.; Curry, E.J.; Chorsi, H.T.; Das, R.; Baroody, J.; Purohit, P.K.; Ilies, H.; Nguyen, T.D. Piezoelectric Biomaterials for Sensors and Actuators. *Adv. Mater.* **2019**, *31*, 1802084, doi:10.1002/ADMA.201802084.
9. Wu, X.; Ma, Y.; Zhang, G.; Chu, Y.; Du, J.; Zhang, Y.; Li, Z.; Duan, Y.; Fan, Z.; Huang, J. Thermally stable, biocompatible, and flexible organic field effect transistors and their application in temperature sensing arrays for artificial skin. *Adv. Funct. Mater.* **2015**, *25*, 2138–2146, doi:10.1002/adfm.201404535.
10. Amjadi, M.; Kyung, K.U.; Park, I.; Sitti, M. Stretchable, Skin-Mountable, and

Wearable Strain Sensors and Their Potential Applications: A Review. *Adv. Funct. Mater.* **2016**, *26*, 1678–1698, doi:10.1002/adfm.201504755.

11. Bariya, M.; Nyein, H.Y.Y.; Javey, A. Wearable sweat sensors. *Nat. Electron.* **2018**, *1*, 160–171, doi:10.1038/s41928-018-0043-y.
12. Dunn, J.; Runge, R.; Snyder, M. Wearables and the medical revolution. *Per. Med.* 2018, *15*, 429–448.
13. Huang, B.; He, Y.; Wang, L.; Shi, J.; Hu, J.; Rofaani, E.; Yamada, A.; Chen, Y. Microfluidic channel with embedded monolayer nanofibers for cell culture and co-culture. *Microelectron. Eng.* **2020**, *225*, doi:10.1016/j.mee.2020.111235.
14. Bariya, M.; Nyein, H.Y.Y.; Javey, A. Wearable sweat sensors. *Nat. Electron.* 2018, *1*, 160–171.
15. Rodgers, M.M.; Pai, V.M.; Conroy, R.S. Recent advances in wearable sensors for health monitoring. *IEEE Sens. J.* **2015**, *15*, 3119–3126, doi:10.1109/JSEN.2014.2357257.
16. Luka, G.; Ahmadi, A.; Najjaran, H.; Alocilja, E.; Derosa, M.; Wolthers, K.; Malki, A.; Aziz, H.; Althani, A.; Hoorfar, M. Microfluidics integrated biosensors: A leading technology towards lab-on-A-chip and sensing applications. *Sensors (Switzerland)* **2015**, *15*, 30011–30031, doi:10.3390/s151229783.
17. Weng, W.; Chen, P.; He, S.; Sun, X.; Peng, H. Smart electronic textiles. *Angew. Chemie - Int. Ed.* 2016, *55*, 6140–6169.
18. Nasiri, S.; Khosravani, M.R. Progress and challenges in fabrication of wearable sensors for health monitoring. *Sensors Actuators, A Phys.* 2020, *312*, 112105.
19. Balageas, D.; Fritzen, C.-P.; Güemes, A. Structural health monitoring. In *Futures in Mechanics of Structures and Materials*; 2020; pp. 785–820.
20. Li, G.; Wen, D. Wearable biochemical sensors for human health monitoring: sensing materials and manufacturing technologies. *J. Mater. Chem. B* 2020, *8*, 3423–3436.
21. Raymond, S.A.; Gordon, G.E.; Singer, D.B. *III United States Patent (19) Patent Number: Date of Patent: 5,778,882*; 1998;

22. Homayounfar, S.Z.; Andrew, T.L. Wearable Sensors for Monitoring Human Motion: A Review on Mechanisms, Materials, and Challenges. *SLAS Technol.* 2020, *25*, 9–24.
23. Bötzel, K.; Marti, F.M.; Rodríguez, M.Á.C.; Plate, A.; Vicente, A.O. Gait recording with inertial sensors - How to determine initial and terminal contact. *J. Biomech.* **2016**, *49*, 332–337, doi:10.1016/j.jbiomech.2015.12.035.
24. Yang, S.; Li, Q. Inertial sensor-based methods in walking speed estimation: A systematic review. *Sensors (Switzerland)* 2012, *12*, 6102–6116.
25. Bavan, L.; Surmacz, K.; Beard, D.; Mellon, S.; Rees, J. Adherence monitoring of rehabilitation exercise with inertial sensors: A clinical validation study. *Gait Posture* **2019**, *70*, 211–217, doi:10.1016/j.gaitpost.2019.03.008.
26. Muro-de-la-Herran, A.; Garcia-Zapirain, B.; Mendez-Zorrilla, A. Gait Analysis Methods: An Overview of Wearable and Non-Wearable Systems, Highlighting Clinical Applications. *Sensors* **2014**, *14*, 3362–3394, doi:10.3390/s140203362.
27. Babchenko, A.; Maryles, J. A sensing element based on 3D imperfected polymer optical fibre. *J. Opt. A Pure Appl. Opt.* **2007**, *9*, 1–5, doi:10.1088/1464-4258/9/1/001.
28. Daum, W.; Krauser, J.; Zamzow, P.E.; Ziemann, O. *POF — Polymer Optical Fibers for Data Communication*; Springer Berlin Heidelberg, 2002;
29. Kuang, K.S.C.; Quek, S.T.; Koh, C.G.; Cantwell, W.J.; Scully, P.J. Plastic optical fibre sensors for structural health monitoring: A review of recent progress. *J. Sensors* **2009**, *2009*, doi:10.1155/2009/312053.
30. Kuang, K.S.C.; Cantwell, W.J.; Scully, P.J. An evaluation of a novel plastic optical fibre sensor for axial strain and bend measurements. *Meas. Sci. Technol.* **2002**, *13*, 1523–1534, doi:10.1088/0957-0233/13/10/303.
31. Faisal, A.I.; Majumder, S.; Mondal, T.; Cowan, D.; Naseh, S.; Deen, M.J. Monitoring Methods of Human Body Joints: State-of-the-Art and Research Challenges. *Sensors* **2019**, *19*, 2629, doi:10.3390/s19112629.
32. Grieshaber, D.; MacKenzie, R.; Vörös, J.; Reimhult, E. Electrochemical

Biosensors - Sensor Principles and Architectures. *Sensors* **2008**, *8*, 1400–1458, doi:10.3390/s80314000.

33. Park, H.; Jeong, Y.R.; Yun, J.; Hong, S.Y.; Jin, S.; Lee, S.J.; Zi, G.; Ha, J.S. Stretchable Array of Highly Sensitive Pressure Sensors Consisting of Polyaniline Nanofibers and Au-Coated Polydimethylsiloxane Micropillars. *ACS Nano* **2015**, *9*, 9974–9985, doi:10.1021/acsnano.5b03510.
34. Park, S.W.; Das, P.S.; Chhetry, A.; Park, J.Y. A Flexible Capacitive Pressure Sensor for Wearable Respiration Monitoring System. *IEEE Sens. J.* **2017**, *17*, 6558–6564, doi:10.1109/JSEN.2017.2749233.
35. Wu, D.; Huang, S.; Xiao, Z.; Yu, L.; Wang, L.; Sun, D.; Lin, L. Poly (vinylidene fluoride) piezoelectric nanofibers fabricated by non-uniform field electrospinning. *Int. J. Nanomanuf.* **2015**, *11*, 297–310, doi:10.1504/IJNM.2015.075239.
36. Liu, N.; Fang, G.; Wan, J.; Zhou, H.; Long, H.; Zhao, X. Electrospun PEDOT:PSS-PVA nanofiber based ultrahigh-strain sensors with controllable electrical conductivity. *J. Mater. Chem.* **2011**, *21*, 18962–18966, doi:10.1039/c1jm14491j.
37. Roh, E.; Hwang, B.U.; Kim, D.; Kim, B.Y.; Lee, N.E. Stretchable, Transparent, Ultrasensitive, and Patchable Strain Sensor for Human-Machine Interfaces Comprising a Nanohybrid of Carbon Nanotubes and Conductive Elastomers. *ACS Nano* **2015**, *9*, 6252–6261, doi:10.1021/acsnano.5b01613.
38. Yao, S.; Zhu, Y. Wearable multifunctional sensors using printed stretchable conductors made of silver nanowires. *Nanoscale* **2014**, *6*, 2345–2352, doi:10.1039/c3nr05496a.
39. Cohen, D.J.; Mitra, D.; Peterson, K.; Maharbiz, M.M. A highly elastic, capacitive strain gauge based on percolating nanotube networks. *Nano Lett.* **2012**, *12*, 1821–1825, doi:10.1021/nl204052z.
40. Cai, L.; Song, L.; Luan, P.; Zhang, Q.; Zhang, N.; Gao, Q.; Zhao, D.; Zhang, X.; Tu, M.; Yang, F.; et al. Super-stretchable, transparent carbon nanotube-based capacitive strain sensors for human motion detection. *Sci. Rep.* **2013**, *3*, 1–9, doi:10.1038/srep03048.
41. Lee, J.; Kwon, H.; Seo, J.; Shin, S.; Koo, J.H.; Pang, C.; Son, S.; Kim, J.H.;

Jang, Y.H.; Kim, D.E.; et al. Conductive Fiber-Based Ultrasensitive Textile Pressure Sensor for Wearable Electronics. *Adv. Mater.* **2015**, *27*, 2433–2439, doi:10.1002/adma.201500009.

42. Frutiger, A.; Muth, J.T.; Vogt, D.M.; Mengüç, Y.; Campo, A.; Valentine, A.D.; Walsh, C.J.; Lewis, J.A. Capacitive Soft Strain Sensors via Multicore-Shell Fiber Printing. *Adv. Mater.* **2015**, *27*, 2440–2446, doi:10.1002/adma.201500072.
43. Sheng, L.; Teo, S.; Liu, J. Liquid-Metal-Painted Stretchable Capacitor Sensors for Wearable Healthcare Electronics. *J. Med. Biol. Eng.* **2016**, *36*, 265–272, doi:10.1007/s40846-016-0129-9.
44. Zhang, J.; Wan, L.; Gao, Y.; Fang, X.; Lu, T.; Pan, L.; Xuan, F. Highly Stretchable and Self-Healable MXene/Polyvinyl Alcohol Hydrogel Electrode for Wearable Capacitive Electronic Skin. *Adv. Electron. Mater.* **2019**, *5*, 1900285, doi:10.1002/aelm.201900285.
45. Lei, Z.; Wang, Q.; Sun, S.; Zhu, W.; Wu, P. A Bioinspired Mineral Hydrogel as a Self-Healable, Mechanically Adaptable Ionic Skin for Highly Sensitive Pressure Sensing. *Adv. Mater.* **2017**, *29*, 1700321, doi:10.1002/adma.201700321.
46. Hasegawa, Y.; Shikida, M.; Ogura, D.; Suzuki, Y.; Sato, K. Fabrication of a wearable fabric tactile sensor produced by artificial hollow fiber. *J. Micromechanics Microengineering* **2008**, *18*, 085014, doi:10.1088/0960-1317/18/8/085014.
47. Ge, G.; Huang, W.; Shao, J.; Dong, X. Recent progress of flexible and wearable strain sensors for human-motion monitoring. *J. Semicond.* **2018**, *39*, 011012, doi:10.1088/1674-4926/39/1/011012.
48. Seyedin, S.; Moradi, S.; Singh, C.; Razal, J.M. Continuous production of stretchable conductive multifilaments in kilometer scale enables facile knitting of wearable strain sensing textiles. *Appl. Mater. Today* **2018**, *11*, 255–263, doi:10.1016/j.apmt.2018.02.012.
49. Yamada, T.; Hayamizu, Y.; Yamamoto, Y.; Yomogida, Y.; Izadi-Najafabadi, A.; Futaba, D.N.; Hata, K. A stretchable carbon nanotube strain sensor for human-motion detection. *Nat. Nanotechnol.* **2011**, *6*, 296–301,

doi:10.1038/nnano.2011.36.

50. Zheng, X.; Wang, Q.; Luan, J.; Li, Y.; Wang, N. Patterned Metal/Polymer Strain Sensor with Good Flexibility, Mechanical Stability and Repeatability for Human Motion Detection. *Micromachines* **2019**, *10*, 472, doi:10.3390/mi10070472.
51. Sadeqi, A.; Rezaei Nejad, H.; Alaimo, F.; Yun, H.; Punjiya, M.; Sonkusale, S.R. Washable Smart Threads for Strain Sensing Fabrics. *IEEE Sens. J.* **2018**, *18*, 9137–9144, doi:10.1109/JSEN.2018.2870640.
52. Wu, X.; Han, Y.; Zhang, X.; Zhou, Z.; Lu, C. Large-Area Compliant, Low-Cost, and Versatile Pressure-Sensing Platform Based on Microcrack-Designed Carbon Black@Polyurethane Sponge for Human-Machine Interfacing. *Adv. Funct. Mater.* **2016**, *26*, 6246–6256, doi:10.1002/adfm.201601995.
53. Choong, C.-L.; Shim, M.-B.; Lee, B.-S.; Jeon, S.; Ko, D.-S.; Kang, T.-H.; Bae, J.; Lee, S.H.; Byun, K.-E.; Im, J.; et al. Highly Stretchable Resistive Pressure Sensors Using a Conductive Elastomeric Composite on a Micropyramid Array. *Adv. Mater.* **2014**, *26*, 3451–3458, doi:10.1002/adma.201305182.
54. Mao, Y.; Ji, B.; Chen, G.; Hao, C.; Zhou, B.; Tian, Y. Robust and Wearable Pressure Sensor Assembled from AgNW-Coated PDMS Micropillar Sheets with High Sensitivity and Wide Detection Range. *ACS Appl. Nano Mater.* **2019**, *2*, 3196–3205, doi:10.1021/acsanm.9b00503.
55. Dan, L.; Shi, S.; Chung, H.J.; Elias, A. Porous Polydimethylsiloxane-Silver Nanowire Devices for Wearable Pressure Sensors. *ACS Appl. Nano Mater.* **2019**, *2*, 4869–4878, doi:10.1021/acsanm.9b00807.
56. Cheng, Y.; Wang, R.; Sun, J.; Gao, L. A Stretchable and Highly Sensitive Graphene-Based Fiber for Sensing Tensile Strain, Bending, and Torsion. *Adv. Mater.* **2015**, *27*, 7365–7371, doi:10.1002/adma.201503558.
57. Ge, J.; Sun, L.; Zhang, F.-R.; Zhang, Y.; Shi, L.-A.; Zhao, H.-Y.; Zhu, H.-W.; Jiang, H.-L.; Yu, S.-H. A Stretchable Electronic Fabric Artificial Skin with Pressure-, Lateral Strain-, and Flexion-Sensitive Properties. *Adv. Mater.* **2016**, *28*, 722–728, doi:10.1002/adma.201504239.
58. Li, G.; Dai, K.; Ren, M.; Wang, Y.; Zheng, G.; Liu, C.; Shen, C. Aligned flexible conductive fibrous networks for highly sensitive, ultrastretchable and

wearable strain sensors. *J. Mater. Chem. C* **2018**, *6*, 6575–6583, doi:10.1039/c8tc01924j.

59. Zhu, L.; Zhou, X.; Liu, Y.; Fu, Q. Highly Sensitive, Ultrastretchable Strain Sensors Prepared by Pumping Hybrid Fillers of Carbon Nanotubes/Cellulose Nanocrystal into Electrospun Polyurethane Membranes. *ACS Appl. Mater. Interfaces* **2019**, *11*, 12968–12977, doi:10.1021/acsami.9b00136.
60. Fang, X.; Tan, J.; Gao, Y.; Lu, Y.; Xuan, F. High-performance wearable strain sensors based on fragmented carbonized melamine sponges for human motion detection. *Nanoscale* **2017**, *9*, 17948–17956, doi:10.1039/c7nr05903e.
61. Azizkhani, M.; Rastgordani, S.; Anaraki, A.P.; Kadkhodapour, J.; Hadavand, B.S. Highly sensitive and stretchable strain sensors based on chopped carbon fibers sandwiched between silicone rubber layers for human motion detections. *J. Compos. Mater.* **2020**, *54*, 423–434, doi:10.1177/0021998319855758.
62. Lim, G.H.; Lee, N.E.; Lim, B. Highly sensitive, tunable, and durable gold nanosheet strain sensors for human motion detection. *J. Mater. Chem. C* **2016**, *4*, 5642–5647, doi:10.1039/c6tc00251j.
63. Suzuki, K.; Yataka, K.; Okumiya, Y.; Sakakibara, S.; Sako, K.; Mimura, H.; Inoue, Y. Rapid-Response, Widely Stretchable Sensor of Aligned MWCNT/Elastomer Composites for Human Motion Detection. *ACS Sensors* **2016**, *1*, 817–825, doi:10.1021/acssensors.6b00145.
64. Kim, K.; Jung, M.; Jeon, S.; Bae, J. Robust and scalable three-dimensional spacer textile pressure sensor for human motion detection. *Smart Mater. Struct.* **2019**, *28*, 065019, doi:10.1088/1361-665X/ab1adf.
65. Sheng, L.; Liang, Y.; Jiang, L.; Wang, Q.; Wei, T.; Qu, L.; Fan, Z. Bubble-Decorated Honeycomb-Like Graphene Film as Ultrahigh Sensitivity Pressure Sensors. *Adv. Funct. Mater.* **2015**, *25*, 6545–6551, doi:10.1002/adfm.201502960.
66. Lee, S.; Shin, S.; Lee, S.; Seo, J.; Lee, J.; Son, S.; Cho, H.J.; Algadi, H.; Al-Sayari, S.; Kim, D.E.; et al. Ag Nanowire Reinforced Highly Stretchable

Conductive Fibers for Wearable Electronics. *Adv. Funct. Mater.* **2015**, *25*, 3114–3121, doi:10.1002/adfm.201500628.

67. Lu, Y.; Liu, Z.; Yan, H.; Peng, Q.; Wang, R.; Barkey, M.E.; Jeon, J.W.; Wujcik, E.K. Ultrastretchable Conductive Polymer Complex as a Strain Sensor with a Repeatable Autonomous Self-Healing Ability. *ACS Appl. Mater. Interfaces* **2019**, *11*, 20453–20464, doi:10.1021/acsami.9b05464.
68. Park, H.; Jeong, Y.R.; Yun, J.; Hong, S.Y.; Jin, S.; Lee, S.J.; Zi, G.; Ha, J.S. Stretchable Array of Highly Sensitive Pressure Sensors Consisting of Polyaniline Nanofibers and Au-Coated Polydimethylsiloxane Micropillars. *ACS Nano* **2015**, *9*, 9974–9985, doi:10.1021/acsnano.5b03510.
69. Ding, Y.; Yang, J.; Tolle, C.R.; Zhu, Z. Flexible and Compressible PEDOT:PSS@Melamine Conductive Sponge Prepared via One-Step Dip Coating as Piezoresistive Pressure Sensor for Human Motion Detection. *ACS Appl. Mater. Interfaces* **2018**, *10*, 16077–16086, doi:10.1021/acsami.8b00457.
70. Massaglia, G.; Chiodoni, A.; Salvador, G.P.; Delmondo, L.; Muñoz-Tabares, J.A.; Bocchini, S.; Sacco, A.; Bianco, S.; Saracco, G.; Quaglio, M. Defining the role of nanonetting in the electrical behaviour of composite nanofiber/nets. *RSC Adv.* **2017**, *7*, 38812–38818, doi:10.1039/c7ra05573k.
71. Souri, H.; Bhattacharyya, D. Highly Stretchable Multifunctional Wearable Devices Based on Conductive Cotton and Wool Fabrics. *ACS Appl. Mater. Interfaces* **2018**, *10*, 20845–20853, doi:10.1021/acsami.8b04775.
72. Mi, Q.; Wang, Q.; Zang, S.; Mao, G.; Zhang, J.; Ren, X. RGO-coated elastic fibres as wearable strain sensors for full-scale detection of human motions. *Smart Mater. Struct.* **2018**, *27*, 015014, doi:10.1088/1361-665X/aa9aff.
73. Park, J.J.; Hyun, W.J.; Mun, S.C.; Park, Y.T.; Park, O.O. Highly stretchable and wearable graphene strain sensors with controllable sensitivity for human motion monitoring. *ACS Appl. Mater. Interfaces* **2015**, *7*, 6317–6324, doi:10.1021/acsami.5b00695.
74. Yu, X.-G.; Li, Y.-Q.; Zhu, W.-B.; Huang, P.; Wang, T.-T.; Hu, N.; Fu, S.-Y. A wearable strain sensor based on a carbonized nano-sponge/silicone

composite for human motion detection. *Nanoscale* **2017**, *9*, 6680–6685, doi:10.1039/C7NR01011G.

75. Liu, Z.; Zhang, S.; Jin, Y.M.; Ouyang, H.; Zou, Y.; Wang, X.X.; Xie, L.X.; Li, Z. Flexible piezoelectric nanogenerator in wearable self-powered active sensor for respiration and healthcare monitoring. *Semicond. Sci. Technol.* **2017**, *32*, 064004, doi:10.1088/1361-6641/AA68D1.
76. Cauda, V.; Stassi, S.; Bejtka, K.; Canavese, G. Nanoconfinement: An effective way to enhance PVDF piezoelectric properties. *ACS Appl. Mater. Interfaces* **2013**, *5*, 6430–6437, doi:10.1021/am4016878.
77. Stadlober, B.; Zirkl, M.; Irimia-Vladu, M. Route towards sustainable smart sensors: ferroelectric polyvinylidene fluoride-based materials and their integration in flexible electronics. *Chem. Soc. Rev.* **2019**, *48*, 1787–1825, doi:10.1039/C8CS00928G.
78. Wang, A.; Hu, M.; Zhou, L.; Qiang, X. Self-powered wearable pressure sensors with enhanced piezoelectric properties of aligned P(VDF-TrFE)/MWCNT composites for monitoring human physiological and muscle motion signs. *Nanomaterials* **2018**, *8*, doi:10.3390/nano8121021.
79. Bae, S.-H.; Kahya, O.; Sharma, B.K.; Kwon, J.; Cho, H.J.; Özyilmaz, B.; Ahn, J.-H. Graphene-P(VDF-TrFE) Multilayer Film for Flexible Applications. *ACS Nano* **2013**, *7*, 3130–3138, doi:10.1021/NN400848J.
80. Guo, W.; Tan, C.; Shi, K.; Li, J.; Wang, X.-X.; Sun, B.; Huang, X.; Long, Y.-Z.; Jiang, P. Wireless piezoelectric devices based on electrospun PVDF/BaTiO3 NW nanocomposite fibers for human motion monitoring. *Nanoscale* **2018**, *10*, 17751–17760, doi:10.1039/C8NR05292A.
81. Aziz, S.; Chang, S.H. Smart-fabric sensor composed of single-walled carbon nanotubes containing binary polymer composites for health monitoring. *Compos. Sci. Technol.* **2018**, *163*, 1–9, doi:10.1016/j.compscitech.2018.05.012.
82. Zhu, J.; Jia, L.; Huang, R. Electrospinning poly(l-lactic acid) piezoelectric ordered porous nanofibers for strain sensing and energy harvesting. *J. Mater. Sci. Mater. Electron. 2017, Vol. 28, Pages 12080-12085* **2017**, *28*, 12080–12085, doi:10.1007/S10854-017-7020-5.

83. Joseph, J.; Singh, S.G.; Vanjari, S.R.K. Leveraging Innate Piezoelectricity of Ultra-Smooth Silk Thin Films for Flexible and Wearable Sensor Applications. *IEEE Sens. J.* **2017**, *17*, 8306–8313, doi:10.1109/JSEN.2017.2766163.

84. Ghosh, S.K.; Mandal, D. Sustainable Energy Generation from Piezoelectric Biomaterial for Noninvasive Physiological Signal Monitoring. *ACS Sustain. Chem. Eng.* **2017**, *5*, 8836–8843, doi:10.1021/ACSSUSCHEMENG.7B01617.

85. Chander, H.; Burch, R.F.; Talegaonkar, P.; Saucier, D.; Luczak, T.; Ball, J.E.; Turner, A.; Kodithuwakku Arachchige, S.N.K.; Carroll, W.; Smith, B.K.; et al. Wearable Stretch Sensors for Human Movement Monitoring and Fall Detection in Ergonomics. *Int. J. Environ. Res. Public Health* **2020**, *17*, 3554, doi:10.3390/ijerph17103554.

86. Pang, C.; Lee, G.Y.; Kim, T. Il; Kim, S.M.; Kim, H.N.; Ahn, S.H.; Suh, K.Y. A flexible and highly sensitive strain-gauge sensor using reversible interlocking of nanofibres. *Nat. Mater.* **2012**, *11*, 795–801, doi:10.1038/nmat3380.

87. Boutry, C.M.; Nguyen, A.; Lawal, Q.O.; Chortos, A.; Rondeau-Gagné, S.; Bao, Z. A Sensitive and Biodegradable Pressure Sensor Array for Cardiovascular Monitoring. *Adv. Mater.* **2015**, *27*, 6954–6961, doi:10.1002/ADMA.201502535.

88. Bae, G.Y.; Pak, S.W.; Kim, D.; Lee, G.; Kim, D.H.; Chung, Y.; Cho, K. Linearly and Highly Pressure-Sensitive Electronic Skin Based on a Bioinspired Hierarchical Structural Array. *Adv. Mater.* **2016**, *28*, 5300–5306, doi:10.1002/ADMA.201600408.

89. Seshadri, D.R.; Li, R.T.; Voos, J.E.; Rowbottom, J.R.; Alfes, C.M.; Zorman, C.A.; Drummond, C.K. Wearable sensors for monitoring the physiological and biochemical profile of the athlete. *npj Digit. Med.* **2019**, *2*, 1–16, doi:10.1038/s41746-019-0150-9.

90. Hong, S.Y.; Lee, Y.H.; Park, H.; Jin, S.W.; Jeong, Y.R.; Yun, J.; You, I.; Zi, G.; Ha, J.S. Stretchable Active Matrix Temperature Sensor Array of Polyaniline Nanofibers for Electronic Skin. *Adv. Mater.* **2016**, *28*, 930–935, doi:10.1002/ADMA.201504659.

91. Honda, W.; Harada, S.; Arie, T.; Akita, S.; Takei, K. Wearable, human-interactive, health-monitoring, wireless devices fabricated by macroscale printing techniques. *Adv. Funct. Mater.* **2014**, *24*, 3299–3304, doi:10.1002/adfm.201303874.
92. Wang, C.; Xia, K.; Zhang, M.; Jian, M.; Zhang, Y. An All-Silk-Derived Dual-Mode E-skin for Simultaneous Temperature-Pressure Detection. *ACS Appl. Mater. Interfaces* **2017**, *9*, 39484–39492, doi:10.1021/acsami.7b13356.
93. Biochemical Microsensors.
94. Zeng, X.; Zhang, Y.; Du, X.; Li, Y.; Tang, W. A highly sensitive glucose sensor based on a gold nanoparticles/polyaniline/multi-walled carbon nanotubes composite modified glassy carbon electrode. *New J. Chem.* **2018**, *42*, 11944–11953, doi:10.1039/C7NJ04327A.
95. Jeerapan, I.; Sempionatto, J.R.; Pavinatto, A.; You, J.M.; Wang, J. Stretchable biofuel cells as wearable textile-based self-powered sensors. *J. Mater. Chem. A* **2016**, *4*, 18342–18353, doi:10.1039/C6TA08358G.
96. Kim, J.; Imani, S.; de Araujo, W.R.; Warchall, J.; Valdés-Ramírez, G.; Paixão, T.R.L.C.; Mercier, P.P.; Wang, J. Wearable salivary uric acid mouthguard biosensor with integrated wireless electronics. *Biosens. Bioelectron.* **2015**, *74*, 1061–1068, doi:10.1016/j.bios.2015.07.039.
97. Choi, J.; Bandodkar, A.J.; Reeder, J.T.; Ray, T.R.; Turnquist, A.; Kim, S.B.; Nyberg, N.; Hourlier-Fargette, A.; Model, J.B.; Aranyosi, A.J.; et al. Soft, skin-integrated multifunctional microfluidic systems for accurate colorimetric analysis of sweat biomarkers and temperature. *ACS Sensors* **2019**, *4*, 379–388, doi:10.1021/acssensors.8b01218.
98. Zhou, J.; Ma, Z.; Hong, X.; Wu, H.M.; Ma, S.Y.; Li, Y.; Chen, D.J.; Yu, H.Y.; Huang, X.J. Top-Down Strategy of Implantable Biosensor Using Adaptable, Porous Hollow Fibrous Membrane. *ACS Sensors* **2019**, *4*, 931–937, doi:10.1021/acssensors.9b00035.
99. Strambini, L.M.; Longo, A.; Scarano, S.; Prescimone, T.; Palchetti, I.; Minunni, M.; Giannessi, D.; Barillaro, G. Self-powered microneedle-based biosensors for pain-free high-accuracy measurement of glycaemia in interstitial fluid. *Biosens. Bioelectron.* **2015**, *66*, 162–168,

doi:10.1016/j.bios.2014.11.010.

100. Wang, L.; Ye, Y.; Zhu, H.; Song, Y.; He, S.; Xu, F.; Hou, H. Controllable growth of Prussian blue nanostructures on carboxylic group-functionalized carbon nanofibers and its application for glucose biosensing. *Nanotechnology* **2012**, *23*, doi:10.1088/0957-4484/23/45/455502.
101. Huang, Y.; Miao, Y.E.; Ji, S.; Tjiu, W.W.; Liu, T. Electrospun carbon nanofibers decorated with Ag-Pt bimetallic nanoparticles for selective detection of dopamine. *ACS Appl. Mater. Interfaces* **2014**, *6*, 12449–12456, doi:10.1021/am502344p.
102. Wu, J.; Yin, F. Studies on the electrocatalytic oxidation of dopamine at phosphotungstic acid-ZnO spun fiber-modified electrode. *Sensors Actuators, B Chem.* **2013**, *185*, 651–657, doi:10.1016/j.snb.2013.05.052.
103. Jia, W.; Bandodkar, A.J.; Valdés-Ramírez, G.; Windmiller, J.R.; Yang, Z.; Ramírez, J.; Chan, G.; Wang, J. Electrochemical tattoo biosensors for real-time noninvasive lactate monitoring in human perspiration. *Anal. Chem.* **2013**, *85*, 6553–6560, doi:10.1021/ac401573r.
104. Liu, L.; Wang, Z.; Yang, J.; Liu, G.; Li, J.; Guo, L.; Chen, S.; Guo, Q. NiCo2O4 nanoneedle-decorated electrospun carbon nanofiber nanohybrids for sensitive non-enzymatic glucose sensors. *Sensors Actuators, B Chem.* **2018**, *258*, 920–928, doi:10.1016/j.snb.2017.11.118.
105. Zhou, C.; Xu, L.; Song, J.; Xing, R.; Xu, S.; Liu, D.; Song, H. Ultrasensitive non-enzymatic glucose sensor based on three-dimensional network of ZnO-CuO hierarchical nanocomposites by electrospinning. *Sci. Rep.* **2014**, *4*, 1–9, doi:10.1038/srep07382.
106. Ding, Y.; Wang, Y.; Su, L.; Bellagamba, M.; Zhang, H.; Lei, Y. Electrospun Co3O4 nanofibers for sensitive and selective glucose detection. *Biosens. Bioelectron.* **2010**, *26*, 542–548, doi:10.1016/j.bios.2010.07.050.
107. Ding, Y.; Liu, Y.; Zhang, L.; Wang, Y.; Bellagamba, M.; Parisi, J.; Li, C.M.; Lei, Y. Sensitive and selective nonenzymatic glucose detection using functional NiO-Pt hybrid nanofibers. *Electrochim. Acta* **2011**, *58*, 209–214, doi:10.1016/j.electacta.2011.09.039.
108. Tierney, M.J.; Tamada, J.A.; Potts, R.O.; Jovanovic, L.; Garg, S. Clinical

evaluation of the GlucoWatch® biographer: A continual, non-invasive glucose monitor for patients with diabetes. In Proceedings of the Biosensors and Bioelectronics; Elsevier, 2001; Vol. 16, pp. 621–629.

109. Potts, R.O.; Tamada, J.A.; Tierney, M.J. Glucose monitoring by reverse iontophoresis. *Diabetes. Metab. Res. Rev.* **2002**, *18*, S49–S53, doi:10.1002/dmrr.210.

110. Bandodkar, A.J.; You, J.M.; Kim, N.H.; Gu, Y.; Kumar, R.; Mohan, A.M.V.; Kurniawan, J.; Imani, S.; Nakagawa, T.; Parish, B.; et al. Soft, stretchable, high power density electronic skin-based biofuel cells for scavenging energy from human sweat. *Energy Environ. Sci.* **2017**, *10*, 1581–1589, doi:10.1039/c7ee00865a.

111. Sempionatto, J.R.; Brazaca, L.C.; García-Carmona, L.; Bolat, G.; Campbell, A.S.; Martin, A.; Tang, G.; Shah, R.; Mishra, R.K.; Kim, J.; et al. Eyeglasses-based tear biosensing system: Non-invasive detection of alcohol, vitamins and glucose. *Biosens. Bioelectron.* **2019**, *137*, 161–170, doi:10.1016/j.bios.2019.04.058.

112. Zhai, Q.; Gong, S.; Wang, Y.; Lyu, Q.; Liu, Y.; Ling, Y.; Wang, J.; Simon, G.P.; Cheng, W. Enokitake Mushroom-like Standing Gold Nanowires toward Wearable Noninvasive Bimodal Glucose and Strain Sensing. *ACS Appl. Mater. Interfaces* **2019**, *11*, 9724–9729, doi:10.1021/acsami.8b19383.

113. Zhu, N.; Gu, L.; Wang, J.; Li, X.; Liang, G.; Zhou, J.; Zhang, Z. Novel and Sensitive Chemiluminescence Sensors Based on 2D-MOF Nanosheets for One-Step Detection of Glucose in Human Urine. *J. Phys. Chem. C* **2019**, *123*, 9388–9393, doi:10.1021/acs.jpcc.9b00671.

114. Lee, H.; Choi, T.K.; Lee, Y.B.; Cho, H.R.; Ghaffari, R.; Wang, L.; Choi, H.J.; Chung, T.D.; Lu, N.; Hyeon, T.; et al. A graphene-based electrochemical device with thermoresponsive microneedles for diabetes monitoring and therapy. *Nat. Nanotechnol.* **2016**, *11*, 566–572, doi:10.1038/nnano.2016.38.

115. Hua, L.; Wu, X.; Wang, R. Glucose sensor based on an electrochemical reduced graphene oxide-poly(l-lysine) composite film modified GC electrode. *Analyst* **2012**, *137*, 5716–5719, doi:10.1039/c2an35612k.

116. Xu, Q.; Gu, S.X.; Jin, L.; Zhou, Y.E.; Yang, Z.; Wang, W.; Hu, X. Graphene/polyaniline/gold nanoparticles nanocomposite for the direct electron transfer of glucose oxidase and glucose biosensing. *Sensors Actuators, B Chem.* **2014**, *190*, 562–569, doi:10.1016/j.snb.2013.09.049.

117. Alwarappan, S.; Liu, C.; Kumar, A.; Li, C.Z. Enzyme-doped graphene nanosheets for enhanced glucose biosensing. *J. Phys. Chem. C* **2010**, *114*, 12920–12924, doi:10.1021/jp103273z.

118. Tang, H.; Chen, J.; Yao, S.; Nie, L.; Deng, G.; Kuang, Y. Amperometric glucose biosensor based on adsorption of glucose oxidase at platinum nanoparticle-modified carbon nanotube electrode. *Anal. Biochem.* **2004**, *331*, 89–97, doi:10.1016/j.ab.2004.05.005.

119. Loh, K.P.; Liang Zhao, S.; De Zhang, W. Diamond and carbon nanotube glucose sensors based on electropolymerization. *Diam. Relat. Mater.* **2004**, *13*, 1075–1079, doi:10.1016/j.diamond.2003.11.009.

120. Nagata, R.; Clark, S.A.; Yokoyama, K.; Tamiya, E.; Karube, I. Amperometric glucose biosensor manufactured by a printing technique. *Anal. Chim. Acta* **1995**, *304*, 157–164, doi:10.1016/0003-2670(94)00612-P.

121. Nagata, R.; Yokoyama, K.; Durliat, H.; Comtat, M.; Clark, S.A.; Karube, I. An enzyme-containing ink for screen-printed glucose sensors. *Electroanalysis* **1995**, *7*, 1027–1031, doi:10.1002/elan.1140071106.

122. Nagata, R.; Yokoyama, K.; Clark, S.A.; Karube, I. A glucose sensor fabricated by the screen printing technique. *Biosens. Bioelectron.* **1995**, *10*, 261–267, doi:10.1016/0956-5663(95)96845-P.

123. Genies, E.M.; Marchesiello, M. Conducting polymers for biosensors, application to new glucose sensors GOD entrapped into polypyrrole, GOD adsorbed on poly (3-methylthiophene). *Synth. Met.* **1993**, *57*, 3677–3682, doi:10.1016/0379-6779(93)90496-J.

124. Imani, S.; Bandodkar, A.J.; Mohan, A.M.V.; Kumar, R.; Yu, S.; Wang, J.; Mercier, P.P. A wearable chemical-electrophysiological hybrid biosensing system for real-time health and fitness monitoring. *Nat. Commun.* **2016**, *7*, 1–7, doi:10.1038/ncomms11650.

125. Yoon, H.; Xuan, X.; Jeong, S.; Park, J.Y. Wearable, robust, non-enzymatic

continuous glucose monitoring system and its in vivo investigation. *Biosens. Bioelectron.* **2018**, *117*, 267–275, doi:10.1016/j.bios.2018.06.008.

126. Toi, P.T.; Trung, T.Q.; Dang, T.M.L.; Bae, C.W.; Lee, N.E. Highly Electrocatalytic, Durable, and Stretchable Nanohybrid Fiber for On-Body Sweat Glucose Detection. *ACS Appl. Mater. Interfaces* **2019**, *11*, 10707–10717, doi:10.1021/acsami.8b20583.
127. Bae, C.W.; Toi, P.T.; Kim, B.Y.; Lee, W. Il; Lee, H.B.; Hanif, A.; Lee, E.H.; Lee, N.E. Fully Stretchable Capillary Microfluidics-Integrated Nanoporous Gold Electrochemical Sensor for Wearable Continuous Glucose Monitoring. *ACS Appl. Mater. Interfaces* **2019**, *11*, 14567–14575, doi:10.1021/acsami.9b00848.
128. Oh, S.Y.; Hong, S.Y.; Jeong, Y.R.; Yun, J.; Park, H.; Jin, S.W.; Lee, G.; Oh, J.H.; Lee, H.; Lee, S.S.; et al. Skin-Attachable, Stretchable Electrochemical Sweat Sensor for Glucose and pH Detection. *ACS Appl. Mater. Interfaces* **2018**, *10*, 13729–13740, doi:10.1021/acsami.8b03342.
129. Skaria, E.; Patel, B.A.; Flint, M.S.; Ng, K.W. Poly(lactic acid)/Carbon Nanotube Composite Microneedle Arrays for Dermal Biosensing. *Anal. Chem.* **2019**, *91*, 4436–4443, doi:10.1021/acs.analchem.8b04980.
130. Qing, X.; Wang, Y.; Zhang, Y.; Ding, X.; Zhong, W.; Wang, D.; Wang, W.; Liu, Q.; Liu, K.; Li, M.; et al. Wearable Fiber-Based Organic Electrochemical Transistors as a Platform for Highly Sensitive Dopamine Monitoring. *ACS Appl. Mater. Interfaces* **2019**, *11*, 13105–13113, doi:10.1021/acsami.9b00115.
131. Emaminejad, S.; Gao, W.; Wu, E.; Davies, Z.A.; Nyein, H.Y.Y.; Challa, S.; Ryan, S.P.; Fahad, H.M.; Chen, K.; Shahpar, Z.; et al. Autonomous sweat extraction and analysis applied to cystic fibrosis and glucose monitoring using a fully integrated wearable platform. *Proc. Natl. Acad. Sci. U. S. A.* **2017**, *114*, 4625–4630, doi:10.1073/pnas.1701740114.
132. Parrilla, M.; Ortiz-Gómez, I.; Cánovas, R.; Salinas-Castillo, A.; Cuartero, M.; Crespo, G.A. Wearable Potentiometric Ion Patch for On-Body Electrolyte Monitoring in Sweat: Toward a Validation Strategy to Ensure Physiological Relevance. *Anal. Chem.* **2019**, *91*, 8644–8651,

doi:10.1021/acs.analchem.9b02126.

133. Sempionatto, J.R.; Nakagawa, T.; Pavinatto, A.; Mensah, S.T.; Imani, S.; Mercier, P.; Wang, J. Eyeglasses based wireless electrolyte and metabolite sensor platform. *Lab Chip* **2017**, *17*, 1834–1842, doi:10.1039/c7lc00192d.
134. Li, P.; Zhang, D.; Wu, Z. Flexible MoS2 sensor arrays for high performance label-free ion sensing. *Sensors Actuators, A Phys.* **2019**, *286*, 51–58, doi:10.1016/j.sna.2018.12.026.
135. Bao, C.; Kaur, M.; Kim, W.S. Toward a highly selective artificial saliva sensor using printed hybrid field effect transistors. *Sensors Actuators, B Chem.* **2019**, *285*, 186–192, doi:10.1016/j.snb.2019.01.062.
136. Kim, J.; De Araujo, W.R.; Samek, I.A.; Bandodkar, A.J.; Jia, W.; Brunetti, B.; Paixão, T.R.L.C.; Wang, J. Wearable temporary tattoo sensor for real-time trace metal monitoring in human sweat. *Electrochem. commun.* **2015**, *51*, 41–45, doi:10.1016/j.elecom.2014.11.024.
137. Anastasova, S.; Crewther, B.; Bembnowicz, P.; Curto, V.; Ip, H.M.; Rosa, B.; Yang, G.Z. A wearable multisensing patch for continuous sweat monitoring. *Biosens. Bioelectron.* **2017**, *93*, 139–145, doi:10.1016/j.bios.2016.09.038.
138. Nakata, S.; Shiomi, M.; Fujita, Y.; Arie, T.; Akita, S.; Takei, K. A wearable pH sensor with high sensitivity based on a flexible charge-coupled device. *Nat. Electron.* **2018**, *1*, 596–603, doi:10.1038/s41928-018-0162-5.
139. Goh, G.L.; Agarwala, S.; Tan, Y.J.; Yeong, W.Y. A low cost and flexible carbon nanotube pH sensor fabricated using aerosol jet technology for live cell applications. *Sensors Actuators, B Chem.* **2018**, *260*, 227–235, doi:10.1016/j.snb.2017.12.127.
140. Lei, Y.; Zhao, W.; Zhang, Y.; Jiang, Q.; He, J.H.; Baeumner, A.J.; Wolfbeis, O.S.; Wang, Z.L.; Salama, K.N.; Alshareef, H.N. A MXene-Based Wearable Biosensor System for High-Performance In Vitro Perspiration Analysis. *Small* **2019**, *15*, 1901190, doi:10.1002/smll.201901190.
141. Li, G.; Wen, D. Wearable biochemical sensors for human health monitoring: sensing materials and manufacturing technologies. *J. Mater. Chem. B* 2020, *8*, 3423–3436.

142. Roy, S.; David-Pur, M.; Hanein, Y. Carbon Nanotube-Based Ion Selective Sensors for Wearable Applications. *ACS Appl. Mater. Interfaces* **2017**, *9*, 35169–35177, doi:10.1021/acsami.7b07346.

143. An, Q.; Gan, S.; Xu, J.; Bao, Y.; Wu, T.; Kong, H.; Zhong, L.; Ma, Y.; Song, Z.; Niu, L. A multichannel electrochemical all-solid-state wearable potentiometric sensor for real-time sweat ion monitoring. *Electrochem. commun.* **2019**, *107*, 106553, doi:10.1016/j.elecom.2019.106553.

144. Qin, Y.; Alam, A.U.; Howlader, M.M.R.; Hu, N.X.; Deen, M.J. Inkjet Printing of a Highly Loaded Palladium Ink for Integrated, Low-Cost pH Sensors. *Adv. Funct. Mater.* **2016**, *26*, 4923–4933, doi:10.1002/adfm.201600657.

145. Arida, H. Novel pH microsensor based on a thin film gold electrode modified with lead dioxide nanoparticles. *Microchim. Acta* **2015**, *182*, 149–156, doi:10.1007/s00604-014-1311-9.

146. Hwang, S.W.; Lee, C.H.; Cheng, H.; Jeong, J.W.; Kang, S.K.; Kim, J.H.; Shin, J.; Yang, J.; Liu, Z.; Ameer, G.A.; et al. Biodegradable elastomers and silicon nanomembranes/nanoribbons for stretchable, transient electronics, and biosensors. *Nano Lett.* **2015**, *15*, 2801–2808, doi:10.1021/nl503997m.

147. Smith, R.E.; Totti, S.; Velliou, E.; Campagnolo, P.; Hingley-Wilson, S.M.; Ward, N.I.; Varcoe, J.R.; Crean, C. Development of a novel highly conductive and flexible cotton yarn for wearable pH sensor technology. *Sensors Actuators, B Chem.* **2019**, *287*, 338–345, doi:10.1016/j.snb.2019.01.088.

148. Kim, B.Y.; Lee, H.B.; Lee, N.E. A durable, stretchable, and disposable electrochemical biosensor on three-dimensional micro-patterned stretchable substrate. *Sensors Actuators, B Chem.* **2019**, *283*, 312–320, doi:10.1016/j.snb.2018.12.045.

149. Hao, Z.; Pan, Y.; Shao, W.; Lin, Q.; Zhao, X. Graphene-based fully integrated portable nanosensing system for on-line detection of cytokine biomarkers in saliva. *Biosens. Bioelectron.* **2019**, *134*, 16–23, doi:10.1016/j.bios.2019.03.053.

150. Colozza, N.; Kehe, K.; Dionisi, G.; Popp, T.; Tsoutsoulopoulos, A.; Steinritz, D.; Moscone, D.; Arduini, F. A wearable origami-like paper-based

electrochemical biosensor for sulfur mustard detection. *Biosens. Bioelectron.* **2019**, *129*, 15–23, doi:10.1016/j.bios.2019.01.002.

151. Mishra, R.K.; Martín, A.; Nakagawa, T.; Barfidokht, A.; Lu, X.; Sempionatto, J.R.; Lyu, K.M.; Karajic, A.; Musameh, M.M.; Kyratzis, I.L.; et al. Detection of vapor-phase organophosphate threats using wearable conformable integrated epidermal and textile wireless biosensor systems. *Biosens. Bioelectron.* **2018**, *101*, 227–234, doi:10.1016/j.bios.2017.10.044.
152. Mishra, R.K.; Vinu Mohan, A.M.; Soto, F.; Chrostowski, R.; Wang, J. A microneedle biosensor for minimally-invasive transdermal detection of nerve agents. *Analyst* **2017**, *142*, 918–924, doi:10.1039/c6an02625g.
153. Hondred, J.A.; Medintz, I.L.; Claussen, J.C. Enhanced electrochemical biosensor and supercapacitor with 3D porous architectured graphene via salt impregnated inkjet maskless lithography. *Nanoscale Horizons* **2019**, *4*, 735–746, doi:10.1039/c8nh00377g.
154. Amit, M.; Mishra, R.K.; Hoang, Q.; Galan, A.M.; Wang, J.; Ng, T.N. Point-of-use robotic sensors for simultaneous pressure detection and chemical analysis. *Mater. Horizons* **2019**, *6*, 604–611, doi:10.1039/c8mh01412d.
155. Long, K.D.; Woodburn, E. V.; Le, H.M.; Shah, U.K.; Lumetta, S.S.; Cunningham, B.T. Multimode smartphone biosensing: The transmission, reflection, and intensity spectral (TRI)-analyzer. *Lab Chip* **2017**, *17*, 3246–3257, doi:10.1039/c7lc00633k.
156. Barfidokht, A.; Mishra, R.K.; Seenivasan, R.; Liu, S.; Hubble, L.J.; Wang, J.; Hall, D.A. Wearable electrochemical glove-based sensor for rapid and on-site detection of fentanyl. *Sensors Actuators, B Chem.* **2019**, *296*, 126422, doi:10.1016/j.snb.2019.04.053.
157. Gao, W.; Emaminejad, S.; Nyein, H.Y.Y.; Challa, S.; Chen, K.; Peck, A.; Fahad, H.M.; Ota, H.; Shiraki, H.; Kiriya, D.; et al. Fully integrated wearable sensor arrays for multiplexed in situ perspiration analysis. *Nature* **2016**, *529*, 509–514, doi:10.1038/nature16521.
158. Bhardwaj, N.; Kundu, S.C. Electrospinning: A fascinating fiber fabrication technique. *Biotechnol. Adv.* **2010**, *28*, 325–347, doi:10.1016/j.biotechadv.2010.01.004.

159. Thenmozhi, S.; Dharmaraj, N.; Kadirvelu, K.; Kim, H.Y. Electrospun nanofibers: New generation materials for advanced applications. *Mater. Sci. Eng. B Solid-State Mater. Adv. Technol.* **2017**, *217*, 36–48, doi:10.1016/j.mseb.2017.01.001.

160. ++2017_Recent Advances in Electrospun Nanofiber Interfaces for Biosensing Devices.pdf.

161. Windmiller, J.R.; Wang, J. Wearable Electrochemical Sensors and Biosensors: A Review. *Electroanalysis* 2013, *25*, 29–46.

162. Greiner, A.; Wendorff, J.H. Electrospinning: A fascinating method for the preparation of ultrathin fibers. *Angew. Chemie - Int. Ed.* **2007**, *46*, 5670–5703, doi:10.1002/anie.200604646.

163. Baji, A.; Mai, Y.W.; Wong, S.C.; Abtahi, M.; Chen, P. Electrospinning of polymer nanofibers: Effects on oriented morphology, structures and tensile properties. *Compos. Sci. Technol.* **2010**, *70*, 703–718, doi:10.1016/j.compscitech.2010.01.010.

164. Mao, X.; Tian, W.; Hatton, T.A.; Rutledge, G.C. Advances in electrospun carbon fiber-based electrochemical sensing platforms for bioanalytical applications. *Anal. Bioanal. Chem.* **2016**, *408*, 1307–1326, doi:10.1007/s00216-015-9209-x.

165. Sapountzi, E.; Braiek, M.; Chateaux, J.F.; Jaffrezic-Renault, N.; Lagarde, F. Recent advances in electrospun nanofiber interfaces for biosensing devices. *Sensors (Switzerland)* **2017**, *17*, doi:10.3390/s17081887.

166. Li, L.; Mun Lee, P.; Yang, G.; Liu, E. A Review on Electrospun Nanofibers-based Electrochemical Sensor. *Curr. Nanosci.* **2015**, *11*, 710–721, doi:10.2174/1573413711666150505223215.

167. Mao, X.; Simeon, F.; Rutledge, G.C.; Hatton, T.A. Electrospun carbon nanofiber webs with controlled density of states for sensor applications. *Adv. Mater.* **2013**, *25*, 1309–1314, doi:10.1002/adma.201203045.

168. Cai, J.; Chawla, S.; Naraghi, M. Piezoresistive effect of individual electrospun carbon nanofibers for strain sensing. *Carbon N. Y.* **2014**, *77*, 738–746, doi:10.1016/j.carbon.2014.05.078.

169. Cai, C.; Gong, H.; Li, W.; Gao, F.; Jiang, Q.; Cheng, Z.; Han, Z.; Li, S. A flexible

and highly sensitive pressure sensor based on three-dimensional electrospun carbon nanofibers. *RSC Adv.* **2021**, *11*, 13898–13905, doi:10.1039/d0ra10803k.

170. Sengupta, D.; Chen, S.H.; Michael, A.; Kwok, C.Y.; Lim, S.; Pei, Y.; Kottapalli, A.G.P. Single and bundled carbon nanofibers as ultralightweight and flexible piezoresistive sensors. *npj Flex. Electron.* **2020**, *4*, 1–11, doi:10.1038/s41528-020-0072-2.
171. Ding, Y.; Yang, J.; Tolle, C.R.; Zhu, Z. A highly stretchable strain sensor based on electrospun carbon nanofibers for human motion monitoring. *RSC Adv.* **2016**, *6*, 79114–79120, doi:10.1039/c6ra16236c.
172. Liu, D.; Zhang, X.; You, T. Electrochemical performance of electrospun free-standing nitrogen-doped carbon nanofibers and their application for glucose biosensing. In Proceedings of the ACS Applied Materials and Interfaces; American Chemical Society, 2014; Vol. 6, pp. 6275–6280.
173. Li, D.; Luo, L.; Pang, Z.; Ding, L.; Wang, Q.; Ke, H.; Huang, F.; Wei, Q. Novel phenolic biosensor based on a magnetic polydopamine-laccase-nickel nanoparticle loaded carbon nanofiber composite. *ACS Appl. Mater. Interfaces* **2014**, *6*, 5144–5151, doi:10.1021/am500375n.
174. Fu, J.; Qiao, H.; Li, D.; Luo, L.; Chen, K.; Wei, Q. Laccase biosensor based on electrospun copper/carbon composite nanofibers for catechol detection. *Sensors (Switzerland)* **2014**, *14*, 3543–3556, doi:10.3390/s140203543.
175. Zang, Y.; Zhang, F.; Di, C.A.; Zhu, D. Advances of flexible pressure sensors toward artificial intelligence and health care applications. *Mater. Horizons* 2015, *2*, 140–156.
176. Xiao, X.; Song, Y.; Liu, H.; Xie, M.; Hou, H.; Wang, L.; Li, Z. Electrospun carbon nanofibers with manganese dioxide nanoparticles for nonenzymatic hydrogen peroxide sensing. *J. Mater. Sci.* **2013**, *48*, 4843–4850, doi:10.1007/s10853-013-7202-3.
177. Yang, Y.; Fu, R.; Wang, H.; Wang, C. Carbon nanofibers decorated with platinum nanoparticles: A novel three-dimensional platform for non-enzymatic sensing of hydrogen peroxide. *Microchim. Acta* **2013**, *180*, 1249–1255, doi:10.1007/s00604-013-1041-4.

178. Lu, Y.; Luo, L.; Ding, Y.; Wang, Y.; Zhou, M.; Zhou, T.; Zhu, D.; Li, X. Electrospun nickel loaded porous carbon nanofibers for simultaneous determination of adenine and guanine. *Electrochim. Acta* **2015**, *174*, 191–198, doi:10.1016/j.electacta.2015.05.165.

179. Huang, J.; Wang, D.; Hou, H.; You, T. Electrospun palladium nanoparticle-loaded carbon nanofibers and their electrocatalytic activities towards hydrogen peroxide and NADH. *Adv. Funct. Mater.* **2008**, *18*, 441–448, doi:10.1002/adfm.200700729.

180. Hu, G.; Zhou, Z.; Guo, Y.; Hou, H.; Shao, S. Electrospun rhodium nanoparticle-loaded carbon nanofibers for highly selective amperometric sensing of hydrazine. *Electrochem. commun.* **2010**, *12*, 422–426, doi:10.1016/j.elecom.2010.01.009.

181. Zhang, X.; Liu, D.; Li, L.; You, T. Direct electrochemistry of glucose oxidase on novel free-standing nitrogen-doped carbon nanospheres@carbon nanofibers composite film. *Sci. Rep.* **2015**, *5*, 1–11, doi:10.1038/srep09885.

182. Wang, Z.G.; Wan, L.S.; Liu, Z.M.; Huang, X.J.; Xu, Z.K. Enzyme immobilization on electrospun polymer nanofibers: An overview. *J. Mol. Catal. B Enzym.* **2009**, *56*, 189–195, doi:10.1016/j.molcatb.2008.05.005.

183. Lin, Z.; Ji, L.; Medford, A.J.; Shi, Q.; Krause, W.E.; Zhang, X. Electrocatalytic interaction of nano-engineered palladium on carbon nanofibers with hydrogen peroxide and β-NADH. *J. Solid State Electrochem.* **2011**, *15*, 1287–1294, doi:10.1007/s10008-010-1218-2.

184. Bae, T.S.; Shin, E.; Im, J.S.; Kim, J.G.; Lee, Y.S. Effects of carbon structure orientation on the performance of glucose sensors fabricated from electrospun carbon fibers. *J. Non. Cryst. Solids* **2012**, *358*, 544–549, doi:10.1016/j.jnoncrysol.2011.11.002.

185. Ali, M.A.; Mondal, K.; Singh, C.; Dhar Malhotra, B.; Sharma, A. Anti-epidermal growth factor receptor conjugated mesoporous zinc oxide nanofibers for breast cancer diagnostics. *Nanoscale* **2015**, *7*, 7234–7245, doi:10.1039/c5nr00194c.

186. Paul, K.B.; Singh, V.; Vanjari, S.R.K.; Singh, S.G. One step biofunctionalized

electrospun multiwalled carbon nanotubes embedded zinc oxide nanowire interface for highly sensitive detection of carcinoma antigen-125. *Biosens. Bioelectron.* **2017**, *88*, 144–152, doi:10.1016/j.bios.2016.07.114.

187. Brince Paul, K.; Kumar, S.; Tripathy, S.; Vanjari, S.R.K.; Singh, V.; Singh, S.G. A highly sensitive self assembled monolayer modified copper doped zinc oxide nanofiber interface for detection of Plasmodium falciparum histidine-rich protein-2: Targeted towards rapid, early diagnosis of malaria. *Biosens. Bioelectron.* **2016**, *80*, 39–46, doi:10.1016/j.bios.2016.01.036.
188. Tripathy, S.; Krishna Vanjari, S.R.; Singh, V.; Swaminathan, S.; Singh, S.G. Electrospun manganese (III) oxide nanofiber based electrochemical DNA-nanobiosensor for zeptomolar detection of dengue consensus primer. *Biosens. Bioelectron.* **2017**, *90*, 378–387, doi:10.1016/j.bios.2016.12.008.
189. Mondal, K.; Ali, M.A.; Agrawal, V. V.; Malhotra, B.D.; Sharma, A. Highly sensitive biofunctionalized mesoporous electrospun TiO2 nanofiber based interface for biosensing. *ACS Appl. Mater. Interfaces* **2014**, *6*, 2516–2527, doi:10.1021/am404931f.
190. Li, Q.; Liu, D.; Xu, L.; Xing, R.; Liu, W.; Sheng, K.; Song, H. Wire-in-Tube IrOx Architectures: Alternative Label-Free Immunosensor for Amperometric Immunoassay toward α-Fetoprotein. *ACS Appl. Mater. Interfaces* **2015**, *7*, 22719–22726, doi:10.1021/acsami.5b07895.
191. Liu, Y.; Wang, H.; Zhao, W.; Zhang, M.; Qin, H.; Xie, Y. Flexible, Stretchable Sensors for Wearable Health Monitoring: Sensing Mechanisms, Materials, Fabrication Strategies and Features. *Sensors* **2018**, *18*, 645, doi:10.3390/s18020645.
192. Mondal, K.; Sharma, A. Recent advances in electrospun metal-oxide nanofiber based interfaces for electrochemical biosensing. *RSC Adv.* **2016**, *6*, 94595–94616, doi:10.1039/c6ra21477k.
193. Ahmad, M.; Pan, C.; Luo, Z.; Zhu, J. A single ZnO nanofiber-based highly sensitive amperometric glucose biosensor. *J. Phys. Chem. C* **2010**, *114*, 9308–9313, doi:10.1021/jp102505g.
194. Brince Paul, K.; Panigrahi, A.K.; Singh, V.; Singh, S.G. Nonlithographic

Fabrication of Plastic-Based Nanofibers Integrated Microfluidic Biochip for Sensitive Detection of Infectious Biomarker. *ACS Appl. Mater. Interfaces* **2017**, *9*, 39994–40005, doi:10.1021/acsami.7b11331.

195. Mondal, K.; Ali, M.A.; Srivastava, S.; Malhotra, B.D.; Sharma, A. Electrospun functional micro/nanochannels embedded in porous carbon electrodes for microfluidic biosensing. *Sensors Actuators, B Chem.* **2016**, *229*, 82–91, doi:10.1016/j.snb.2015.12.108.
196. Tang, C.; Saquing, C.D.; Morton, S.W.; Glatz, B.N.; Kelly, R.M.; Khan, S.A. Cross-linked polymer nanofibers for hyperthermophilic enzyme immobilization: Approaches to improve enzyme performance. *ACS Appl. Mater. Interfaces* **2014**, *6*, 11899–11906, doi:10.1021/am5033633.
197. Thenmozhi, S.; Dharmaraj, N.; Kadirvelu, K.; Kim, H.Y. Electrospun nanofibers: New generation materials for advanced applications. *Mater. Sci. Eng. B Solid-State Mater. Adv. Technol.* **2017**, *217*, 36–48, doi:10.1016/j.mseb.2017.01.001.
198. Rahman, M.M.; Ahammad, A.J.S.; Jin, J.H.; Ahn, S.J.; Lee, J.J. A comprehensive review of glucose biosensors based on nanostructured metal-oxides. *Sensors* **2010**, *10*, 4855–4886, doi:10.3390/s100504855.
199. Xia, L.; Wei, Z.; Wan, M. Conducting polymer nanostructures and their application in biosensors. *J. Colloid Interface Sci.* **2010**, *341*, 1–11, doi:10.1016/j.jcis.2009.09.029.
200. Rezaei, B.; Ghani, M.; Shoushtari, A.M.; Rabiee, M. Electrochemical biosensors based on nanofibres for cardiac biomarker detection: A comprehensive review. *Biosens. Bioelectron.* **2016**, *78*, 513–523, doi:10.1016/j.bios.2015.11.083.
201. Anwar, R.M.; Vattipalli, K.; Myrah, E.; Asmatulu, R.; Prasad, S. Highly Sensitive Conductive Polymer Nanofibers for Applications in Cardiac Biomarker Detection. *Adv. Sci. Eng. Med.* **2013**, *5*, 633–640, doi:10.1166/asem.2013.1297.
202. Rodthongkum, N.; Ruecha, N.; Rangkupan, R.; Vachet, R.W.; Chailapakul, O. Graphene-loaded nanofiber-modified electrodes for the ultrasensitive determination of dopamine. *Anal. Chim. Acta* **2013**, *804*, 84–91,

doi:10.1016/j.aca.2013.09.057.

203. Kumar, S.; Rai, P.; Sharma, J.G.; Sharma, A.; Malhotra, B.D. PEDOT:PSS/PVA-Nanofibers-Decorated Conducting Paper for Cancer Diagnostics. *Adv. Mater. Technol.* **2016**, *1*, 1–8, doi:10.1002/admt.201600056.

204. Hou, X.; Zhou, Y.; Liu, Y.; Wang, L.; Wang, J. Coaxial electrospun flexible PANI//PU fibers as highly sensitive pH wearable sensor. *J. Mater. Sci.* **2020**, *55*, 16033–16047, doi:10.1007/s10853-020-05110-7.

205. Liu, K.; Zhou, Z.; Yan, X.; Meng, X.; Tang, H.; Qu, K.; Gao, Y.; Li, Y.; Yu, J.; Li, L. Polyaniline nanofiber wrapped fabric for high performance flexible pressure sensors. *Polymers (Basel).* **2019**, *11*, 1120, doi:10.3390/polym11071120.

206. Nan, N.; He, J.; You, X.; Sun, X.; Zhou, Y.; Qi, K.; Shao, W.; Liu, F.; Chu, Y.; Ding, B. A Stretchable, Highly Sensitive, and Multimodal Mechanical Fabric Sensor Based on Electrospun Conductive Nanofiber Yarn for Wearable Electronics. *Adv. Mater. Technol.* **2019**, *4*, 1800338, doi:10.1002/admt.201800338.

207. Verpoorten, E.; Massaglia, G.; Ciardelli, G.; Fabrizio Pirri, C.; Quaglio, M. Design and Optimization of Piezoresistive PEO/PEDOT:PSS Electrospun Nanofibers for Wearable Flex Sensors. *Nanomater. 2020, Vol. 10, Page 2166* **2020**, *10*, 2166, doi:10.3390/nano10112166.

208. Zhang, M.; Zhao, X.; Zhang, G.; Wei, G.; Su, Z. Electrospinning design of functional nanostructures for biosensor applications. *J. Mater. Chem. B* **2017**, *5*, 1699–1711, doi:10.1039/c6tb03121h.

209. Wang, Y.R.; Zheng, J.M.; Ren, G.Y.; Zhang, P.H.; Xu, C. A flexible piezoelectric force sensor based on PVDF fabrics. *Smart Mater. Struct.* **2011**, *20*, 045009, doi:10.1088/0964-1726/20/4/045009.

210. Li, Z.; Zhang, X.; Li, G. In situ ZnO nanowire growth to promote the PVDF piezo phase and the ZnO-PVDF hybrid self-rectified nanogenerator as a touch sensor. *Phys. Chem. Chem. Phys.* **2014**, *16*, 5475–5479, doi:10.1039/c3cp54083a.

211. Hosseini, S.M.; Yousefi, A.A. Piezoelectric sensor based on electrospun

PVDF-MWCNT-Cloisite 30B hybrid nanocomposites. *Org. Electron.* **2017**, *50*, 121–129, doi:10.1016/j.orgel.2017.07.035.

212. Li, B.; Zheng, J.; Xu, C. Silver nanowire dopant enhancing piezoelectricity of electrospun PVDF nanofiber web. In Proceedings of the Fourth International Conference on Smart Materials and Nanotechnology in Engineering; SPIE, 2013; Vol. 8793, p. 879314.
213. Merlini, C.; Barra, G.M.O.; Medeiros Araujo, T.; Pegoretti, A. Electrically pressure sensitive poly(vinylidene fluoride)/polypyrrole electrospun mats. *RSC Adv.* **2014**, *4*, 15749–15758, doi:10.1039/c4ra01058b.
214. Merlini, C.; Almeida, R.D.S.; D'Ávila, M.A.; Schreiner, W.H.; De Oliveira Barra, G.M. Development of a novel pressure sensing material based on polypyrrole-coated electrospun poly(vinylidene fluoride) fibers. *Mater. Sci. Eng. B Solid-State Mater. Adv. Technol.* **2014**, *179*, 52–59, doi:10.1016/j.mseb.2013.10.003.
215. Park, S.H.; Lee, H.B.; Yeon, S.M.; Park, J.; Lee, N.K. Flexible and Stretchable Piezoelectric Sensor with Thickness-Tunable Configuration of Electrospun Nanofiber Mat and Elastomeric Substrates. *ACS Appl. Mater. Interfaces* **2016**, *8*, 24773–24781, doi:10.1021/acsami.6b07833.
216. Mandal, D.; Yoon, S.; Kim, K.J. Origin of piezoelectricity in an electrospun poly(vinylidene fluoride-trifluoroethylene) nanofiber web-based nanogenerator and nano-pressure sensor. *Macromol. Rapid Commun.* **2011**, *32*, 831–837, doi:10.1002/marc.201100040.
217. Ren, G.; Cai, F.; Li, B.; Zheng, J.; Xu, C. Flexible pressure sensor based on a poly(VDF-TrFE) nanofiber web. *Macromol. Mater. Eng.* **2013**, *298*, 541–546, doi:10.1002/mame.201200218.
218. Ke, J.-Y.; Chu, H.-J.; Hsu, Y.-H.; Lee, C.-K. A highly flexible piezoelectret-fiber pressure sensor based on highly aligned P(VDF-TrFE) electrospun fibers. In Proceedings of the Active and Passive Smart Structures and Integrated Systems 2017; SPIE, 2017; Vol. 10164, p. 101642X.
219. Lou, Z.; Chen, S.; Wang, L.; Jiang, K.; Shen, G. An ultra-sensitive and rapid response speed graphene pressure sensors for electronic skin and health monitoring. *Nano Energy* **2016**, *23*, 7–14,

doi:10.1016/j.nanoen.2016.02.053.

220. Wang, X.; Wang, X.; Wang, X.; Chen, F.; Zhu, K.; Xu, Q.; Tang, M. Novel electrochemical biosensor based on functional composite nanofibers for sensitive detection of p53 tumor suppressor gene. *Anal. Chim. Acta* **2013**, *765*, 63–69, doi:10.1016/j.aca.2012.12.037.

221. Devadoss, A.; Han, H.; Song, T.; Kim, Y.P.; Paik, U. Gold nanoparticle-composite nanofibers for enzymatic electrochemical sensing of hydrogen peroxide. *Analyst* **2013**, *138*, 5025–5030, doi:10.1039/c3an00317e.

222. Li, P.; Zhang, M.; Liu, X.; Su, Z.; Wei, G. Electrostatic assembly of platinum nanoparticles along electrospun polymeric nanofibers for high performance electrochemical sensors. *Nanomaterials* **2017**, *7*, doi:10.3390/nano7090236.

223. Zhang, P.; Zhao, X.; Zhang, X.; Lai, Y.; Wang, X.; Li, J.; Wei, G.; Su, Z. Electrospun doping of carbon nanotubes and platinum nanoparticles into the β-phase polyvinylidene difluoride nanofibrous membrane for biosensor and catalysis applications. *ACS Appl. Mater. Interfaces* **2014**, *6*, 7563–7571, doi:10.1021/am500908v.

224. Wang, X.; Wang, X.; Wang, X.; Chen, F.; Zhu, K.; Xu, Q.; Tang, M. Novel electrochemical biosensor based on functional composite nanofibers for sensitive detection of p53 tumor suppressor gene. *Anal. Chim. Acta* **2013**, *765*, 63–69, doi:10.1016/j.aca.2012.12.037.

225. Manesh, K.M.; Kim, H.T.; Santhosh, P.; Gopalan, A.I.; Lee, K.P. A novel glucose biosensor based on immobilization of glucose oxidase into multiwall carbon nanotubes-polyelectrolyte-loaded electrospun nanofibrous membrane. *Biosens. Bioelectron.* **2008**, *23*, 771–779, doi:10.1016/j.bios.2007.08.016.

226. Pavinatto, A.; Mercante, L.A.; Facure, M.H.M.; Pena, R.B.; Sanfelice, R.C.; Mattoso, L.H.C.; Correa, D.S. Ultrasensitive biosensor based on polyvinylpyrrolidone/chitosan/reduced graphene oxide electrospun nanofibers for 17α – Ethinylestradiol electrochemical detection. *Appl. Surf. Sci.* **2018**, *458*, 431–437, doi:10.1016/j.apsusc.2018.07.035.

227. Ahn, Y.C.; Park, S.K.; Kim, G.T.; Hwang, Y.J.; Lee, C.G.; Shin, H.S.; Lee, J.K.

Development of high efficiency nanofilters made of nanofibers. *Curr. Appl. Phys.* **2006**, *6*, 1030–1035, doi:10.1016/j.cap.2005.07.013.

228. Zeleny, J. The electrical discharge from liquid points, and a hydrostatic method of measuring the electric intensity at their surfaces. *Phys. Rev.* **1914**, *3*, 69–91, doi:10.1103/PhysRev.3.69.
229. Subbiah, T.; Bhat, G.S.; Tock, R.W.; Parameswaran, S.; Ramkumar, S.S. Electrospinning of nanofibers. *J. Appl. Polym. Sci.* **2005**, *96*, 557–569, doi:10.1002/app.21481.
230. Sautter, B.P. Continuous Polymer Nanofibers Using Electrospinning. *Mech. Eng.* **2005**.
231. Frenot, A.; Chronakis, I.S. Polymer nanofibers assembled by electrospinning. *Curr. Opin. Colloid Interface Sci.* 2003, *8*, 64–75.
232. MacDiarmid, A.G.; Jones, W.E.; Norris, I.D.; Gao, J.; Johnson, A.T.; Pinto, N.J.; Hone, J.; Han, B.; Ko, F.K.; Okuzaki, H.; et al. Electrostatically-generated nanofibers of electronic polymers. *Synth. Met.* **2001**, *119*, 27–30, doi:10.1016/S0379-6779(00)00597-X.
233. Reneker, D.H.; Yarin, A.L. Electrospinning jets and polymer nanofibers. *Polymer (Guildf).* **2008**, *49*, 2387–2425, doi:10.1016/j.polymer.2008.02.002.
234. Sun, D.; Chang, C.; Li, S.; Lin, L. Near-field electrospinning. *Nano Lett.* **2006**, *6*, 839–842, doi:10.1021/nl0602701.
235. Reneker, D.H.; Chun, I. Nanometre diameter fibres of.pdf. **1996**, *7*, 216–223.
236. Sun, B.; Long, Y.Z.; Zhang, H.D.; Li, M.M.; Duvail, J.L.; Jiang, X.Y.; Yin, H.L. Advances in three-dimensional nanofibrous macrostructures via electrospinning. *Prog. Polym. Sci.* **2014**, *39*, 862–890, doi:10.1016/j.progpolymsci.2013.06.002.
237. Doshi, J.; Reneker, D.H. Electrospinning process and applications of electrospun fibers. *Conf. Rec. - IAS Annu. Meet. (IEEE Ind. Appl. Soc.* **1993**, *3*, 1698–1703, doi:10.1109/ias.1993.299067.
238. Bellan, L.M.; Craighead, H.G. Applications of controlled electrospinning systems. *Polym. Adv. Technol.* **2011**, *22*, 304–309, doi:10.1002/pat.1790.

239. Zander, N.E. Hierarchically structured electrospun fibers. *Polymers (Basel).* **2013**, *5*, 19–44, doi:10.3390/polym5010019.

240. Srivastava, Y.; Marquez, M.; Thorsen, T. Multijet electrospinning of conducting nanofibers from microfluidic manifolds. *J. Appl. Polym. Sci.* **2007**, *106*, 3171–3178, doi:10.1002/APP.26810.

241. Li, D.; Wang, Y.; Xia, Y. Electrospinning Nanofibers as Uniaxially Aligned Arrays and Layer-by-Layer Stacked Films. *Adv. Mater.* **2004**, *16*, 361–366, doi:10.1002/adma.200306226.

242. Agarwal, S.; Greiner, A.; Wendorff, J.H. Functional materials by electrospinning of polymers. *Prog. Polym. Sci.* **2013**, *38*, 963–991, doi:10.1016/j.progpolymsci.2013.02.001.

243. Ding, Z.; Salim, A.; Ziaie, B. Selective nanofiber deposition through field-enhanced electrospinning. *Langmuir* **2009**, *25*, 9648–9652, doi:10.1021/la901924z.

244. Zuo, W.; Zhu, M.; Yang, W.; Yu, H.; Chen, Y.; Zhang, Y. Experimental study on relationship between jet instability and formation of beaded fibers during electrospinning. *Polym. Eng. Sci.* **2005**, *45*, 704–709, doi:10.1002/pen.20304.

245. Liu, Y.; He, J.-H.; Yu, J.; Zeng, H. Controlling numbers and sizes of beads in electrospun nanofibers. *Polym. Int.* **2008**, *57*, 632–636, doi:10.1002/PI.2387.

246. Li, D.; Luo, L.; Pang, Z.; Ding, L.; Wang, Q.; Ke, H.; Huang, F.; Wei, Q. Novel phenolic biosensor based on a magnetic polydopamine-laccase-nickel nanoparticle loaded carbon nanofiber composite. *ACS Appl. Mater. Interfaces* **2014**, *6*, 5144–5151, doi:10.1021/am500375n.

247. Beachley, V.; Wen, X. Effect of electrospinning parameters on the nanofiber diameter and length. *Mater. Sci. Eng. C* **2009**, *29*, 663–668, doi:10.1016/j.msec.2008.10.037.

248. Fong, H.; Chun, I.; Reneker, D.H. <1-s2.0-S0032386199000683-main.pdf>. *Polymer (Guildf).* **1999**, *40*, 4585–4592, doi:10.1016/S0032-3861(99)00068-3.

249. Zargham, S.; Bazgir, S.; Tavakoli, A.; Rashidi, A.S.; Damerchely, R. The

effect of flow rate on morphology and deposition area of electrospun nylon 6 nanofiber. *J. Eng. Fiber. Fabr.* **2012**, *7*, 42–49, doi:10.1177/155892501200700414.

250. Huang, Z.M.; Zhang, Y.Z.; Kotaki, M.; Ramakrishna, S. A review on polymer nanofibers by electrospinning and their applications in nanocomposites. *Compos. Sci. Technol.* **2003**, *63*, 2223–2253, doi:10.1016/S0266-3538(03)00178-7.
251. Kumar, P. Effect of Collector on Electrospinning To Fabricate Aligned Nanofiber Effect of Collector on Electrospinning To Fabricate Aligned Nanofiber. *Natl. Inst. Technol.* **2012**, 1–40.
252. Katta, P.; Alessandro, M.; Ramsier, R.D.; Chase, G.G. Continuous electrospinning of aligned polymer nanofibers onto a wire drum collector. *Nano Lett.* **2004**, *4*, 2215–2218, doi:10.1021/nl0486158.
253. Pham, Q.P.; Sharma, U.; Mikos, A.G. Electrospinning of polymeric nanofibers for tissue engineering applications: A review. *Tissue Eng.* **2006**, *12*, 1197–1211, doi:10.1089/ten.2006.12.1197.
254. Perumal, V.; Hashim, U. Advances in biosensors: Principle, architecture and applications. *J. Appl. Biomed.* **2014**, *12*, 1–15, doi:10.1016/j.jab.2013.02.001.
255. de Rooij, D.M.R. Electrochemical Methods: Fundamentals and Applications. *Anti-Corrosion Methods Mater.* **2003**, *50*, doi:10.1108/acmm.2003.12850eae.001.
256. Latessa, G.; Brunetti, F.; Reale, A.; Saggio, G.; Di Carlo, A. Piezoresistive behaviour of flexible PEDOT:PSS based sensors. *Sensors Actuators, B Chem.* **2009**, *139*, 304–309, doi:10.1016/j.snb.2009.03.063.
257. Du, L.; Li, T.; Jin, F.; Wang, Y.; Li, R.; Zheng, J.; Wang, T.; Feng, Z.Q. Design of high conductive and piezoelectric poly (3,4-ethylenedioxythiophene)/chitosan nanofibers for enhancing cellular electrical stimulation. *J. Colloid Interface Sci.* **2020**, *559*, 65–75, doi:10.1016/j.jcis.2019.10.003.
258. Liu, Nishuang and Fang, Guojia and Wan, Jiawei and Zhou, Hai and Long, Hao and Zhao, X. Electrospun PEDOT: PSS--PVA nanofiber based ultrahigh-

strain sensors with controllable electrical conductivity. *J. Mater. Chem.* **2011**, *21*, 18962--18966.

259. Zubair N.A., R.N.A.; H.N., L.; M., Z.R.; Y., S. Electrochemical properties of PVA–GO/PEDOT nanofibers prepared using electrospinning and electropolymerization techniques. *RSC Adv.* **2016**, *6*, 17720–17727.
260. N., L.; G., F.; J., W.; H., Z.; H., L.; X., Z. Electrospun PEDOT:PSS–PVA nanofiber based ultrahigh-strain sensors with controllable electrical conductivity. *J. Mater. Chem.* **2011**, *21*, 18962–18966.
261. Choi, J.; Lee, J.; Choi, J.; Jung, D.; Shim, S.E. Electrospun PEDOT:PSS/PVP nanofibers as the chemiresistor in chemical vapour sensing. *Synth. Met.* **2010**, *160*, 1415–1421, doi:10.1016/j.synthmet.2010.04.021.
262. Huang, T.M.; Batra, S.; Hu, J.; Miyoshi, T.; Cakmak, M. Chemical cross-linking of conducting poly(3,4-ethylenedioxythiophene): poly(styrenesulfonate) (PEDOT:PSS) using poly(ethylene oxide) (PEO). *Polymer (Guildf).* **2013**, *54*, 6455–6462, doi:10.1016/j.polymer.2013.09.046.
263. Massaglia, G.; Chiodoni, A.; Marasso, S.L.; Pirri, C.F.; Quaglio, M. Electrical conductivity modulation of crosslinked composite nanofibers based on PEO and PEDOT:PSS. *J. Nanomater.* **2018**, *2018*, doi:10.1155/2018/3286901.
264. Huang, T.; Batra, S.; Hu, J.; Miyoshi, T. Chemical cross-linking of conducting poly (3 , 4-ethylenedioxythio- phene): poly (styrenesulfonate) (PEDOT : PSS) using poly (ethylene oxide) (PEO). **2013**, *54*, 6455–6462.
265. Shi, H.; Liu, C.; Jiang, Q.; Xu, J. Effective Approaches to Improve the Electrical Conductivity of PEDOT:PSS: A Review. *Adv. Electron. Mater.* **2015**, *1*, 1–16, doi:10.1002/aelm.201500017.
266. Zubair, N. A., Rahman, N. A., Lim, H. N., Zawawi, R. M., & Sulaiman, Y. Electrochemical properties of PVA–GO/PEDOT nanofibers prepared using electrospinning and electropolymerization techniques. *Rsc Adv.* **2016**, *6*, 17720–17727.
267. Bessaire, B.; Mathieu, M.; Salles, V.; Yeghoyan, T.; Celle, C.; Simonato, J.P.; Brioude, A. Synthesis of continuous conductive PEDOT: PSS nanofibers by

electrospinning: A conformal coating for optoelectronics. *ACS Appl. Mater. Interfaces* **2017**, *9*, 950–957, doi:10.1021/acsami.6b13453.

268. Pinto, N.J.; Rivera, D.; Melendez, A.; Ramos, I.; Lim, J.H.; Johnson, A.T.C. Electrical response of electrospun PEDOT-PSSA nanofibers to organic and inorganic gases. *Sensors Actuators, B Chem.* **2011**, *156*, 849–853, doi:10.1016/j.snb.2011.02.053.
269. Takano, T.; Masunaga, H.; Fujiwara, A.; Okuzaki, H.; Sasaki, T. PEDOT nanocrystal in highly conductive PEDOT:PSS polymer films. *Macromolecules* **2012**, *45*, 3859–3865, doi:10.1021/ma300120g.
270. Antiohos, D.; Folkes, G.; Sherrell, P.; Ashraf, S.; Wallace, G.G.; Aitchison, P.; Harris, A.T.; Chen, J.; Minett, A.I. Compositional effects of PEDOT-PSS/single walled carbon nanotube films on supercapacitor device performance. *J. Mater. Chem.* **2011**, *21*, 15987–15994, doi:10.1039/c1jm12986d.
271. Saggio, G.; Riillo, F.; Sbernini, L.; Quitadamo, L.R. Resistive flex sensors: A survey. *Smart Mater. Struct.* **2015**, *25*, 13001, doi:10.1088/0964-1726/25/1/013001.
272. Saggio, G.; Orengo, G. Flex sensor characterization against shape and curvature changes. *Sensors Actuators, A Phys.* **2018**, *273*, 221–231, doi:10.1016/j.sna.2018.02.035.
273. Verpoorten, E.; Massaglia, G.; Pirri, C.F.; Quaglio, M. Electrospun PEO/PEDOT:PSS Nanofibers for Wearable Physiological Flex Sensors. *Sensors 2021, Vol. 21, Page 4110* **2021**, *21*, 4110, doi:10.3390/S21124110.
274. Saggio, G. Mechanical model of flex sensors used to sense finger movements. *Sensors Actuators, A Phys.* **2012**, *185*, 53–58, doi:10.1016/j.sna.2012.07.023.
275. Takamatsu, S.; Takahata, T.; Muraki, M.; Iwase, E.; Matsumoto, K.; Shimoyama, I. Transparent conductive-polymer strain sensors for touch input sheets of flexible displays. *J. Micromechanics Microengineering* **2010**, *20*, doi:10.1088/0960-1317/20/7/075017.
276. Lang, U.; Rust, P.; Schoberle, B.; Dual, J. Piezoresistive properties of PEDOT:PSS. *Microelectron. Eng.* **2009**, *86*, 330–334,

doi:10.1016/j.mee.2008.10.024.

277. Lang, U.; Rust, P.; Dual, J. Towards fully polymeric MEMS: Fabrication and testing of PEDOT/PSS strain gauges. *Microelectron. Eng.* **2008**, *85*, 1050–1053, doi:10.1016/j.mee.2008.01.051.

278. Ghoneim, M.T.; Nguyen, A.; Dereje, N.; Huang, J.; Moore, G.C.; Murzynowski, P.J.; Dagdeviren, C. Recent Progress in Electrochemical pH-Sensing Materials and Configurations for Biomedical Applications. *Chem. Rev.* 2019, *119*, 5248–5297.

279. Shaju, K.S.; Joby Thomas, K.; Raphael, V.P.; Paul, A. Electrochemical and Surface Morphological Studies of Carbon Steel Corrosion by a Novel Polynuclear Schiff Base in HCl Solution. *ISRN Electrochem.* **2013**, *2013*, 1–8, doi:10.1155/2013/820548.

280. El Azhar, M.; Mernari, B.; Traisnel, M.; Bentiss, F.; Lagrenée, M. Corrosion inhibition of mild steel by the new class of inhibitors [2,5-bis(n-pyridyl)-1,3,4-thiadiazoles] in acidic media. *Corros. Sci.* **2001**, *43*, 2229–2238, doi:10.1016/S0010-938X(01)00034-8.

281. Mitreva, M. the Microbiome of Healthy. In *Skin Microbiome Handbook*; Wiley, 2020; pp. 1–32.

282. Samandari, M.; Julia, M.G.; Rice, A.; Chronopoulos, A.; del Rio Hernandez, A.E. Liquid biopsies for management of pancreatic cancer. *Transl. Res.* **2018**, *201*, 98–127, doi:10.1016/j.trsl.2018.07.008.

283. Khanmohammadi, A.; Aghaie, A.; Vahedi, E.; Qazvini, A.; Ghanei, M.; Afkhami, A.; Hajian, A.; Bagheri, H. Electrochemical biosensors for the detection of lung cancer biomarkers: A review. *Talanta* **2020**, *206*, 120251, doi:10.1016/j.talanta.2019.120251.

284. Labib, M.; Khan, N.; Ghobadloo, S.M.; Cheng, J.; Pezacki, J.P.; Berezovski, M. V. Three-mode electrochemical sensing of ultralow MicroRNA levels. *J. Am. Chem. Soc.* **2013**, *135*, 3027–3038, doi:10.1021/ja308216z.

285. Maduraiveeran, G.; Sasidharan, M.; Ganesan, V. Electrochemical sensor and biosensor platforms based on advanced nanomaterials for biological and biomedical applications. *Biosens. Bioelectron.* **2018**, *103*, 113–129, doi:10.1016/j.bios.2017.12.031.

286. Bertok, T.; Sediva, A.; Katrlik, J.; Gemeiner, P.; Mikula, M.; Nosko, M.; Tkac, J. Label-free detection of glycoproteins by the lectin biosensor down to attomolar level using gold nanoparticles. *Talanta* **2013**, *108*, 11–18, doi:10.1016/j.talanta.2013.02.052.

287. Guo, J.; Yuan, C.; Yan, Q.; Duan, Q.; Li, X.; Yi, G. An electrochemical biosensor for microRNA-196a detection based on cyclic enzymatic signal amplification and template-free DNA extension reaction with the adsorption of methylene blue. *Biosens. Bioelectron.* **2018**, *105*, 103–108, doi:10.1016/j.bios.2018.01.036.

288. Cardoso, A.R.; Moreira, F.T.C.; Fernandes, R.; Sales, M.G.F. Novel and simple electrochemical biosensor monitoring attomolar levels of miRNA-155 in breast cancer. *Biosens. Bioelectron.* **2016**, *80*, 621–630, doi:10.1016/j.bios.2016.02.035.

289. Zeng, Y.; Bao, J.; Zhao, Y.; Huo, D.; Chen, M.; Yang, M.; Fa, H.; Hou, C. A sensitive label-free electrochemical immunosensor for detection of cytokeratin 19 fragment antigen 21-1 based on 3D graphene with gold nanopaticle modified electrode. *Talanta* **2018**, *178*, 122–128, doi:10.1016/j.talanta.2017.09.020.

290. 2014_Electrochemical Performance of Electrospun Free-Standing Nitrogen- Doped Carbon Nanofibers and Their Application for Glucose Biosensing.pdf.

291. Tang, H.; Yan, F.; Tai, Q.; Chan, H.L.W. The improvement of glucose bioelectrocatalytic properties of platinum electrodes modified with electrospun TiO2 nanofibers. *Biosens. Bioelectron.* **2010**, *25*, 1646–1651, doi:10.1016/j.bios.2009.11.027.

292. Waifalkar, P.P.; Chougale, A.D.; Kollu, P.; Patil, P.S.; Patil, P.B. Magnetic nanoparticle decorated graphene based electrochemical nanobiosensor for H2O2 sensing using HRP. *Colloids Surfaces B Biointerfaces* **2018**, *167*, 425–431, doi:10.1016/j.colsurfb.2018.04.042.

293. Liu, S.; Wang, Y.; Xu, W.; Leng, X.; Wang, H.; Guo, Y.; Huang, J. A novel sandwich-type electrochemical aptasensor based on GR-3D Au and aptamer-AuNPs-HRP for sensitive detection of oxytetracycline. *Biosens.*

Bioelectron. **2017**, *88*, 181–187, doi:10.1016/j.bios.2016.08.019.

294. Ruiz-Vega, G.; Arias-Alpízar, K.; de la Serna, E.; Borgheti-Cardoso, L.N.; Sulleiro, E.; Molina, I.; Fernàndez-Busquets, X.; Sánchez-Montalvá, A.; del Campo, F.J.; Baldrich, E. Electrochemical POC device for fast malaria quantitative diagnosis in whole blood by using magnetic beads, Poly-HRP and microfluidic paper electrodes. *Biosens. Bioelectron.* **2020**, *150*, 111925, doi:10.1016/j.bios.2019.111925.
295. Zhang, Y.; Zhang, B.; Ye, X.; Yan, Y.; Huang, L.; Jiang, Z.; Tan, S.; Cai, X. Electrochemical immunosensor for interferon-γ based on disposable ITO detector and HRP-antibody-conjugated nano gold as signal tag. *Mater. Sci. Eng. C* **2016**, *59*, 577–584, doi:10.1016/j.msec.2015.10.066.
296. Chen, P.; Hua, X.; Liu, J.; Liu, H.; Xia, F.; Tian, D.; Zhou, C. A dual amplification electrochemical immunosensor based on HRP-Au@Ag NPs for carcinoembryonic antigen detection. *Anal. Biochem.* **2019**, *574*, 23–30, doi:10.1016/j.ab.2019.03.003.
297. Li, W.; Ma, C.; Song, Y.; Hong, C.; Qiao, X.; Yin, B. Sensitive detection of carcinoembryonic antigen (CEA) by a sandwich-type electrochemical immunosensor using MOF-Ce@HA/Ag-HRP-Ab2 as a nanoprobe. *Nanotechnology* **2020**, *31*, 12, doi:10.1088/1361-6528/ab70d3.
298. Cai, H.; Lee, T.M.H.; Hsing, I.M. Label-free protein recognition using an aptamer-based impedance measurement assay. *Sensors Actuators, B Chem.* **2006**, *114*, 433–437, doi:10.1016/j.snb.2005.06.017.
299. Li, D.; Xia, Y. Electrospinning of nanofibers: Reinventing the wheel? *Adv. Mater.* **2004**, *16*, 1151–1170, doi:10.1002/adma.200400719.
300. Lee, S.; Jeon, S. Laser-Induced Graphitization of Cellulose Nanofiber Substrates under Ambient Conditions. *ACS Sustain. Chem. Eng.* **2019**, *7*, 2270–2275, doi:10.1021/acssuschemeng.8b04955.
301. Eklund, L.; Saharinen, P. Angiopoietin signaling in the vasculature. *Exp. Cell Res.* 2013, *319*, 1271–1280.
302. Saharinen, P.; Eklund, L.; Pulkki, K.; Bono, P.; Alitalo, K. VEGF and angiopoietin signaling in tumor angiogenesis and metastasis. *Trends Mol. Med.* 2011, *17*, 347–362.

303. Bach, F.; Uddin, F.J.; Burke, D. Angiopoietins in malignancy. *Eur. J. Surg. Oncol.* 2007, *33*, 7–15.

304. Wu, Q.; Xu, W.D.; Huang, A.F. Role of angiopoietin-2 in inflammatory autoimmune diseases: A comprehensive review. *Int. Immunopharmacol.* 2020, *80*.

305. Sack, K.D.; Kellum, J.A.; Parikh, S.M. The Angiopoietin-Tie2 Pathway in Critical Illness. *Crit. Care Clin.* 2020, *36*, 201–216.

306. Seol, C.H.; Yong, S.H.; Shin, J.H.; Lee, S.H.; Leem, A.Y.; Park, S.M.; Kim, Y.S.; Chung, K.S. The ratio of plasma angiopoietin-2 to angiopoietin-1 as a prognostic biomarker in patients with sepsis. *Cytokine* **2020**, *129*, doi:10.1016/j.cyto.2020.155029.

307. Uchida, T.; Ito, H.; Yamamoto, H.; Ohno, N.; Asahara, M.; Yamada, Y.; Yamaguchi, O.; Tomita, M.; Makita, K. Elevated levels of angiopoietin-2 as a biomarker for respiratory failure after cardiac surgery. *J. Cardiothorac. Vasc. Anesth.* **2014**, *28*, 1293–1301, doi:10.1053/j.jvca.2014.03.004.

308. Rasmi, Y.; Roshani-Asl, E.; KhademAnsari, M.; SeyedMohammadza, M.; Rostamzadeh, A. GW27-e0621 Angiopoietin-2 as a biomarker for patients with Cardiac Syndrome X. *J. Am. Coll. Cardiol.* **2016**, *68*, C24, doi:10.1016/j.jacc.2016.07.092.

309. Schneuer, F.J.; Roberts, C.L.; Ashton, A.W.; Guilbert, C.; Tasevski, V.; Morris, J.M.; Nassar, N. Angiopoietin 1 and 2 serum concentrations in first trimester of pregnancy as biomarkers of adverse pregnancy outcomes. *Am. J. Obstet. Gynecol.* **2014**, *210*, 345.e1-345.e9, doi:10.1016/j.ajog.2013.11.012.

310. Schneuer, F.J.; Nassar, N.; Guilbert, C.; Tasevski, V.; Ashton, A.W.; Morris, J.M.; Roberts, C.L. First trimester screening of serum soluble fms-like tyrosine kinase-1 and placental growth factor predicting hypertensive disorders of pregnancy. *Pregnancy Hypertens.* **2013**, *3*, 215–221, doi:10.1016/j.preghy.2013.04.119.

311. Smadja, D.M.; Guerin, C.L.; Chocron, R.; Yatim, N.; Boussier, J.; Gendron, N.; Khider, L.; Hadjadj, J.; Goudot, G.; Debuc, B.; et al. Angiopoietin-2 as a marker of endothelial activation is a good predictor factor for intensive

care unit admission of COVID-19 patients. *Angiogenesis* **2020**, *23*, 611–620, doi:10.1007/s10456-020-09730-0.

312. Oliveira, J.P.; Prado, A.R.; Keijok, W.J.; Antunes, P.W.P.; Yapuchura, E.R.; Guimarães, M.C.C. Impact of conjugation strategies for targeting of antibodies in gold nanoparticles for ultrasensitive detection of 17β-estradiol. *Sci. Reports 2019 91* **2019**, *9*, 1–8, doi:10.1038/s41598-019-50424-5.
313. Dadafarin, H.; Konkov, E.; Omanovic, S. Electrochemical functionalization of a 316L stainless steel surface with a 11-mercaptoundecanoic acid monolayer: Stability studies. *Int. J. Electrochem. Sci.* **2013**, *8*, 369–389.
314. Sugihara, K.; Shimazu, K.; Uosaki, K. Electrode potential effect on the surface pKa of a self-assembled 15-mercaptohexadecanoic acid monolayer on a gold/quartz crystal microbalance electrode. *Langmuir* **2000**, *16*, 7101–7105, doi:10.1021/la991301t.
315. Cortés, E.; Rubert, A.A.; Benitez, G.; Carro, P.; Vela, M.E.; Salvarezza, R.C. Enhanced stability of thiolate self-assembled monolayers (SAMs) on nanostructured gold substrates. *Langmuir* **2009**, *25*, 5661–5666, doi:10.1021/la804251a.
316. Stettner, J.; Frank, P.; Griesser, T.; Trimmel, G.; Schennach, R.; Gilli, E.; Winkler, A. A study on the formation and thermal stability of 11-MUA SAMs on Au(111)/Mica and on polycrystalline gold foils. *Langmuir* **2009**, *25*, 1427–1433, doi:10.1021/la802534q.
317. Chiadò, A.; Novara, C.; Lamberti, A.; Geobaldo, F.; Giorgis, F.; Rivolo, P. Immobilization of Oligonucleotides on Metal-Dielectric Nanostructures for miRNA Detection. *Anal. Chem.* **2016**, *88*, 9554–9563, doi:10.1021/acs.analchem.6b02186.
318. Palmara, G.; Chiadò, A.; Calmo, R.; Ricciardi, C. Succinic anhydride functionalized microcantilevers for protein immobilization and quantification. *Anal. Bioanal. Chem.* **2016**, *408*, 7917–7926, doi:10.1007/s00216-016-9920-2.
319. Chiadò, A.; Palmara, G.; Ricciardi, S.; Frascella, F.; Castellino, M.; Tortello, M.; Ricciardi, C.; Rivolo, P. Optimization and characterization of a

homogeneous carboxylic surface functionalization for silicon-based biosensing. *Colloids Surfaces B Biointerfaces* **2016**, *143*, 252–259, doi:10.1016/j.colsurfb.2016.03.048.

320. Trilling, A.K.; Beekwilder, J.; Zuilhof, H. Antibody orientation on biosensor surfaces: A minireview. *Analyst* 2013, *138*, 1619–1627.
321. Haji-Hashemi, H.; Norouzi, P.; Safarnejad, M.R.; Ganjali, M.R. Label-free electrochemical immunosensor for direct detection of Citrus tristeza virus using modified gold electrode. *Sensors Actuators B Chem.* **2017**, *244*, 211–216, doi:10.1016/J.SNB.2016.12.135.
322. Campuzano, S.; Pedrero, M.; Montemayor, C.; Fatás, E.; Pingarrón, J.M. Characterization of alkanethiol-self-assembled monolayers-modified gold electrodes by electrochemical impedance spectroscopy. *J. Electroanal. Chem.* **2006**, *586*, 112–121, doi:10.1016/J.JELECHEM.2005.09.007.
323. González-Cortés, A. Electrochemical Impedance Spectroscopy. *Agric. Food Electroanal.* **2015**, 381–419, doi:10.1002/9781118684030.ch14.
324. Riaz, U.; Ashraf, S.M.; Jadoun, S.; Iqbal, A.; Ahmad, S. Silver ferrite and cobalt ferrite dispersed castor oil polyurethane nanocomposites: Quenching studies of bovine serum albumin. *https://doi.org/10.1080/00914037.2017.1393683* **2017**, *67*, 925–933, doi:10.1080/00914037.2017.1393683.
325. Specific Heat of some common Substances. *Eng. Toolbox* 2015.
326. Massaglia, G.; Margaria, V.; Fiorentin, M.R.; Pasha, K.; Sacco, A.; Castellino, M.; Chiodoni, A.; Bianco, S.; Pirri, F.C.; Quaglio, M. Nonwoven mats of N-doped carbon nanofibers as high-performing anodes in microbial fuel cells. *Mater. Today Energy* **2020**, *16*, 100385, doi:10.1016/j.mtener.2020.100385.
327. Massaglia, G.; Sacco, A.; Castellino, M.; Chiodoni, A.; Frascella, F.; Bianco, S.; Pirri, C.F.; Quaglio, M. N-doping modification by plasma treatment in polyacrylonitrile derived carbon-based nanofibers for Oxygen Reduction Reaction. *Int. J. Hydrogen Energy* **2021**, *46*, 13845–13854, doi:10.1016/j.ijhydene.2020.09.149.
328. Massaglia, G.; Margaria, V.; Sacco, A.; Castellino, M.; Chiodoni, A.; Pirri,

F.C.; Quaglio, M. N-doped carbon nanofibers as catalyst layer at cathode in single chamber Microbial Fuel Cells. *Int. J. Hydrogen Energy* **2019**, *44*, 4442–4449, doi:10.1016/j.ijhydene.2018.10.008.

329. Dixon, A.M.; Mather, S.J. What is it and how does it work? *Anaesthesia* **1981**, *36*, 230–231, doi:10.1111/j.1365-2044.1981.tb08760.x.